COMPLETION OPTIMIZATION IN THE MONTNEY FORMATION, TOWN FIELD, BRITISH COLUMBIA, CANADA

A Dissertation

by

SIMIN SADEGHI

Submitted to the Office of Graduate and Professional Studies of
Texas A&M University
in partial fulfillment of the requirements for the degree of

DOCTOR OF PHILOSOPHY

Chair of Committee,	Duane A. McVay
Co-Chair of Committee,	George W. Voneiff
Committee Members,	Elizabeth Y. Kolodziej
	Jerome Schubert
Head of Department,	Jeff Spath

August 2019

Major Subject: Petroleum Engineering

ABSTRACT

Completion optimization is a process of identifying completion parameters (e.g., lateral length, number of entry points and sand intensity) that maximize economics. Completion optimization is difficult to accomplish due to large heterogeneity in unconventional rock properties and the high cost of trying new completion practices. On the other hand, optimal development of these unconventional resources has significant economic potential. Therefore, it is critical to develop methodologies to identify optimum completion practices.

This research consists of two objectives: first, to develop methodologies to determine the economic optimum completion within and beyond the current industry practices in a low-permeability heterogeneous formation that requires horizontal wells and hydraulic fracturing to flow at commercial rates, and, second, to apply those methodologies to the Town field in the Town field in Montney formation in British Columbia, Canada.

To achieve these objectives, I developed multivariable regression models for the entire Montney along with three subset fields (Town, Altares and Parkland). Then, I built a physics-based reservoir simulation model, calibrated it against the production type curve, and used it to predict well performance. Third, I defined 300 different completion designs and performed economic analysis on production forecasts generated with both the regression and simulation models. Finally, I identified the completion design that yields the maximum rate of return (ROR) and present value at 10% discount rate (PV10) as the optimum completion.

For Altares and Parkland fields, there was no meaningful difference between the full and reduced models; however, for the Town field, the reduced dataset generated a better predictive model. I then focused on the 44-well Town field for the remainder of my study. Both

multivariable regression and simulation models in the Town field do a poor job in predicting individual well performance. For the completion parameters that are well inside the boundary of current practices and toward the average designs, the regression model has less uncertainty and is more suitable. However, for completion parameters that are closer to the upper boundary of current practices, the simulation model does a better job in predicting well performance.

The results show that within current completion practices in the industry, the two models suggest the same optimal completion design of 6,560 ft of lateral length, 942 lb/ft of sand intensity and 50 entry points, which is at the upper limit of current practices for all completion parameters.

Beyond current completion designs, the multivariable regression and simulation models generate different optimal completion designs. In both methodologies, lateral length and number of entry points of the optimum completion designs (by ROR and PV10) are greater than the upper limits of values currently used in the Town field. The optimized sand intensities (ROR and PV10) using the regression method are considerably higher than the upper limit of sand intensities currently used in the Town field. In the simulation method, optimized sand intensities for ROR are within observed field practices and optimized sand intensities for PV10 are at the upper end and beyond current practices used in the Town field, depending on commodity prices. In summary, these results suggest that the overall optimal completion is a more aggressive completion than current industry practices in the Town field.

DEDICATION

I dedicate this dissertation to the person nearest and dearest to my heart, my sister, Mahnoosh.

She is my backbone in all ups and downs of life.

ACKNOWLEDGMENTS

I would like to thank Prof. Duane A. McVay and Prof. George Voneiff for serving as the chair and co-chair of my graduate committee and for their guidance and support without which this project would not have come to fruition. I would like to thank you Mr. Peter Bastian and Mr. John Jochen, Mr. Brad Wolters for their great support and encouragement.

I would like to thank my committee members, Dr. Kolodziej, Dr. Schubert for their guidance and support throughout the course of this research.

Thanks also go to my friends and colleagues and the department faculty and staff for making my time at Texas A&M University a great experience.

CONTRIBUTORS AND FUNDING SOURCES

Contributors

This work was supervised by a dissertation committee consisting of Professors Duane A. McVay [advisor], George W. Voneiff [co-advisor] and Jerome Schubert of the Department of Petroleum Engineering and Elizabeth Y. Kolodziej of the Department of Statistics at Texas A&M University. All other work conducted for the dissertation was completed by the student independently.

Funding Sources

There are no outside funding contributions to acknowledge related to the research and compilation of this document.

NOMENCLATURE

$	US Dollar
$\gamma_{o,API}$	Specific gravity of gas (^{o}API)
λ	Box-Cox exponent
AECO	Alberta Energy Company
BC	British Columbia
bbl	Barrel
EP	Total entry points
EUR	Estimated ultimate recovery
DA	Data analytics
Di	Initial production decline
CAD	Canadian dollar
E&P	Exploration and production
FirstFracYear	First fracturing year
LL	Lateral Length
lb	pound
md	Millidarcy
MVR	Multivariable regression
Mcf	Thousand cubic feet
nd	Nano Darcy
NEB	National Energy Board

NGL	Natural Gas Liquids
OGIP	Original gas in place
qi	Initial production rate
PV10	Net present value
ROR	Rate of return
PC	Perforation cluster per stage
scf	Standard cubic feet
Sim	Simulation
SRV	Stimulated reservoir volume
ST	Stages
S_w	Water saturation (no unit)
t	t-test
tep	Transformed entry points
TR	Transformation ratio (no unit)
T_{res}	Reservoir temperature (^oF)
tsand	Transformed injected sand
T_{surf}	Surface temperature (^oF)
Tcf	Trillion cubic feet
ttvd	Transformed true vertical depth
Vs	Slurry volume
VIF	Variance inflation factor
UGR	Unconventional Gas Resources LLC

UGRFieldname	Field name as assigned by UGR
WHP	Wellhead Pressure
x_f	Fracture half-length

TABLE OF CONTENTS

Page

LIST OF FIGURES

Page

LIST OF TABLES

Page

CHAPTER 1 INTRODUCTION

Selection of the values of completion design components (lateral length, sand intensity, injected fluid, number of clusters) to maximize economic value is called completion optimization. Completion optimization in heterogeneous unconventional plays is a difficult problem to solve due to large variability in critical reservoir parameters, numerous variables that can be chosen in the completion design, and the high cost of trying new completions in the field.

Reservoir properties, various completion designs, and well spacing are factors that should be considered when deciding to drill a well in low-permeability plays. In addition to drilling in the good-quality acreage, appropriate completion designs are essential for a long-term successful investment outcome in low-permeability plays such as the Montney. However, identifying the best completion design is a challenging task due to the inherent complexities and great uncertainty in these unconventional resources. Some exploration and production (E&P) companies apply time-consuming, costly numerical methods (such as reservoir simulation), while others replicate neighbor operators' designs to test completion strategies. These methods, however, may fall short in determining the values of the most significant completion parameters for shale assets because they fail to account for rock variation within these plays.

Shale gas has become an increasingly important source of energy in the last decade, especially in the U.S. and Canada. The U.S. Energy Information Administration (2015) reported that shale-gas reservoirs produced more than 56% of the total U.S. dry-gas production, and it is estimated that by 2040 around 70 Tcf of the world's annual gas production (out of 203 Tcf) will be obtained from unconventional resources.

Optimizing completions is materially important to the oil and gas industry. Well performance continues to increase with increasing stimulation properties, such as horizontal well length, mass of injected sand, volume of injected fluid and number of clusters, suggesting that current practices have not yet reached the optimal (Curtis 2017). The U.S. Energy Information Administration (2016) reported that the total cost of horizontal wells ranges from $6 to $8 million in the U.S and completion costs constitute more than 50% of those costs. Optimized completion practices improve well economics by maximizing rate of return (ROR) or present value at 10% discount rate (PV10), or whatever economic measure is the object of maximization. There are hundreds of thousands of potential well locations in US and Canadian plays and improving completion technologies in horizontal wells places these plays among the most attractive investment opportunities in the oil and gas industry. For instance, the Montney, with more than 8,000 wells, is a massive resource play in Canada that has drawn significant amounts of interest, investment and activity in recent years. Reimer (2015) suggested if the Montney were fully developed, there would be 150,000 wells in the play. With an average $5 million completion cost per well, the total completion capital expenditure would be $750 billion. Current practices to determine the best completion designs, such as field experiments and numerical simulation, are useful; however, they are expensive, time-consuming, and difficult to optimize with spatially changing rock properties.

1.1 Status of the Question

An early study of the optimization of hydraulically-fractured-well completions was conducted by R.W. Veatch in 1983. He summarized three basic requirements for fracture-treatment design in his early studies: 1) determine the expected oil and gas producing rates from

a given reservoir with given fracture half-lengths and conductivities; 2) determine treatment cost for a range of lengths and conductivities; and 3) maximize a specific economic parameter such as the net present value or rate of return. These concepts are illustrated in (Fig. 1.1).

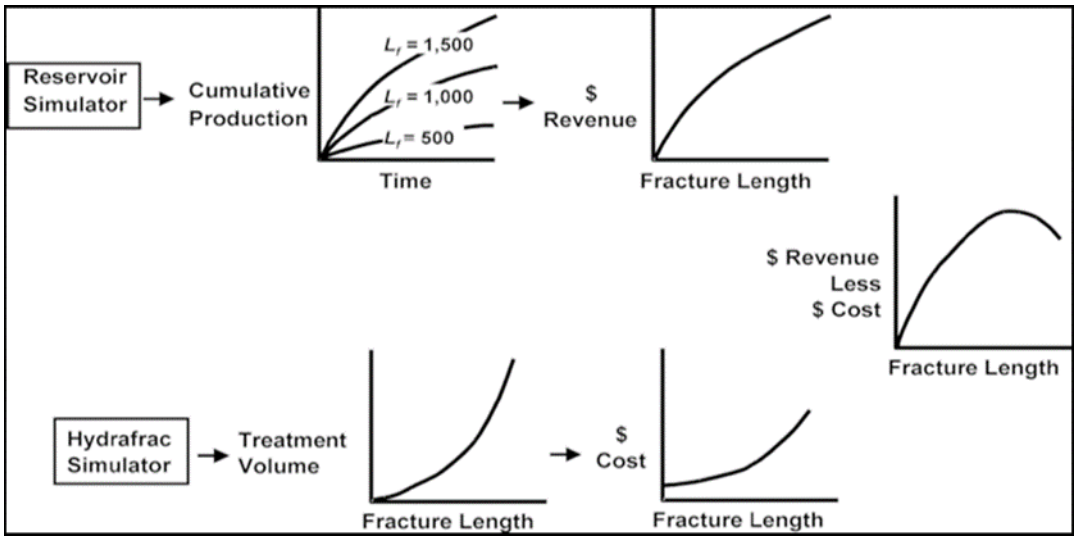

Fig. 1.1—Overview of current hydraulic fracturing design and treatment technology (Adapted from Veatch 1983)

Fig. 1.1 must be understood in the following order to optimize completions: calculate fracture half-length, forecast production rates, and estimate revenue. In this methodology, a fracture-propagation simulator computes propped fracture half-length and conductivity as a function of the treatment volume. A reservoir simulator then provides production forecasts for various fracture half-lengths and conductivities. From these production forecasts, a revenue estimate for each treatment volume is generated. A cost estimate subsequently is generated from the treatment volume. The last step is to calculate the profit by using treatment cost, production revenue and other economic data. The user determines the optimum point on the plot of profit versus fracture half-length at which the profit is maximized (Fig. 1.1). Veatch assessed only one fracture stage since multistage hydraulic fracturing was not practiced at the time of his study.

Hryb et al. (2014) used seismic, mineralogy, geomechanics, well plan, drilling, completion, microseismic monitoring, and production data from wells in the Vaca Muerta shale in Argentina to construct a 3D static geologic model to identify the best reservoir quality locations and determine optimal completion design for a well in the Vaca Muerta formation. The stimulation design was determined using a multistage hydraulic-fracture simulator that predicted complex fracture propagation in the shale reservoir. The hydraulic-fracture results were input to a shale-oil numerical simulator and calibrated with the production history of the well. However, numerical reservoir simulation and history matching are costly, difficult and unacceptably time-consuming over a different geographical area in shale formations. The methodology also requires detailed reservoir characterization, which is labor-intensive. Moreover, the authors attempted to optimize completion design by maximizing production, and they did not perform economic analysis.

Many operators have tried to optimize completion design using various data-mining and analytical approaches (Lafollette (2012), Lafollette and Holcomb (2011), Voneiff and Sadeghi (2013, 2014)). LaFollette and Holcomb (2011) and LaFollette (2012) performed extensive data-mining studies in the Barnett shale to correlate production performance to completion and stimulation parameters. They used well location as a proxy for rock quality and concluded that wells with horizontal lengths greater than 3,500 to 4,500 ft are less productive than shorter wells in the Barnett shale in terms of lower production per perforated foot. However, they did not attempt to optimize completions economically.

In another study, Gong et al. (2011) used multivariable statistical analysis in the Barnette shale play. They studied 64 horizontal wells in the Barnett shale play to correlate decline-curve parameters to completion and stimulation parameters such as perforated interval, fluid volume,

proppant mass, and well spacing. The authors used well spacing and fluid volume per interval as variables to predict the ratio of cumulative production at 6 months to 1 month (CP6 to1). As shown in the paper, one of the limitations of the study is that it appears that multivariable coefficient terms are statistically biased. Bias may happen due to a missing important variable in the multivariable model or due to multicollinearity among variables. Additionally, correlation coefficients are low in the model. The authors did not attempt to perform economic analysis.

Companies often conduct A-vs.-B completion experiments in the field to learn the best completion strategy at that location. For example, Shell Canada (2012) studied A-vs.-B completion experiments on the performance of 74 wells in the Montney play with a common and consistent analytical framework. The study spanned five producing areas, two different completion styles (164 vs. 328 ft fracture spacing) and three different initial production strategies including unrestricted, moderately-restricted and highly-restricted flowing tubing pressure. These strategies might correlate to reservoir quality; that is, lower rock quality requires a higher pressure-drawdown to produce gas.

In another study, Wilson et al. (2011) studied A-vs.-B completion experiment by comparing cased-hole and open-hole completion technologies in the lower Montney formation on 15 wells. These wells are in two separate geographical areas within the same field. Comparisons of cased-hole and open-hole technologies included lateral lengths, number of stages, stage spacing, proppant volumes, pump rates, and operational time and cost per well. They concluded that open-hole wells produce hydrocarbons more efficiently. A-vs.-B completion experiments in the field may be applicable to the wells near an area of study; however, the weakness of the methodology is it can be misleading when there are many parameters with large variability.

The research gap in the oil and gas industry is lack of fast, efficient and reliable methodology to identify optimum completion design. Current numerical and field-experiment methodologies applied to find the optimum completion in heterogeneous unconventional plays are slow and inefficient.

1.2 Introduction to the Montney

The Montney gas play is a major shale-gas resource in the U.S. and Canada (Taylor 2009). It extends from British Columbia to Alberta in Canada (Fig. 1.2 and Fig. 1.3). The Triassic over-pressured Montney formation includes dry gas, liquid-rich gas, and oil. In 2013 the US National Energy Board (NEB) estimated that the Montney stretches over 1,640,000 ft in length and covers an area of 50,000 miles^2. The hydrocarbon thickness varies between 328 ft and 984 ft and is thickest along the western edge. Permeability is 20 to 80 times greater than other resource plays in North America and ranges from 1,000 to 100,000 nd. The resources in place are enormous, with a P50 estimate of 4,274 Tcf gas in place, and a P50 estimate of 268 billion bbl oil and natural gas liquids (NGL) in place (Reynolds 2015). Rokosh (2012) claimed the P50 estimate of the total marketable gas was 449 Tcf, and the P50 estimate of marketable oil and NGLs was 15.6 billion bbl in the Montney. Zinselmeyer (2015) pointed out that production volumes from the entire Montney (both Alberta and British Columbia) have increased to 3.9 Bcf/D and 62,000 bbl/D of NGL and oil as of November 2014.

Operators drill horizontal wells in three different zones of the Montney: upper, middle and lower. Approximately 3,500 wells have already been drilled in the Montney. The play is still early in development; however, enough horizontal wells have been drilled and sufficient data have been gathered to start optimizing completion practices.

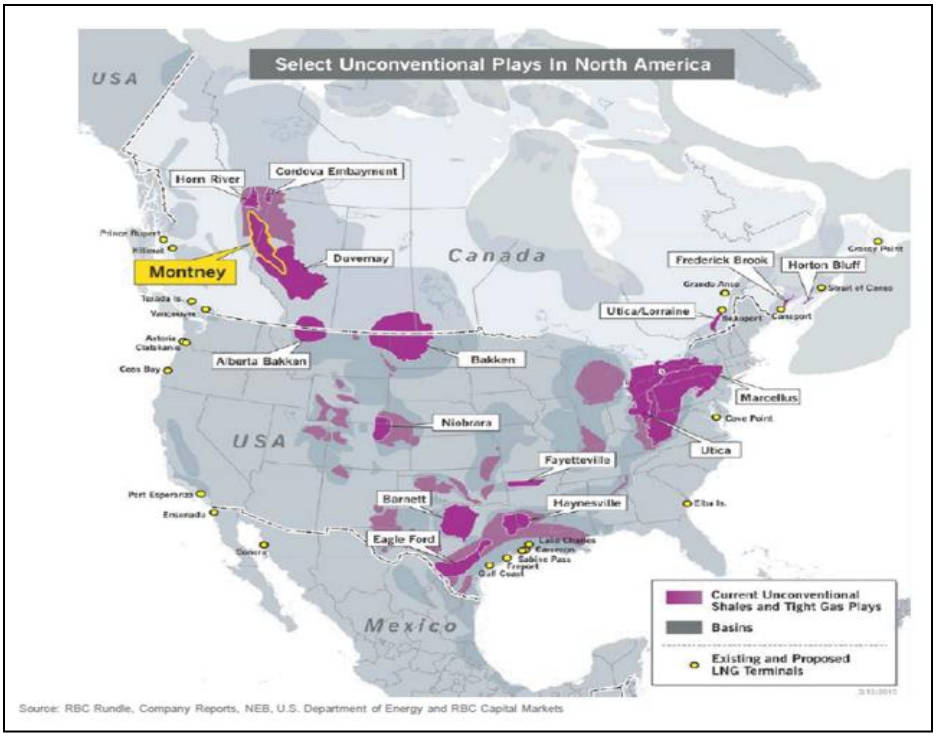

Fig. 1.2—Unconventional plays in North America (Crew Energy Inc. Corporation report 2016)

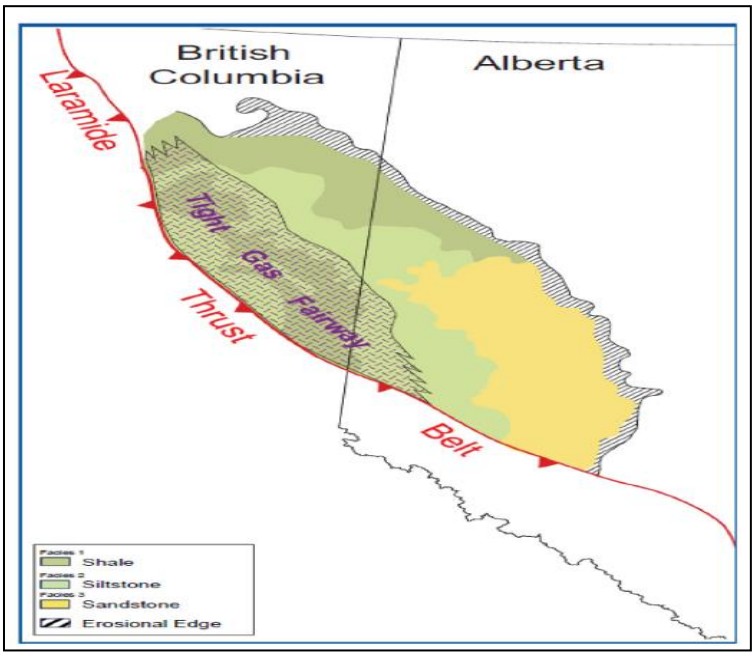

Fig. 1.3—Montney Play (Krause 1994)

1.3 Research Objectives

This research has two objectives. First, develop two different methodologies to determine the economic optimum completion in low-permeability complex heterogeneous horizontal wells that require hydraulic fracturing to flow at commercial rates, both within and beyond the current industry completion practices. Second, apply those methodologies to the Town field in the Montney formation in British Columbia, Canada.

1.4 Overview of Methodology

In this research, I applied the following methodology to 44 wells located in the Town field:

1) Regression method: I applied an integrated statistical methodology using multivariable regression to predict short-term well performance given specific completion design parameters. Then, I generated a type curve production forecast for the Town field. I scaled the type curve given a specific completion design using a scaling ratio. The scaling ratio was defined as a ratio of regressed short-term well performance to the production type curve short-term well performance.
2) Physic-based modeling method: I integrated available production and engineering data using a physics-based reservoir simulation model to estimate monthly gas production over a 40-year period.
3) I defined 300 different completion designs that consist of unique combinations of six values for lateral length, five values for sand intensity and 10 values for entry points. Then, I performed economic analysis on the 300 cases using both the regression and simulation production forecasts. Finally, I identified the completion design that yields the maximum ROR and PV10 as the optimum completion (Fig. 1.4).

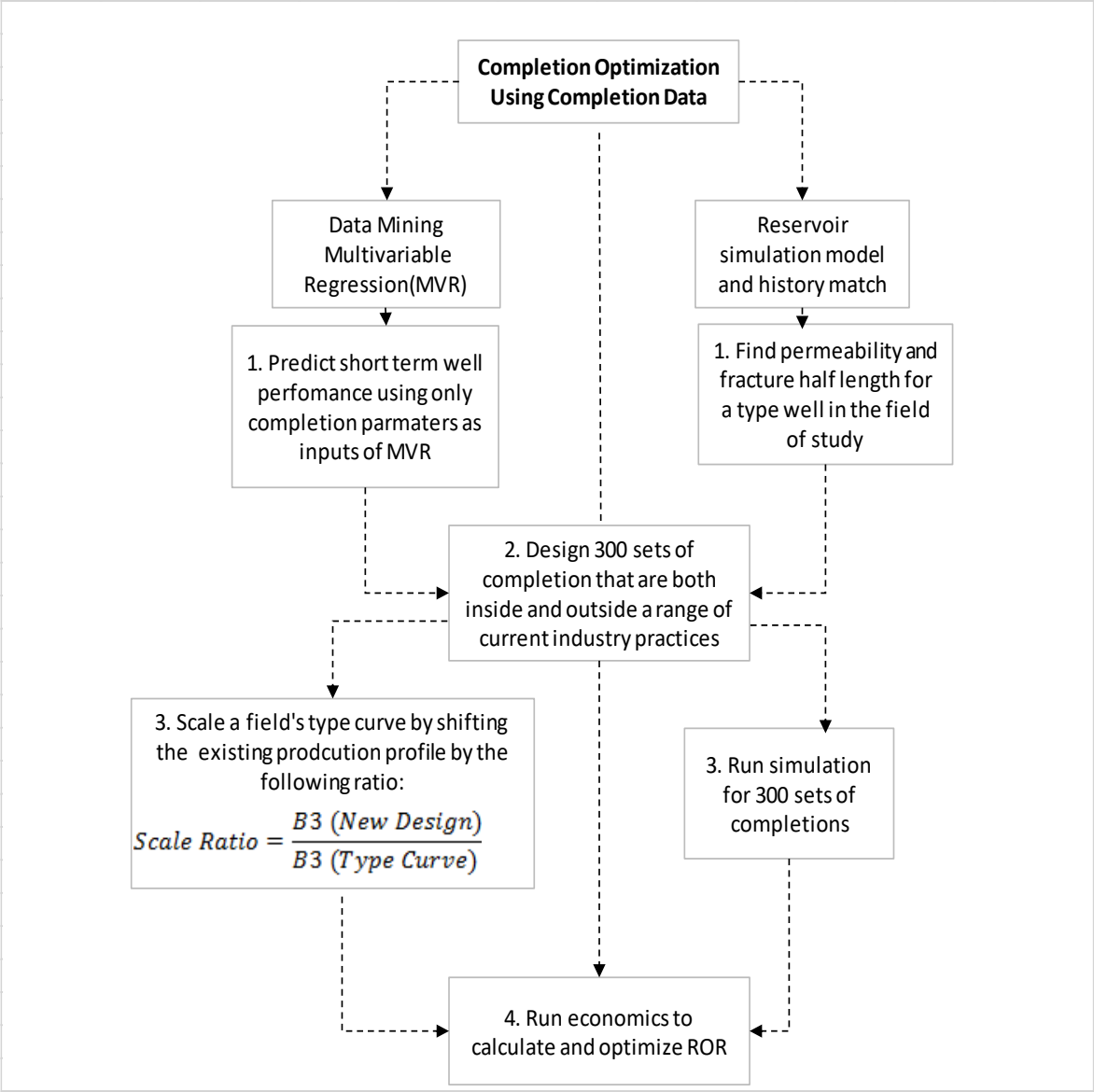

Fig. 1.4—Methodology

CHAPTER 2 SUMMARY OF 2,102 WELLS IN THE MONTNEY FORMATION, BRITISH COLUMBIA

In this chapter, I summarize statistics for 2,102 wells in the British Columbia Montney formation. The daily completion reports were sourced from a commercial data vendor (IHS Markit) that offers Canadian data. The 2,102 wells were not all the Montney wells in British Columbia at the time, but they were all the wells that existed in the IHS dataset at the time of gathering the dataset. I reviewed the daily completion reports on these 2,102 wells and built a dataset of 10 completion and geographical parameters for each well.

The five numerical parameters in the dataset are short-term well performance, sand, fluid, entry points, and lateral length. Five categorical parameters are zone, fluid type, first fracturing year, field name and completion type. The list of completion and geographical parameters and their explanations is shown below (Table 2.1).

Parameters (unit)	Abbreviation	Explanation
B3eq, Mcfed	B3	Best three consecutive months of production
Sand, lb	Sand	Amount of sand injected
Fluid, ft3	Fluid	Amount of fluid injected
Entry Points	EP	Number of entry points
Lateral Length, ft	LL	Completed lateral length
Fluid Type	-	10 Types of fluids are injected for fracturing
First Fracture Year	FirstFracYear	The starting year of fracturing
Field Name	UGRFieldName	32 Fields (a proxy of location)
Completion Type	-	Completion technology (open-hole, cased-hole)
Zone	-	Drilling zone (Middle, Upper, Lower)
True Vertical Depth	TVD	True vertical depth

Table 2.1—Summary of parameters in the 2,102 wells in the dataset in the Montney

The British Columbia (BC) Montney study area has two general areas, Northern Montney and Regional Heritage, which are the BC-government-assigned field names (Fig. 2.1). Since these government-assigned field names cover large geographic areas with varying geologic properties, I used 32 assigned field names provided by Unconventional Gas Resources LLC (UGR) to localize the analysis and reduce reservoir variability. The 32 fields and their well counts are shown in Fig. 2.2.

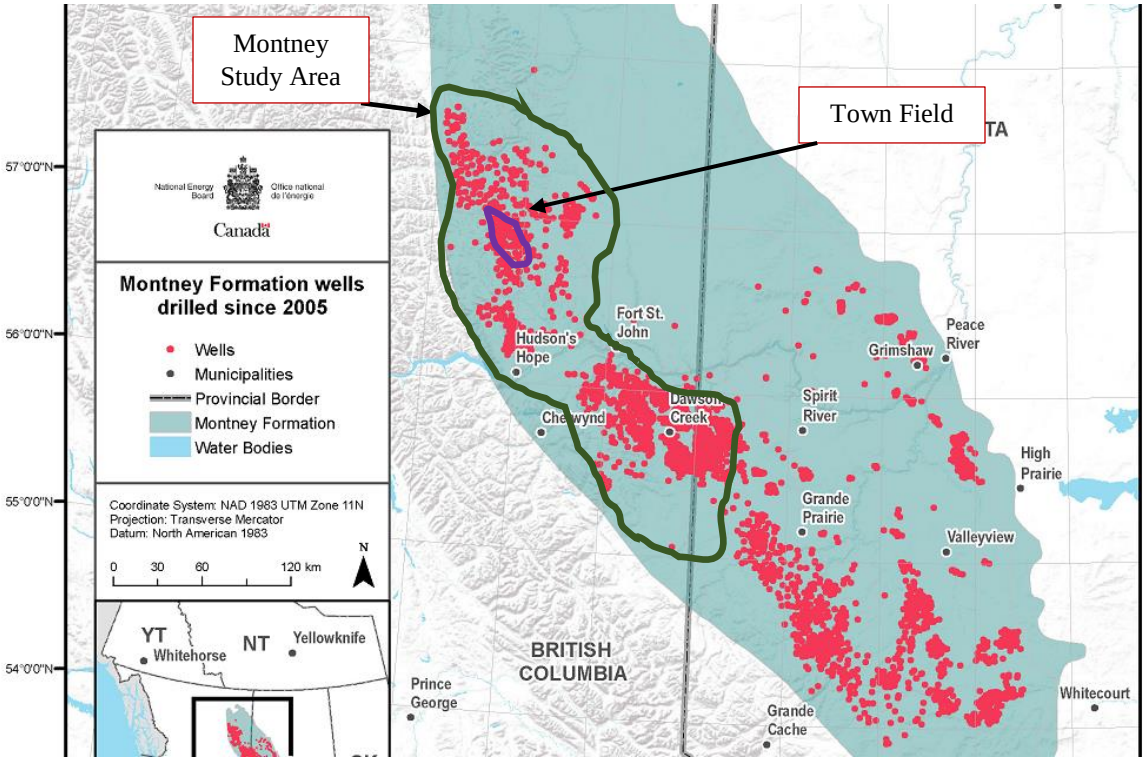

Fig. 2.1—Reference map of Montney (Hislop 2018)

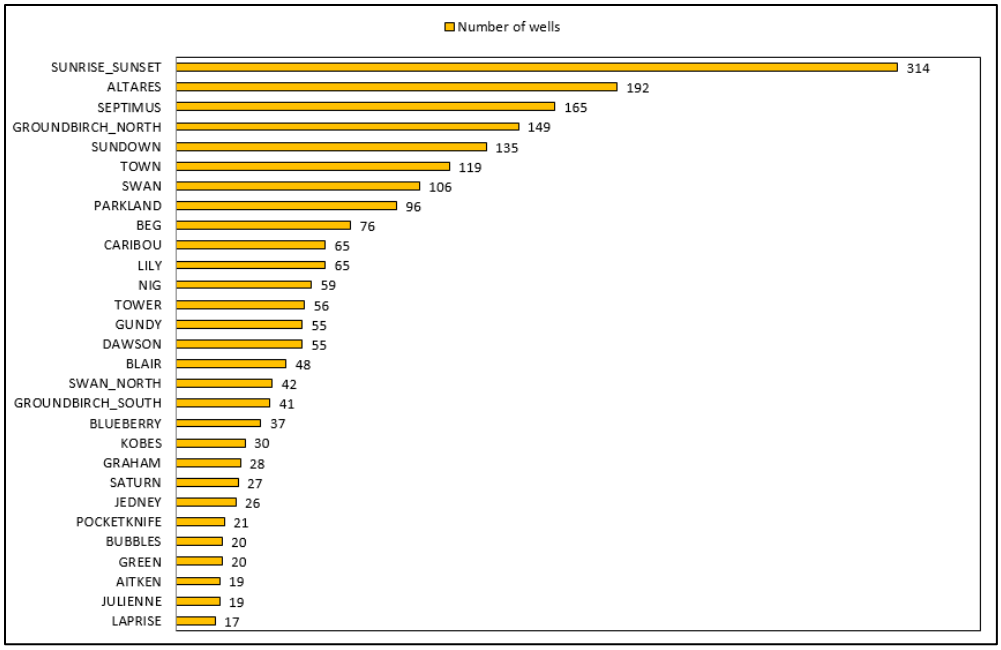

Fig. 2.2—List of 32 fields in the BC Montney and their well counts

The 2,102 wells located in the BC Montney dataset represent 23 operating companies, 32 fields, 3 zones, 10 different fracture-fluid types and two completion types. There is only one zone completed per well.

In this study, I reviewed the daily completion reports on 2,102 wells from the IHS database. Slickwater is the most popular fracturing fluid because it has been proved to be an effective fluid to increase recovery in the shale gas reservoir (Grieser 2003). Among 2,102 wells, 1,539 wells are treated with slickwater as a fracturing fluid. Furthermore, the upper zone of Montney BC contains more highly porous and permeable rock and is the preferred landing zone for operators (Sereda 2017). Among 2,102 wells, 1,291 wells are located in the upper zone. Therefore, I selected wells in the entire Montney BC that are in the upper zone and treated with slickwater as a fracturing fluid. This reduced the 2,102 wells in the dataset down to 1,040 wells. I used these 1,040 wells along with independent variables mentioned in Table 2.1 for multivariable analysis in Chapter 3.

Furthermore, in Chapter 4, reservoir properties are required to do reservoir simulation. Among all 32 fields in the BC Montney, Unconventional Gas Resources LLC operates in the Town field and there is more information available on reservoir properties (such as porosity, water saturation and initial reservoir pressure) in this field. As a result, I focused on 119 wells located in the Town field. All 119 wells in the Town field were fractured by slickwater fluid. Furthermore, to reduce the variability of rock properties and build a dataset of wells with similar geology, I considered only 44 wells located in the upper zone among these 119 wells. I also used these 44 wells in the Town field to perform multivariable regression in Chapter 3. In Fig. 2.3, the blue area with the red rectangle shows the Town field and different colored regions represent the 32 different fields.

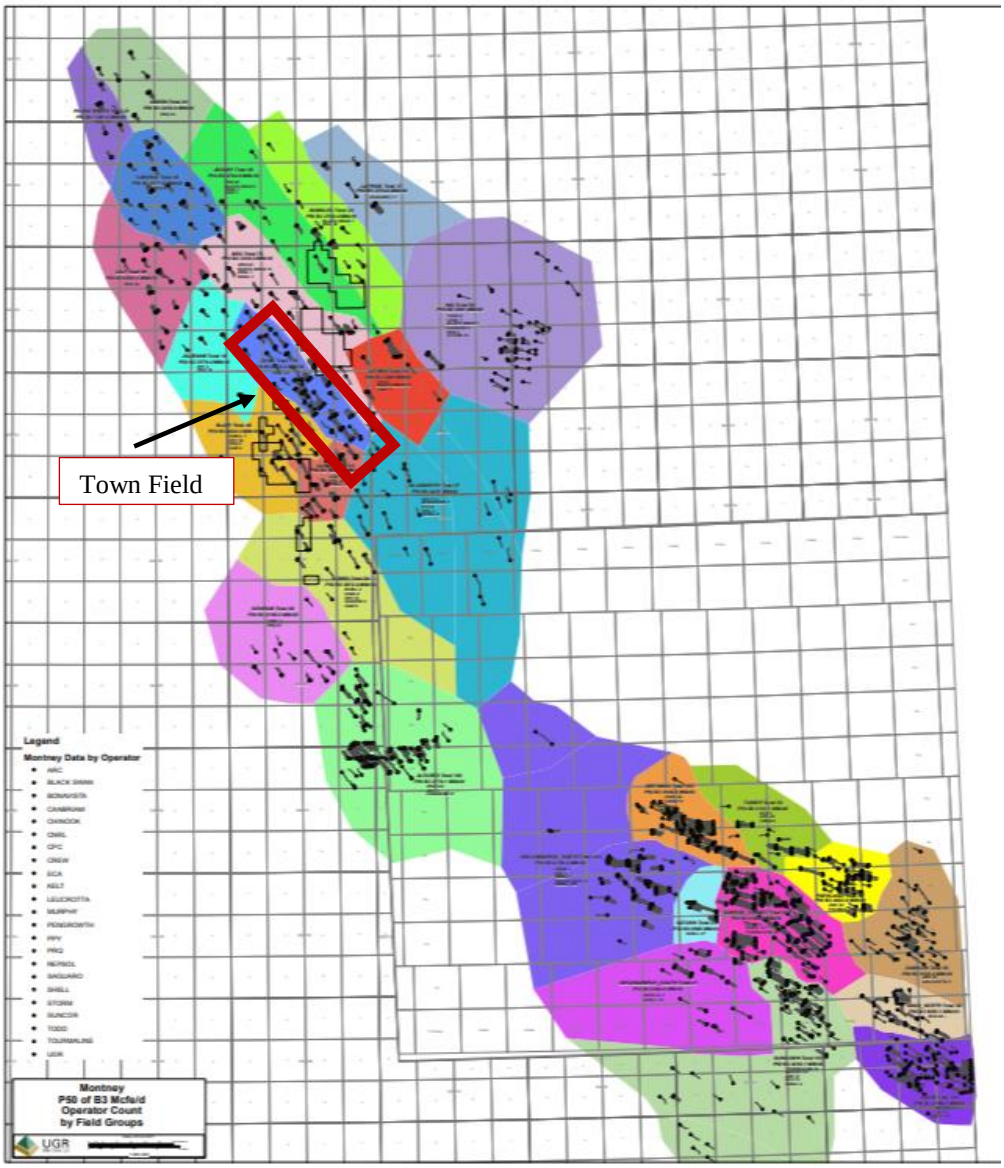

Fig. 2.3—Montney study area color coded by fields, the red rectangle in the map shows the Town field area (obtained from Unconventional Gas Resources LLC 2015)

CHAPTER 3 MULTIVARIABLE REGRESSION ANALYSIS

In this chapter, I developed several multivariable regression models for two different datasets. The first dataset consists of 44 wells in the Town field and the second dataset consists of 1,040 wells in the entire BC Montney. I used multivariable regression to estimate short-term production (B3) from completion and production parameters. In this chapter, I will first give a brief introduction of multivariable regression models, following with the application of multivariable regression for the Town well and BC Montney datasets. At the end of the chapter, I will acknowledge the limitations of data analytics.

3.1 Data Analytics

Data analytics is a field that utilizes statistics, mathematics and computer programming to extract knowledge from data. In the oil and gas industry over the past few decades, a massive amount of exploration, development and production data has been collected and stored on a daily basis. Oil and gas data analytics can help to improve decision making by considering only actual data instead of assumed models and by capturing trends, patterns, and relationships between data. The relationships are used to build algorithms which identify and optimize critical parameters in completion, production and other areas of the oil and gas industry. One of the most popular analytics tools available is multivariable regression. Predictive multivariable regression models bring helpful insights to unconventional resources where reservoir parameters can be highly variable.

3.2 Multivariable Regression

It is likely that more than one independent variable influences a response variable. Fitting predictive regression models to data with more than one independent variable is a common practice. Let $x_1, x_2 \ldots, x_p$ be p independent variables to be related to response variable y. The linear regression model for the ith sample is:

$$y_i = b_0 + b_1 x_{i1} + b_2 x_{i2} \ldots\ldots + b_p x_{ip} + e_i, \quad (1)$$

where e_i is a residual term and $b_i, i = 1, 2 \ldots, p$ are unknown and fixed regression coefficients. b_0 is the intercept and also unknown. The assumption of multivariable regression is that residuals are independent and normally distributed with mean equals zero. This assumption underlies the mathematical development of multivariable regression.

If we write Eq. 1 for a dataset with n records, we have:

$$y_1 = b_0 + b_1 x_{11} + b_2 x_{12} \ldots\ldots + b_p x_{1p} + e_1, \quad (2)$$

$$y_2 = b_0 + b_1 x_{21} + b_2 x_{22} \ldots\ldots + b_p x_{2p} + e_2, \quad (3)$$

.
.
.

$$y_n = b_0 + b_1 x_{n1} + b_2 x_{n2} \ldots\ldots + b_p x_{np} + e_n \quad (4)$$

A convenient way to write the above equations is in a matrix format where Y is a $(n \times 1)$ matrix of the response variable, X is a $n \times (p+1)$ matrix of independent variables, β is a $(p+1) \times 1$ vector of unknown regression coefficients and E is a $(n \times 1)$ vector of residuals. In this section, Y upper case is a matrix and y_i lower case (like the one in Eq. 1) is a sample. Also, X upper case is a matrix and $x_1, x_2 \ldots, x_p$ lower case (like the one in Eq. 1) are one set of sample.

$$Y = \begin{bmatrix} y_1 \\ y_2 \\ . \\ . \\ y_n \end{bmatrix}, X = \begin{bmatrix} 1 & x_{11} & . & . & x_{1p} \\ 1 & x_{21} & . & . & x_{2p} \\ . & . & . & . & . \\ . & . & . & . & . \\ 1 & x_{n1} & . & . & x_{np} \end{bmatrix}, \beta = \begin{bmatrix} b_0 \\ b_1 \\ . \\ . \\ b_p \end{bmatrix}, \quad E = \begin{bmatrix} e_1 \\ e_2 \\ . \\ . \\ e_n \end{bmatrix}$$

Using the above matrices and vectors, we can write Eq. 2 to Eq. 4 in a matrix format:

$$Y = X\beta + E \tag{5}$$

To estimate the unknown values of the vector β, we minimize the sum of squared residuals.

$$Residual\ sum\ of\ the\ squared\ (RSS) = \sum_{i=1}^{n} e_i^2 \tag{6}$$

The inner product of a vector and its transpose is equal to the sum of squares of the vector's components:

$$E' \cdot E = [e_1, e_2, \ldots, e_n] \cdot \begin{bmatrix} e_1 \\ e_2 \\ . \\ . \\ e_n \end{bmatrix} = e_1^2 + e_2^2 + \ldots + e_n^2 = \sum_{i=1}^{n} e_i^2, \tag{7}$$

where apostrophe in E' used as a symbol for transposed vector *E*. Therefore, Eq. 6 equals:

$$\sum_{i=1}^{n} e_i^2 = E' \cdot E \tag{8}$$

From Eq. 5, the residual term can be written as:

$$E = Y - X\beta \tag{9}$$

Below are mathematical statements for transposed matrices that I use to continue the analysis:

$$(c - d)' = c' - d'$$

$$(cd)' = d'c'$$

By using above mathematical statements and combining Eq. 8 and Eq. 9:

$$Residual\ sum\ of\ the\ squared\ (RSS) = \sum_{i=1}^{n} e_i^2 = E' \cdot E\ = \tag{10}$$

$$(Y - X\beta)' \cdot (Y - X\beta) = (Y' - (X\beta)') \cdot (Y - X\beta) = (Y' - \beta' X') \cdot (Y - X\beta)$$

$$= Y'Y - Y'X\beta - \beta'X'Y + \beta'X'X\beta$$

Since $\beta'X'Y$ is a scalar, meaning dimension of 1×1, the transpose of the term is the same term, thus:

$$\beta'X'Y = (\beta'X'Y)' = Y'X\beta \tag{11}$$

Therefore, by using Eq. 11, Eq. 10 can be written as:

$$Residual\ sum\ of\ the\ squared\ (RSS) = \sum_{i=1}^{n} e_i^2 = E' \cdot E\ = (Y - X\beta)' \cdot (Y - X\beta) =$$

$$(Y' - (X\beta)') \cdot (Y - X\beta) = (Y' - \beta' X') \cdot (Y - X\beta) \tag{12}$$

$$= Y'Y - Y'X\beta - \beta'X'Y + \beta'X'X\beta = Y'Y - 2\beta'X'Y + \beta'X'X\beta$$

To minimize Eq. 12 and calculate the unknown values of vector β, we take the derivative of *RSS* with respect to β and set to zero. To do this, we use the following mathematical statements:

$$\frac{\partial \beta' X' Y}{\partial \beta} = X'Y$$

$$\frac{\partial \beta' X' X \beta}{\partial \beta} = 2X'X\beta$$

More information about the above mathematical statements can be found in The Matrix CookBook (Petersen and Pedersen 2012). By applying above statements, the derivation of Eq. 12 is:

$$\frac{\partial RSS}{\partial \beta} = -2X'Y + 2X'X\beta = 0 \quad (13)$$

Eq. 13 can be written as:

$$X'X\beta = X'Y \quad (14)$$

If we assume that the inverse of the matrix ($X'X$) exists, vector β is:

$$\beta = (X'X)^{-1}(X'Y) \quad (15)$$

Values of vector β are the regression coefficients in Eq. 2 to Eq. 4.

3.3 Case Study: Multivariable Regression Models in the Town Field

In this section, I applied a multivariable regression model to the 44 wells in the Town field. In a large heterogeneous geographical area, there is likely a lot of variation in rock properties. In this study, there is no information available on rock properties (e.g., permeability, porosity). Therefore, to reduce the impact of the missing information on multivariable regression models, I built a geologically similar dataset to perform multivariable regression analysis. To build a geologically similar dataset, I selected the Town field among 32 fields in the Montney since Unconventional Gas Resources LLC operates in the field. As discussed earlier in Chapter 2, there are 119 wells in the Town field located in three different zones. The zones are geologically different according to Unconventional Gas Resources LLC. Therefore, I selected 44 wells located in the upper zone of the Town field. Slickwater is the most popular fracturing fluid, and all the 44 wells in the Town field well were treated with slickwater.

I applied multivariable regression to these 44 wells to predict B3 from completion inputs (i.e., lateral length, mass of sand, volume of injected fluid, entry points) in five different models. The only completion type in the dataset is cemented completion and the only fracturing fluid is slickwater. Furthermore, all the 44 wells are landed in the upper zone and have similar true vertical depth. Therefore, the parameters completion type, fracture fluid, true vertical depth, zone and field name mentioned in Table 2.1 are not independent variables in these models. The five predictive models with inputs and output are listed in Table 3.1.

Model	Inputs	Output, unit
Total completion parameters	Sand tonnes, Lateral length m, Fluid m^3, Entry points	B3, Mcfed
Per lateral length	Sand per lateral length tonnes/m, Fluid per lateral length m^3/m, Entry points per lateral length 1/m	B3 per lateral length, Mcfed/m
Per fluid	Sand per fluid tonnes/m^3, Lateral length per fluid m/m^3, Entry points per fluid 1/m^3	B3 per fluid, Mcfed/m^3
Per sand	Fluid per sand m^3/tonnes, Lateral length per sand m/tonnes, Entry points per sand 1/tonnes	B3 per sand, Mcfed/tonnes
Per entry points	Fluid per entry points m^3, Lateral length per entry points m, Sand per entry points tonnes	B3 per entry points, Mcfed

Table 3.1—Multivariable regression model inputs and outputs for the Town field dataset

Table 3.2 shows the multivariable regression models for the 44 wells located in the Town field. I will discuss how I developed the per-fluid model for the 44-well Town field in detail in the next section. The rest of the models are developed similarly.

Total completion parameters	$(B3)^{(0.65)} = -21797.3 * Sand^{-0.75} + 6885 * LL^{-0.60} - 3.1 * EP^{0.54} + 11984 * Fluid^{-0.69} + 199.42$
Per lateral length	$(B3.LL)^{(0.72)} = -1.04 * Sand.LL^{-1.06} + 1.8 * Fluid.\ LL^{-0.95} - 3.5 * EP.LL^{0.75} + 2.7$
Per fluid	$(B3.Fluid)^{(1.1)} = 2.8 * Sand.Fluid^{1.38} + 0.81 * LL.Fluid^{0.33} + 0.11 * EP.Fluid^{0.33} - 0.28$
Per sand	$(B3.Sand)^{(0.85)} = 10.1 * Fluid.Sand^{-1.9} + 0.53 * LL.Sand^{0.98} - 0.26 * EP.Sand^{0.39} + 1.2$
Per entry points	$(B3.EP)^{(0.33)} = -0.9 * Fluid.EP^{0.18} - 14.9 * LL.EP^{-0.33} + 39.1 * Sand.EP^{0.03} - 32.6$

Table 3.2—Multivariable regression models of 44 wells for the Town field dataset

3.3.1 Per Fluid Multivariable Regression in the Town Field

To build the multivariable regression model, first I normalized lateral length, entry points, amount of sand and B3 by the amount of fluid injected. After preparing the dataset, the following six steps were taken:

1. Correlation plots
2. Variable selection
3. Transformation
4. Homoscedasticity
5. Multicollinearity
6. Residuals

I will discuss these steps in detail in the following subsections.

3.3.1.1 Correlation Plots

Correlation plots display relations between pairs of variables as well as the histograms for normalized variables. The independent variables in the dataset are B3 per fluid, sand per fluid, entry point per fluid, and lateral length per fluid. The R^2 values of 2-D plots are in the upper triangular part of the correlation plot in Fig. 3.1. The diagonal elements of the matrix are the histograms for the variables.

Each variable in the dataset has one row and column in the matrix. For example, B3 per fluid is on the first row and column; sand per fluid, lb/ft^3 is on the second row and column. Therefore, row 2 and column 1 is the 2-D plot of B3 per fluid vs. sand per fluid (the plot with the green star). The flipped element on the upper side of the triangular matrix shows an R^2 of 0.44 between B3 per fluid and sand per fluid. The size of R^2 numbers on the upper triangular part of the matrix represents the magnitude of correlation. Pairs with higher correlation have a larger text size R^2 in Fig. 3.1. The objective of 2-D plots is to identify correlated variables that can be used in further steps of multivariable regression. If the magnitude of correlation between two independent variables is more than 0.8, the two independent variables are highly correlated and both of them carry the same information on the response variable. Therefore, those independent variables should be investigated and one of them should be dropped. As shown in Fig. 3.1, there are not any pairs of independent variables that have R^2 more than 0.8.

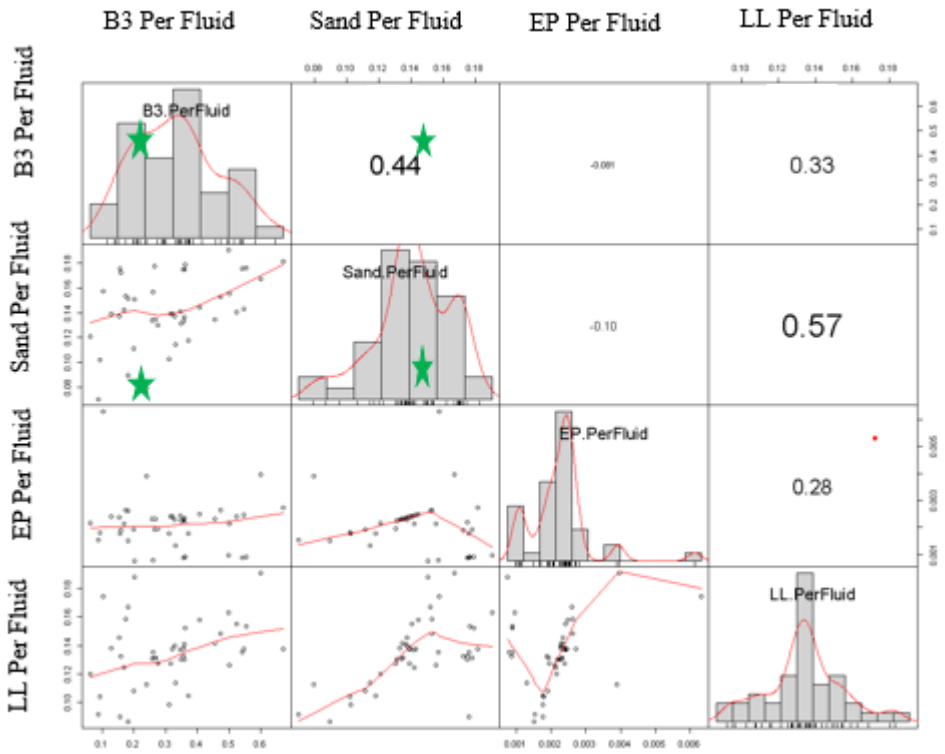

Fig. 3.1—Pairwise 2-D plots and histograms, Upper Montney, per fluid model

3.3.1.2 Variable Selection

For this part, I used a backward procedure to select the most important variables in the model. The backward procedure starts with all independent variables in the model and removes the independent variable with highest p-value that is greater than a critical p-value of 0.05. Then the model is refitted with the remaining independent variables and the variable that has highest p-value more than critical p-value of 0.05 will be dropped again. The algorithm stops when all p-values are less than the critical p-value. The result of backward selection shows that all independent variables in the per-fluid model are important and should be in the model. Refer to

A Modern Approach to Regression with R (Sheather 2009) for more information about variable selection.

3.3.1.3 Transformations

Multivariable linear regression assumes independent variables have normal distributions. Non- normal distributions can distort relationships. Therefore, the first step in the analysis is to look at the initial distribution of numerical input variables and find transformations that make them normal. Fig. 3.2 shows the initial distribution for numerical independent variables in this model, which are sand per fluid, entry points per fluid, and lateral length per fluid. These distributions are not normal.

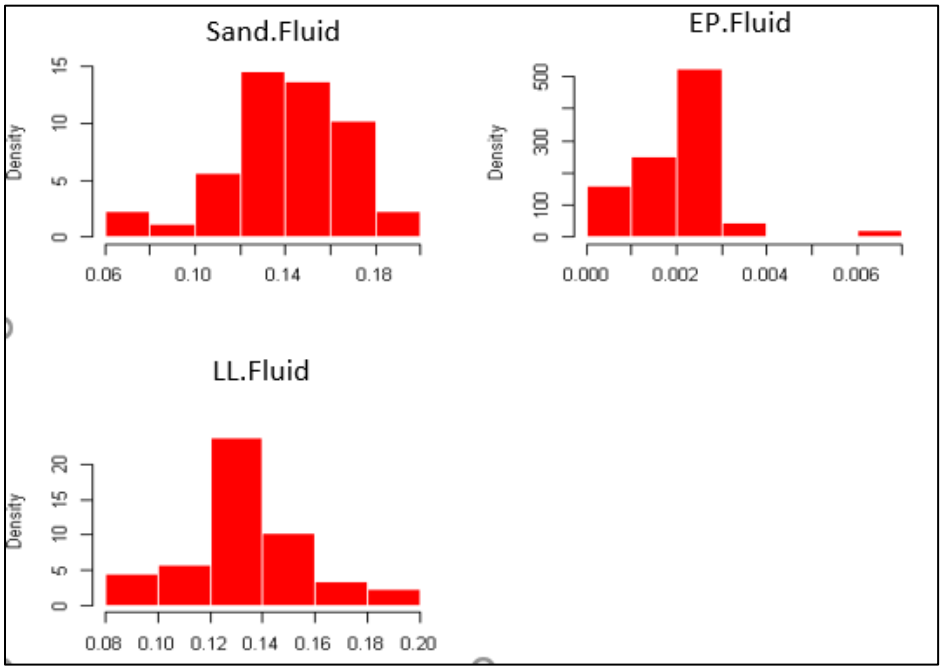

Fig. 3.2—Histograms of initial variables

Box-Cox transformation is a way to transform non-normal distributions. The technique was developed by statisticians George Box and Sir David Roxbee Cox and named after them.

Box-Cox transformation defines a set of exponents called lambda (λ), one for each independent variable, which vary from -5 to 5. A λ equal to zero is a log transformation. All values of λ are considered and the optimal values for different independent variables in the dataset are selected based on linearity and normality of all of independent variables. Therefore, the optimal values for different independent variables are a set of numbers which results in the best approximation of multidimensional normal distribution curve. Refer to A Modern Approach to Regression with R (Sheather 2009) for more information about Box-Cox transformation. Table 3.3 shows the transformations of the numerical variables using Box-Cox. For example, the optimum set of values for sand per fluid, entry point per fluid and lateral length per fluid to be transformed to multidimensional normal distributions are 1.38, 0.33 and 0.33.

Sand Per Fluid	Entry point Per Fluid	Lateral Length Per Fluid
1.38	0.33	0.33

Table 3.3—Transformation of variables

The equation for the multivariable model with transformed inputs is:

$$B3.Fluid = 2.8 * Sand.Fluid^{1.38} + 0.81 * LL.Fluid^{0.33} + 0.11 * EP.Fluid^{0.33} - 0.28 \quad (16)$$

Fig. 3.3 shows histograms of transformed numerical independent variables. These distributions do not appear to be close to normal because they consist of only 44 data points, and the optimization was done by matching the multidimensional normal distribution curve, not the individual distributions.

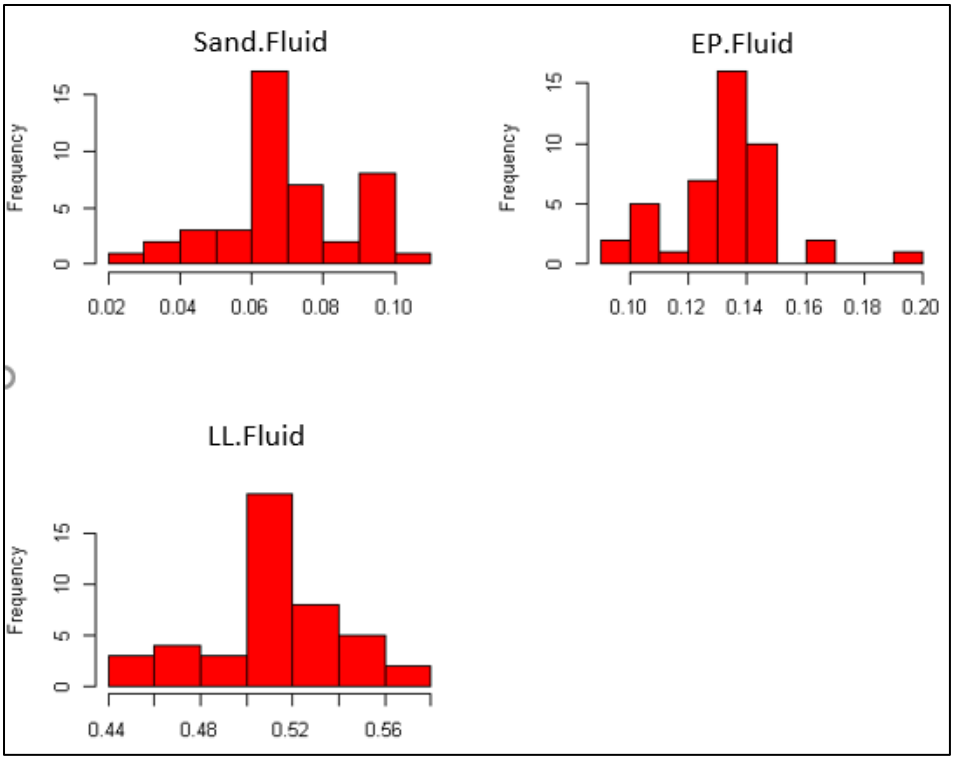

Fig. 3.3—Histograms of transformed variables

3.3.1.4 Homoscedasticity

Homoscedasticity means equal scatter. One of the assumptions of multivariable analysis is equal scatter of residuals over the range of fitted values (homoscedasticity of residuals). Homoscedasticity is important because multivariable regression assumes that all residuals are drawn from a population that has a constant variance.

After transforming the independent variables in the previous subsection, the response variable (B3) should be transformed to achieve linearity and homoscedasticity (constant variance of residuals). To define the transformation for the output (B3 per fluid), I used the Box-Cox technique on the results of the multivariable model. I regressed B3 per fluid as the output

variable on transformed lateral length, sand, and entry points. The calculated transformation for B3 per fluid is 1.1. Therefore, the final linear model is the following:

$$(B3.Fluid)^{(1.1)} = 2.8 * Sand.Fluid^{1.38} + 0.81 * LL.Fluid^{0.33} + 0.11 * EP.Fluid^{0.33} - 0.28 \quad (17)$$

Eq. 17 is the final multivariable model to predict B3 per fluid.

To check the assumption as a next step, I looked at the plot of standardized residual vs. fitted values (Fig. 3.4). The fitted values of B3 per fluid are on the x-axis; the square root of the standardized residual is on the y-axis. Below is the formula to calculate standardized residual:

$$Standardized\ Residual\ i = \frac{Residual\ i}{Standard\ Deviation\ of\ Residual\ i} \quad (18)$$

In Fig. 3.4 the spread of residuals does not have any pattern. In the case of heteroscedasticity (unequal scatter), the spread of the residuals increases in one direction or forms a cone shape. Therefore the per fluid model satisfies the homoscedasticity assumption.

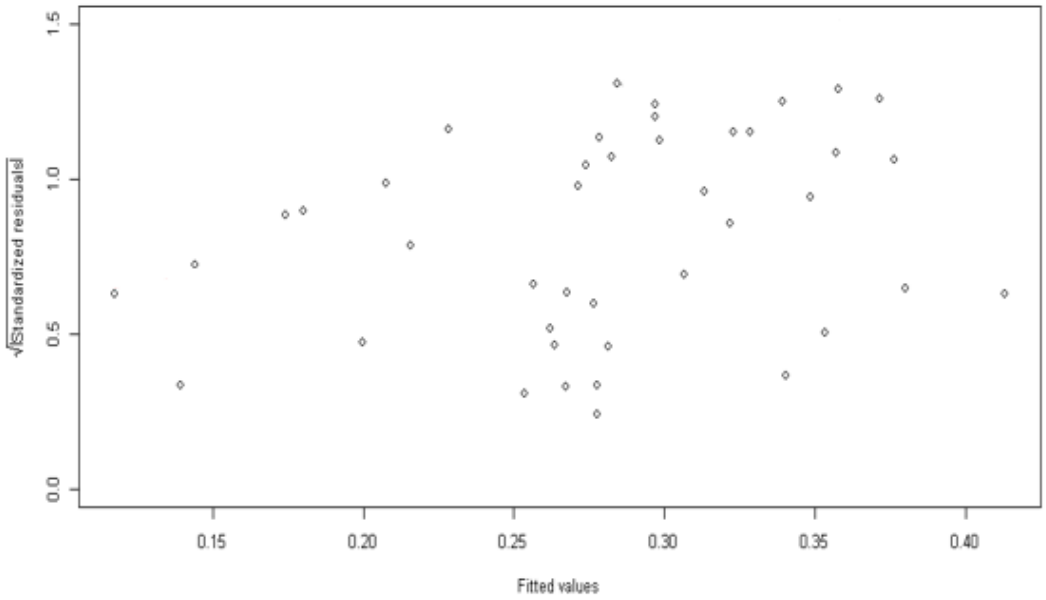

Fig. 3.4—Scale location plot, homoscedasticity

3.3.1.5 Multicollinearity

Multicollinearity occurs when two or more independent variables in a regression model are correlated strongly or moderately. Multivariable linear regression assumes that there is little or no multicollinearity in the data. The interpretation of a regression coefficient is that it represents the mean change in the response variable for each unit change in an independent variable when all of the other independent variables hold constant. Therefore, changing the value of one independent variable should not affect other independent variables. However, when independent variables are correlated, it indicates that changes in one independent variable cause the other correlated variable to change. Therefore, when multicollinearity exists, the estimated regression coefficients are not precise. It also makes it difficult to assess the relative importance

of independent variables in explaining the variation of an output variable. To detect multicollinearity, the Variance Inflation Factor (VIF) is used. The equation for VIF is as follows:

$$VIF_k = \frac{1}{1-R_k^2} \tag{19}$$

where R_k^2 is the R^2 obtained by regressing the K^{th} independent variable on the remaining independent variables.

A VIF of less than 10 indicates there is no multicollinearity. Table 3.4 shows the VIF of independent variables in the model. All the values in the table are less than 10, which indicates there is no multicollinearity among independent variables.

Total Sand Per Fluid	Entry Points Per Fluid	Lateral Length Per Fluid
1.7	1.2	1.7

Table 3.4—VIF of the independent variables, per fluid model

3.3.1.6 Normality of Residuals

Residuals are the differences between the fitted values from regression and actual values of B3 per fluid. Multivariable linear regression assumes that residuals are normally distributed. Satisfaction of this assumption allows generation of a reliable confidence interval. A Q-Q plot of residuals and histogram of residuals can help to assess whether the residuals are approximately normally distributed. If the residuals follow the dash line on the Q-Q plot, they are normally distributed.

Fig. 3.5 is a diagnostic Q-Q plot of standardized residuals. In the Q-Q plot, the data points follow the dash line, which indicates that residuals have an approximate normal distribution. The histogram of residuals in Fig. 3.6 is approximately normal, which satisfies the assumption of normality for the residuals.

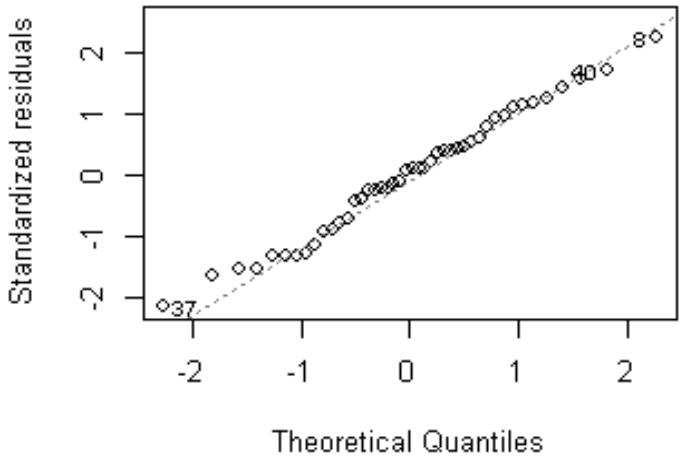

Fig. 3.5 —Q-Q plot of residuals

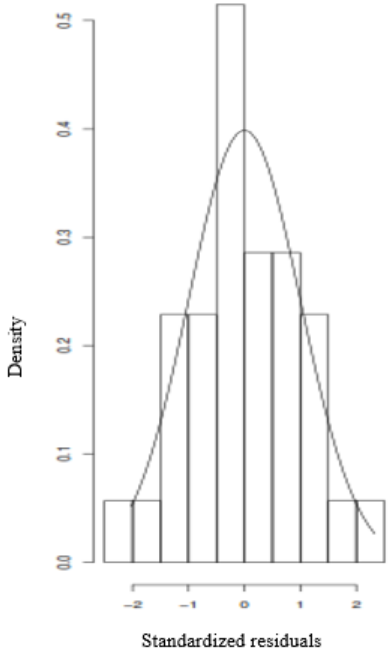

Fig. 3.6—Histogram of residuals for per fluid model in the Town field

Fig. 3.7 is a 2-D graph of predicted B3 per fluid on the y-axis and actual B3 per fluid of 44 wells in the Town field on the x-axis. There are two lines in the figure: unit-slope line (red line) and the regression line for predicted vs. actual B3 per fluid values (blue line). The R^2 of

predicted values vs. actual values is 0.20, which is small compared to the maximum possible value of 1. R^2 of a regression line for predicted vs. actual values represents the predictive power of a model. As R^2 increases, the scatter around the regression line decreases. Slope of a regression line for predicted vs. actual values represents how well a model can predict the entire range of the response variable, especially the extremes. The slope is different between the unit-slope line with R^2 of 1 and the regression line for predicted vs. actual B3 per fluid values in Fig. 3.7, which indicates there is uncertainty in the model due to missing information in the dataset. The missing information includes unavailable data such as rock properties (e.g., permeability, porosity). Including rock properties information in the dataset should result in a more accurate model, in which case the slope of the blue line would be closer to that of the unit-slope line.

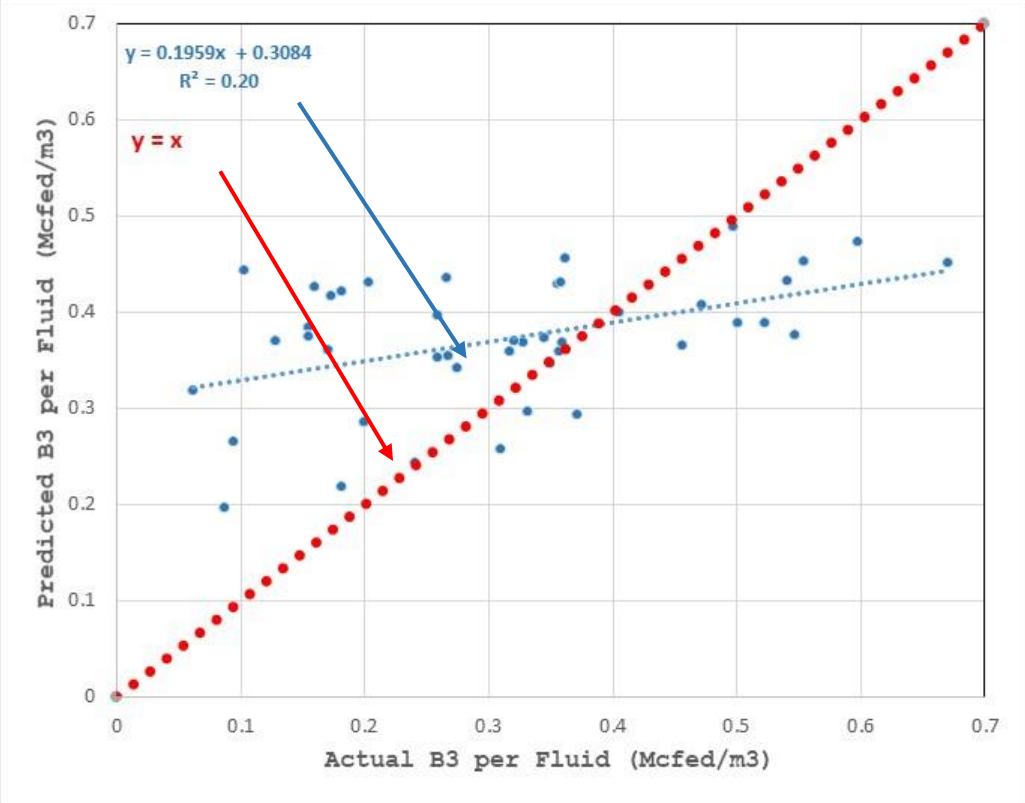

Fig. 3.7—2-D regression line of predicted vs. actual B3 per fluid, Mcfed/ft3 values for 44 wells in the Town field

3.3.2 Selection of the Best Model in the Town field

In the previous section, I explained the details of the per-fluid model for 44 wells in the Town field. I developed four other models in the Town field (Table 3.2)

To choose the best model I initially used the Akaike Information Criterion (AIC) and Bayesian Information Criterion (BIC). AIC is an estimate of relative information lost in the trade-off between model fit and complexity. A lower AIC is preferred and considered more likely to be the true model. BIC is another criterion for model selection. When fitting models, it is possible to increase the likelihood by adding parameters but doing so may lead to overfitting. The BIC penalizes the problem by adding a logarithmic term for the number of parameters in the model. Similarly, a model with lower BIC is preferred (Sheather 2009).

The R^2 shown in Table 3.5 is the 2-D R-squares of predicted vs. observed values. The per-fluid model has the lowest AIC and BIC among the five models, although it does not have the highest R^2 (Table 3.5). Therefore, based on my original criteria (AIC and BIC), I selected the per fluid model as the best model among all five models. Later, I learned that AIC and BIC criteria for selecting the best model can only be used when the dependent variable is the same in the different models. In these five models with five different dependent variables, R^2 should have been used to select the best model. Therefore, in retrospect, the per-entry point model is likely the best model among all five models because it has the highest R^2. However, I used the per-fluid model for the Town field in the remainder of this study. For future work it is recommended to use the per-entry point model if this analysis was to be repeated.

Model	R^2	AIC	BIC
Total completion parameters	0.05	490	501
Per lateral length	0.03	83	92
Per fluid	0.20	-43	-32
Per sand	0.06	102	111
Per entry points	0.58	113	122

Table 3.5—Comparison of the models of 44 wells in the Town dataset

3.4 Case Study: Entire BC Montney Shale-Well Dataset

In this section, I applied multivariable regression model on the 1,040 wells in the entire BC Montney. These 1,040 wells are located in the upper zone and treated with slickwater fluid, as discussed earlier in Chapter 2. I predicted B3, which is the first three consecutive months of production, from completion and production inputs, i.e., sand, fluid, entry points, lateral length, fluid type, first fracture year, field name, completion type, zone and true vertical depth. I developed five predictive models using the independent variables in Table 2.1. However, since all wells in this dataset are treated with slickwater and are in the upper zone, fluid type and zone variables in Table 2.1 are not included in the models. The independent variables and response variable for each model are in Table 3.6.

Model	Inputs	Output
Total completion parameters	Sand tonnes, Lateral length m, Fluid m3, Entry points, True vertical depth m, Completion type, Field name, First fracturing year	B3, Mcfed
Per lateral length	Sand per lateral length tonnes/m, Fluid per lateral length m3/m, Entry points per lateral length 1/m, True vertical depth m, Completion type, Field name, First fracturing year	B3 per lateral length, Mcfed/m
Per fluid	Sand per fluid tonnes/m3, Lateral length per fluid m/m3, Entry points per fluid 1/m3, True vertical depth m, Completion type, Field name, First fracturing year	B3 per fluid, Mcfed/m3
Per sand	Fluid per sand m3/tonnes, Lateral length per sand m/tonnes, Entry points per sand 1/tonnes, True vertical depth m, Completion type, Field name, First fracturing year	B3 per sand, Mcfed/tonnes
Per entry points	Fluid per entry points m3, Lateral length per entry points m, Sand per entry points tonnes, True vertical depth m, Completion type, Field name, First fracturing year	B3 per entry points, Mcfed

Table 3.6—Multivariable regression model inputs and outputs in the entire Montney BC dataset

Table 3.7 shows five multivariable regression models with their coefficients and intercepts. The independent variables in the first model includes total lateral length, volume of fluid, mass of sand, and number of entry points. In the rest of models, the quantitative independent variables models have been normalized based on lateral length, volume of fluid, mass of sand, and number of entry points, respectively. For example, in the per-lateral-length model, volume of fluid, mass of sand, and number of entry points have been divided by total lateral length.

Total completion parameters	$(B3)^{(0.25)} = -17.4 * Sand^{-0.06} + 0.028 * LL^{0.53} - 6.5 * 10^{-4} * Fluid^{0.52} + 1.12 * EP^{0.13} + 119.7 * TVD^{-0.35} + Completion\,Type + UGRFieldName - 0.062 * FirstFracYear + 131.2$
Per lateral length	$(B3.LL)^{(0.31)} = -0.72 * Sand.LL^{-0.19} + 0.007 * Fluid.LL^{0.53} + 0.51 * EP.LL^{0.22} + 30.1 * TVD^{-0.38} + Completion\,Type + UGRFieldName - 0.016 * FirstFracYear + 33.8$
Per fluid	$(B3.Fluid)^{(0.15)} = -0.07 * Sand.Fuid^{-0.37} + 4.22 * LL.Fluid^{0.0035} - 0.61 * EP.Fluid^{-0.108} + 4.17 * TVD^{-0.149} + Completion\,Type + UGRFieldName - 0.006 * FirstFracYear + 8.56$
Per sand	$(B3.Sand)^{(0.34)} = 0.01 * Fluid.Sand^{0.75} + 0.55 * LL.Sand^{0.17} + 1.21 * EP.Sand^{0.18} + 15.48 * TVD^{-0.16} + Completion\,Type + UGRFieldName - 0.02 * FirstFracYear + 42.1$
Per entry points	$(B3.EP)^{(0.1863)} = 0.017 * Fluid.EP^{0.2784} - 3.36 * LL.EP^{-0.1032} - 4.28 * Sand.EP^{-0.0478} - 0.00037 * TVD + Completion\,Type + UGRFieldName - 0.024 * FirstFracYear + 56.9$

Table 3.7—Multivariable regression models for the entire Montney BC dataset

Among the predictive models in Table 3.7, the per-fluid model is likely the best model for the dataset of 1,040 wells in the Montney BC because it has the highest R^2 among the models (Table 3.8). The R^2 shown in Table 3.8 is the 2-D R-squares of predicted vs. observed values.

Model	R^2
Total completion parameters	0.32
Per lateral length	0.33
Per fluid	0.78
Per sand	0.37
Per entry points	0.58

Table 3.8—Comparison of the models of 1,040 wells in the entire Montney BC

Fig. 3.8 is a 2-D graph of predicted B3 per fluid on the y-axis and actual B3 per fluid of 1,040 wells in the entire BC Montney on the x-axis. The R^2 of predicted values vs. actual values for the per-fluid model of 1,040 wells is 0.78, which is relatively close to the maximum R^2 value of 1. As mentioned earlier, R^2 of a regression line for predicted vs. actual values represents the predictive power of a model. Slope of a regression line for predicted vs. actual values represents how well a model can predict the entire range of the response variable, especially the extremes. In the previous section, the per-fluid model for the 44 wells in the Town field has R^2 of 0.20. The R^2 of the per-fluid model for 1,040 wells in the Montney (0.78) is greater than the R^2 of the per-fluid model of 44 wells in the Town field (0.20). The slope of the regression line for predicted vs. actual B3 per-fluid values (blue line) is also closer to 1 than the 44-well Town-Field model. The full-dataset model (1,040 wells) is better than the reduced-dataset model (44 wells) likely because there is more data available in the full-dataset model. However, as shown in Fig. 3.8, the slope of the regression line for predicted vs. actual B3 per fluid values (blue line) is still less than 1. Therefore, there is still uncertainty remaining in the model due to missing information. The missing information is most likely unavailable data such as rock properties (e.g., permeability,

porosity). Including rock properties information in the dataset should result in a more accurate model, in which case the blue line would likely be closer to the unit-slope line (red line).

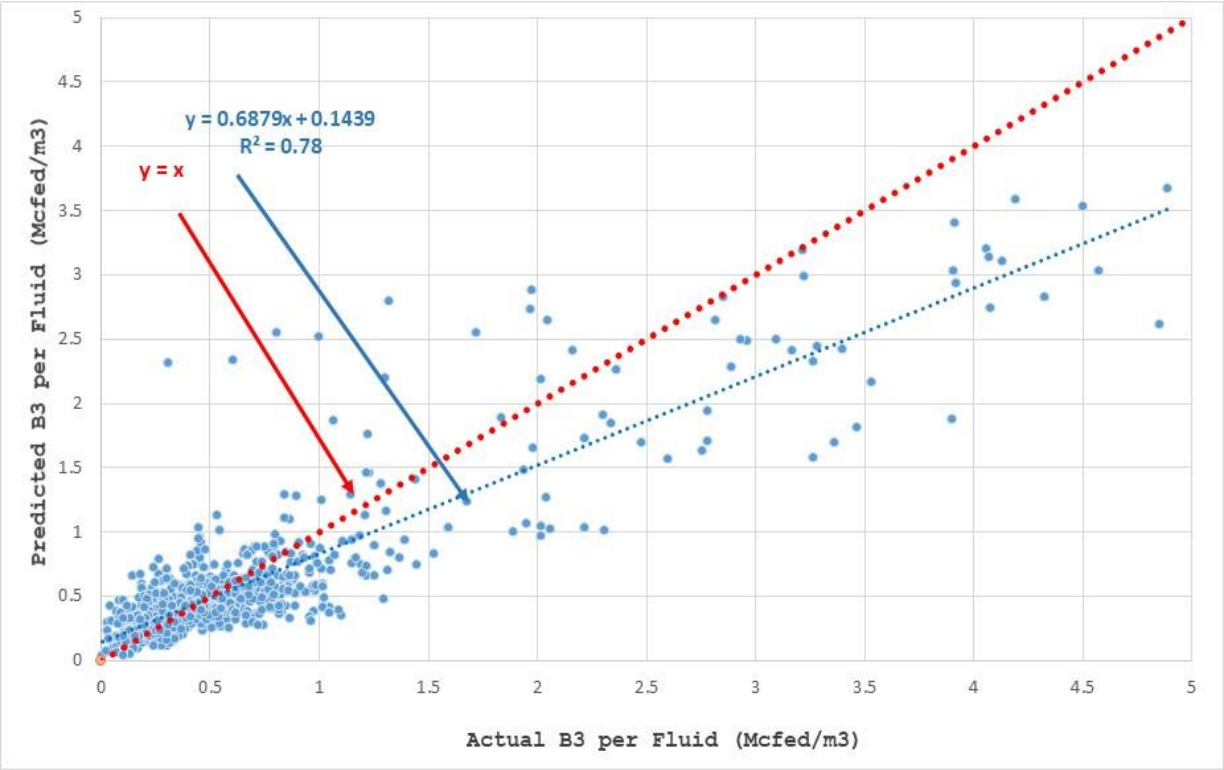

Fig. 3.8—2-D regression line of predicted vs. actual B3 per fluid, Mcfed/ft3 values for 1,040 wells in the BC Montney

3.5 Comparison of Reduced Datasets vs. Full Dataset

In the previous sections, I built multivariable models on the 1,040 wells in the entire BC Montney, including Town field, as well as models on the 44 wells in the Town field. In this section, I will use the full dataset of 1,040 wells along with three different reduced datasets (Town, Altares and Parkland) to build new models and compare their results. The models that are built in this section are independent and different from the models in Sections 3.3 and 3.4. In Section 3.3, the models of 44 wells in the Town field did not include TVD and FirstFracYear;

however, models in this section include TVD and FirstFracYear for 44 wells of Town field, 119 wells of Altares and 63 wells of Parkland. Also, the models built in Section 3.4 did not include interaction terms; however, the model in this section for 1,040 wells has interaction terms. I will define the interaction terms in the following paragraphs.

The main objective of this section is to build two models with the exact same independent variables on two different datasets (full and reduced dataset) for three different fields (Town, Altares and Parkland). In the full dataset case (1,040 wells), there are more data available for modeling; therefore, statistical conclusions are expected to be more statistically significant and reliable compared to the reduced datasets (44 wells in Town, 119 wells in Altares and 63 wells in Parkland). However, the full dataset likely has a higher degree of uncertainty and heterogeneity in reservoir properties because it includes all 32 fields. On the other hand, the wells in the reduced datasets are likely more similar in rock properties since all of them are each in one field. In this section, I am going to assess whether the full dataset yields a more accurate model than the reduced dataset. To answer this question, as mentioned above, I selected three fields in the Northern Montney, Regional Heritage and middle sections of the Montney, which are the Town (44 wells), Altares (119 wells) and Parkland (63 wells) fields. All the wells in the three fields are treated with slickwater and located in the upper zone. The full-dataset model consists of interaction terms (variables in red in Eq. 20) between sand per fluid and UGRFieldname, EP per fluid and UGRFieldname, LL per fluid and UGRFieldname and TVD and UGRFieldname. This means that the coefficients of sand per fluid, EP per fluid, LL per fluid and TVD are different from one field to another field. The full-dataset model is a function of the variables below:

$$(B3.Fluid) =$$

$$f\left(\begin{matrix} sand.fluid, EP.fluid, LL.fluid, TVD, First\ fracyear, UGRFieldname, Completiontype, \\ Sand.fluid * UGRFieldname, EP.fluid * UGRFieldname, LL.fluid * UGRFieldname, \\ TVD * UGRFieldname \end{matrix}\right) \quad (20)$$

The reduced models do not have interaction terms because the dataset belongs to only the Town field or the Altares field or the Parkland field. The reduced models are a function of the variables below:

$$(B3.Fluid) = f(sand.fluid, EP.fluid, LL.fluid, TVD, FirstFracYear) \quad (21)$$

Interaction terms in the full-dataset model measure the effect of one independent variable conditioned on the other independent variable. For example, the effect of sand per fluid on B3 per fluid depends on the field that a well is located within. To measure the impact of sand per fluid on B3 per fluid for different fields, I defined an interaction term in the multivariable regression that consists of sand per fluid and field name, shown as $Sand.Fluid * FieldName$ in Eq. 22. This term means the trend of B3 per fluid vs. sand per fluid varies in the 32 different fields and depends on the field in which a well is located. Therefore, the coefficient of this term $(a8)$ in Eq. 22 holds 32 different values for 32 different fields. For example, for the Parkland field the value of the $a8$ coefficient is 0.27 and for Altares this value is 0.32. However, the value of $a1$ is the same for all 32 fields and equal to -0.34. The explanation is the same for all the other interaction terms in Eq. 22.

$$\boldsymbol{B3} = a0 + \boldsymbol{a1} * \boldsymbol{Sand.Fluid} + a2 * \boldsymbol{EP.Fluid} + a3 * \boldsymbol{LL.Fluid} + a4 * \boldsymbol{TVD} + a5 * \boldsymbol{FirstFracYear} + a6 * \boldsymbol{UGRFieldName} + a7 * \boldsymbol{Completion\,Type} + \boldsymbol{a8} * \boldsymbol{Sand.Fluid} * \boldsymbol{FieldName} + a9 * \boldsymbol{EP.\ Fluid} * \boldsymbol{UGRFieldName} + a10 * \boldsymbol{LL.\ Fluid} * \boldsymbol{UGRFieldName} + a11 * \boldsymbol{TVD} * \boldsymbol{UGRFieldName} \quad (22)$$

Table 3.9 shows the models in Town, Altares, and Parkland for the full and reduced datasets. The differences between Table 3.7 and Table 3.9 are interaction terms. Interaction terms are not included in Table 3.7.

Town full dataset	$(B3.Fluid)^{(0.14)} = -0.35 * Sand.Fuid^{-0.417} - 2.5 * LL.Fluid^{-0.0047} - 0.024 * EP.Fluid^{-0.1009} + 15.8 * TVD^{-0.1347} - 0.006 * FirstFracYear + Completion\,Type + Sand.Fluid * TownField + EP.Fluid * TownField + LL.Fluid * TownField + TVD * TownField + 12.4\ (intercept)$
Town reduced dataset	$(B3.Fluid)^{(0.47)} = 0.50 * Sand.Fuid^{1.17} + 1.25 * LL.Fluid^{0.26} + 0.33 * EP.Fluid^{0.23} + 16.50 * TVD^{-3.43} - 0.013 * FirstFracYear + 26.4\ (intercept)$
Parkland full dataset	$(B3.Fluid)^{(0.14)} = -0.35 * Sand.Fuid^{-0.417} - 2.5 * LL.Fluid^{-0.0047} - 0.024 * EP.Fluid^{-0.1009} + 15.8 * TVD^{-0.1347} - 0.006 * FirstFracYear + Completion\,Type + Sand.Fluid * ParklandField + EP.Fluid * ParklandField + LL.Fluid * ParklandField + TVD * ParklandField + 12.4\ (intercept)$
Parkland reduced dataset	$(B3.Fluid)^{(-0.2)} = 0.018 * Sand.Fuid^{-0.68} + 0.04 * LL.Fluid^{-0.85} + 0.13 * EP.Fluid^{-0.10} - 9.34 * 10^{9} * TVD^{-3.13} + 0.007 * FirstFracYear - 14.4(intercept)$
Altares full dataset	$(B3.Fluid)^{(0.14)} = -0.35 * Sand.Fuid^{-0.417} - 2.5 * LL.Fluid^{-0.0047} - 0.024 * EP.Fluid^{-0.1009} + 15.8 * TVD^{-0.1347} - 0.006 * FirstFracYear + Completion\,Type + Sand.Fluid * AltaresField + EP.Fluid * AltaresField + LL.Fluid * AltaresField + TVD * AltaresField + 12.4\ (intercept)$
Altares Reduced dataset	$Ln(B3.Fluid) = -0.05 * Sand.Fuid^{-0.64} - 1.3 * LL.Fluid^{-0.26} * +5.2 * EP.Fluid^{0.15} - 3.53 * 10^{-12} * TVD^{3.41} - 0.12 * FirstFracYear + 240.1$

Table 3.9—Full and reduced dataset models in Town, Parkland, Altares fields

I plotted predicted vs. actual values from the full and reduced models for the Town, Parkland and Altares fields in Fig. 3.9 to Fig. 3.11. To select the best model between reduced and full dataset models in each field, I based my conclusions on R^2 and the slope of predicted vs. actual values of these plots. For the Town field, the reduced model is better in both respects. The R^2 of the per-fluid model in Section 3.4 was higher than the R^2 of the per-fluid model in Section 3.3. This is probably because the per-fluid model of Section 3.3 did not include TVD and first fracturing year as variables, but the reduced model in this section does include them. Moreover,

the R^2 of the per-fluid model in Section 3.4 is for the entire Montney and not just the Town field. In Parkland and Altares fields, the reduced and full models are similar in both respects, although the full model is slightly better.

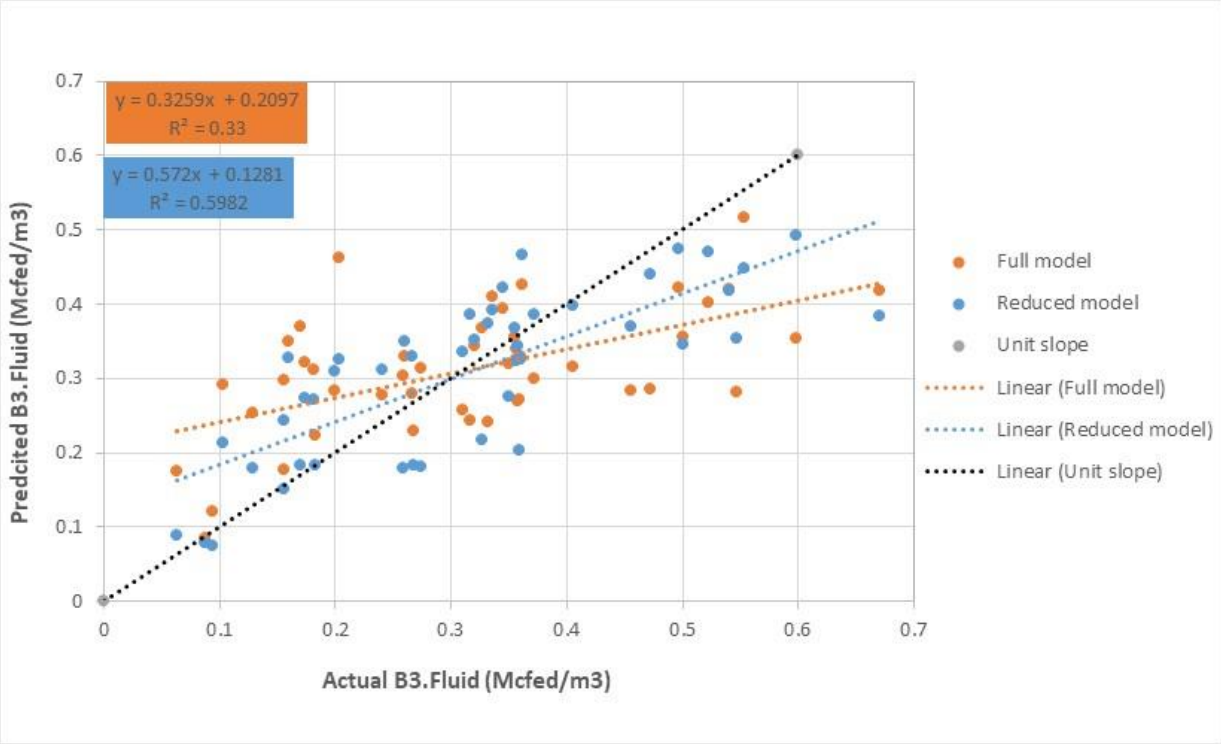

Fig. 3.9—Predicted vs. actual B3 per fluid (Mcfed/ft3) in the Town field for full and reduced models

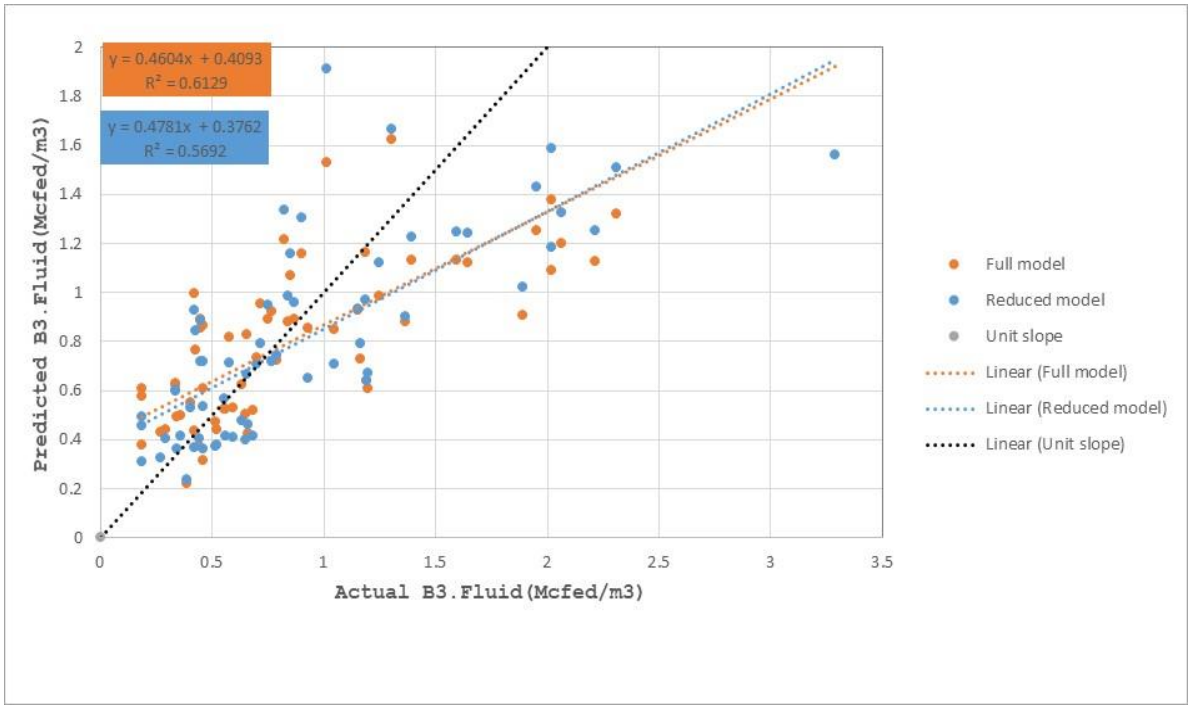

Fig. 3.10—Predicted vs. actual B3 per fluid (Mcfed/ft3) in the Parkland field for full and reduced models

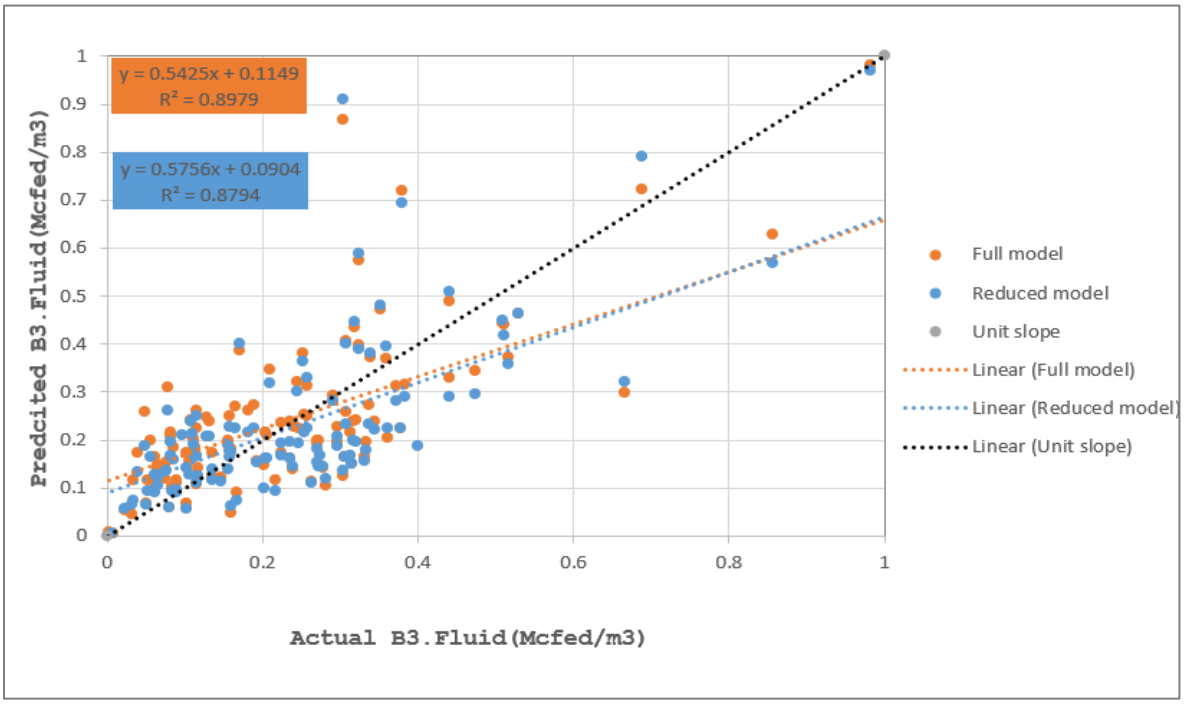

Fig. 3.11—Predicted vs. actual B3 per fluid (Mcfed/ft3) in the Altares field for full and reduced models

Table 3.10 summarizes R^2 and slope for the full and reduced datasets in Town, Altares and Parkland fields. The R^2 shown in Table 3.10 is the 2-D R-squares of predicted vs. observed values.

	Full model R^2	Reduced model R^2	Full model slope	Reduced model slope
Town	0.33	0.60	0.33	0.57
Parkland	0.61	0.57	0.46	0.48
Altares	0.90	0.88	0.54	0.58

Table 3.10—Summary of full and reduced models in the Town, Parkland and Altares fields

I will use the per-fluid model for the Town field selected in Section 3.3.2 in the remainder of this study. In the next section, I will develop a type curve for 44 well in the Town field and use the per-fluid model from Section 3.3.2 to scale the type curve.

3.6 Build Type Curve of 44 Wells in the Town Field

The next step in the analysis was to build the production type curve of the 44 wells in the Town field that is used later in the economic analysis. To build the type curve, I first forecasted 40 years of monthly production for individual wells in the Town field by applying hyperbolic decline curve analysis of the historical data.

These 44 wells started producing on different dates; therefore, I shifted all wells to the same time zero. Zero-time shifting means that the first month of production for all wells is assigned to month one regardless of their start production date, the second month of production for all wells are assigned to month two of production for all wells regardless of their date, and so forth. After applying zero-time shifting to monthly production of the 44 wells, I calculated a final type curve for the area by averaging monthly productions of those wells.

When computing the zero-time average, there is a concern of survivor bias generating artificially high or low tail declines. As time progresses, some of the wells with fewer months of production no longer have data to average; therefore, there is undue focus on wells that have survived. One solution to avoid survivor bias is to include the production forecast for each well in the averaging process. Thus, in the earliest zero-time months the average consists of all historical data and later in time the average grades to all forecasted data.

The zero-time type curve for the Town field, including forecasted data in the average, is the red line in Fig. 3.12. There is an uncertainty in the red line given that is based on forecasts. The green line in Fig. 3.12 illustrates an average curve based solely on historical data and is subject to survivor bias. As seen by inspection, survivor bias in this dataset results in a lower forecast after 50–60 months. The left side of the purple line shows the first 78 months of production, in which more than 50% of wells have historical data. The secondary y-axis shows the well count. It starts from 44 wells and, at month 78, only 23 wells have historical data. I regressed these 78 months of production to forecast 40 years of performance using hyperbolic decline curve analysis (Fig. 3.13). The decline curve with terminal decline of 6% (red curve with dash line in Fig. 3.13) is used as the basis for the reservoir simulation and economic analysis in the next chapters. The terminal decline of 6% is standard in the field and provided by UGR LLC. The q_i, D_i and b of the Town field type curve are 3,366 Mcfed, 1.097 (per year, nominal) and 1.46, respectively. The B3 of the type curve is 3,039 Mcfed.

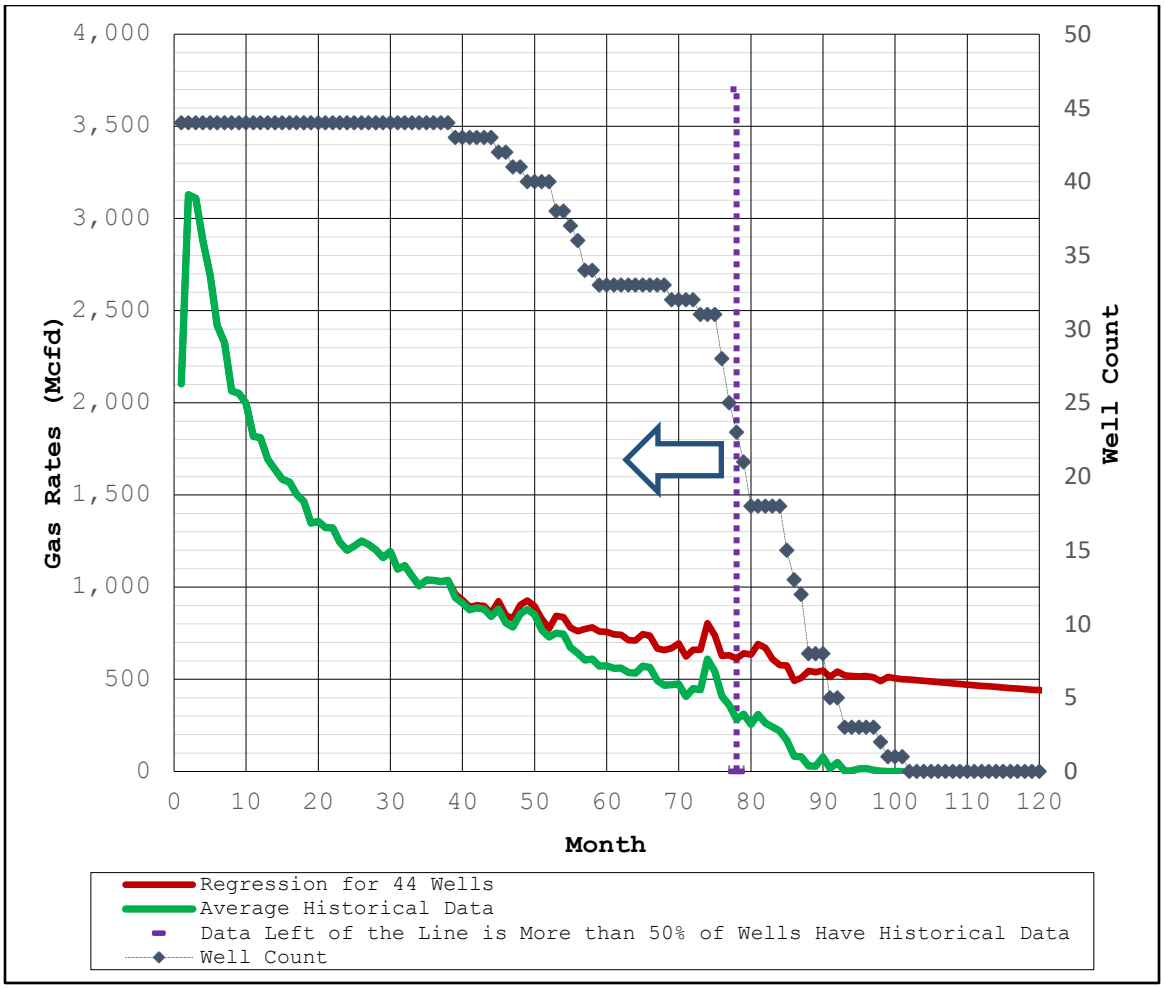

Fig. 3.12—Type curve of 44 wells

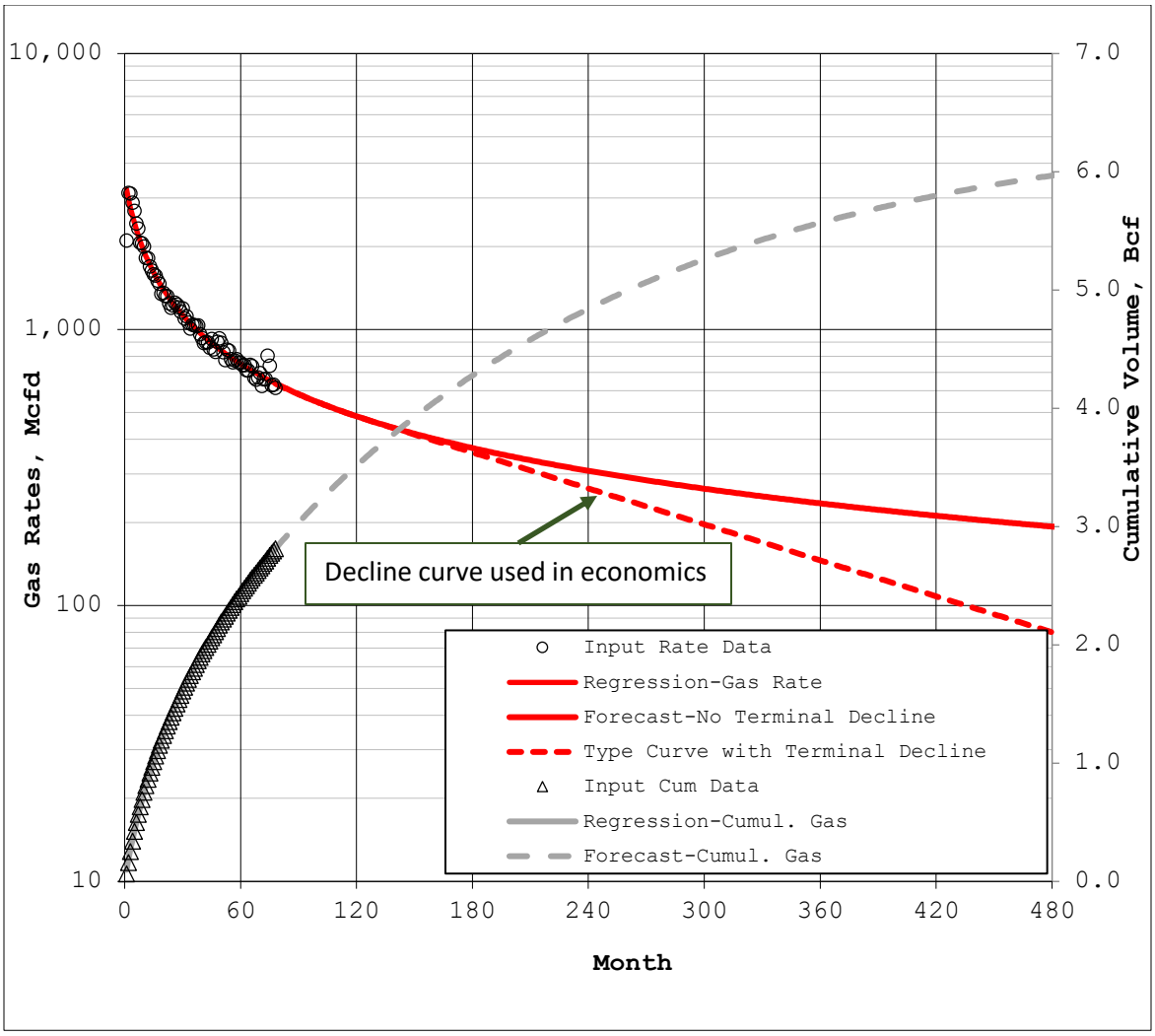

Fig. 3.13—Decline curve of 44 wells

3.7 Calculate Well Spacing for the Town Type Curve

After building the type curve, the objective in this section is to calculate a development well spacing. For this purpose, I first determined if the 44 wells in the Town field are isolated or non-isolated. There are two types of wells:

- Type (a): a horizontal well in isolation (no other wells near enough to constrain any of the well's boundaries). A Type (a) well has maximum distance perpendicular to the lateral that is equal to the radius of a 0.25 miles^2 circle. This

number is provided by UGR based on mapping and the most likely drainage distance. This is 1,489 ft from each side of the lateral (Fig. 3.14).

Drainage area of Type (a) well = Lateral length * Well spacing + 0.25 miles^2 (23)

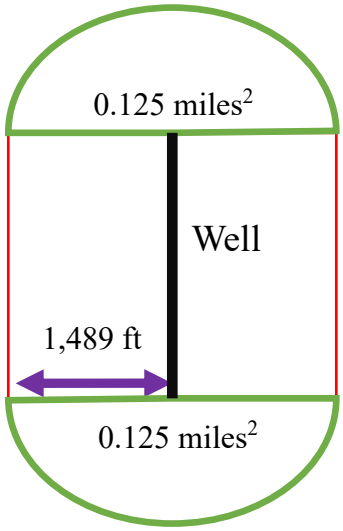

Fig. 3.14—Schematic of drainage area

- Type (b): a horizontal well that is not of Type (a) above, meaning somewhere near the well, there is at least one other well close enough to constrain its boundaries such that it is not a Type (a) well.

If all wells were in isolation (Type (a)), then the drainage distance would be 1,489 ft from each side of the lateral. Therefore, first I drew a line of Type (a) area (assuming the 44 wells are in isolation) vs. lateral length (Fig. 3.15). Then, I added the Voronoi drainage areas vs. lateral length of the 44 wells (Fig. 3.15). As shown, Voronoi drainage areas are below the Type (a) line, indicating all wells in the field are non-isolated.

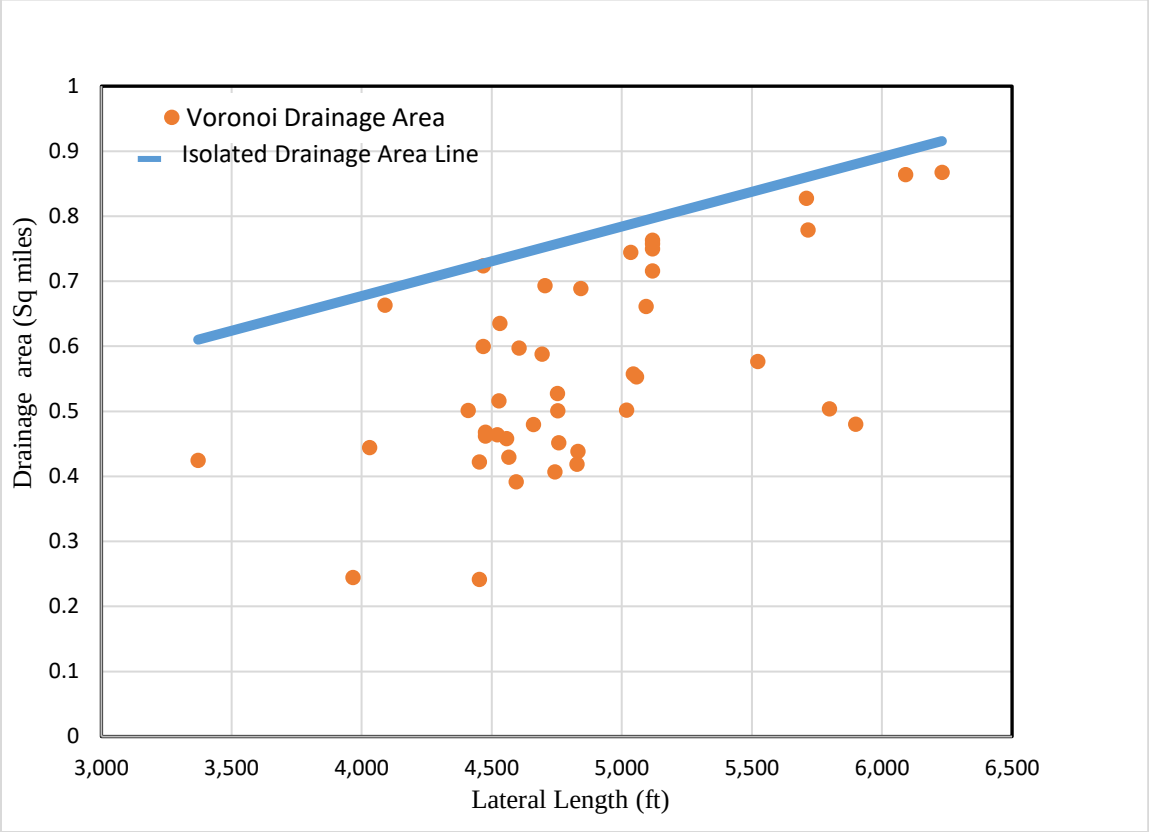

Fig. 3.15 —Voronoi areas of 44 -Well in the Town field

All 44 wells are non-isolated; therefore, to calculate the average well spacing, the relationship between drainage area of the type well in the Town field, lateral length and well spacing can be written as below.

$$\text{Drainage area of type (b) wells} = \text{Lateral length} \times \text{Well spacing} + \pi \times (\text{Well spacing} / 2)^2, \quad (24)$$

By inserting an average lateral length of 4,838 ft and an average Voronoi drainage area of 15,659,832 ft^2 for the 44 wells, I computed the corresponding average well spacing.

$$4{,}838 \times \text{Well spacing} + \pi \times (\text{Well spacing}/2)^2 - 15{,}659{,}832 = 0 \quad (25)$$

Solving Eq. 25, the average well spacing is 2,344 ft. With this average well spacing and porosity of 0.031, water saturation of 0.25, net pay of 262 ft and gas volume factor of 0.00079 bbl/scf (I assumed the porosity value; the other reservoir properties were provided by UGR), I calculate the original gas in place (OGIP) as below:

$$\text{OGIP} = \frac{Average\ drainage\ area \times Porosity \times (1 - Water\ saturation) \times Net\ pay}{gas\ volume\ factor}$$

$$= \frac{15{,}659{,}832 \times 0.031 \times (1 - 0.25) \times 262}{0.00079 \times 5.615}$$

$$= 21.2 \times 10^9 \text{ scf} = 21.2 \text{ Bcf} \quad (26)$$

Using the type curve with terminal decline of 6%, developed in the Section 3.6, yields 6.06 Bcf of estimated ultimate recovery (EUR) based on a 40-year well life. Therefore, the calculated recovery factor is 29% using Eq. 27.

$$R_f = \frac{EUR}{OGIP} \times 100 = \frac{6.06}{21.2} \times 100 = 29\% \quad (27)$$

The calculated 29% recovery factor is far below the typical recovery factor of 65%. It appears that wells on average are not able to effectively drain an area corresponding to an average well spacing of 2,344 ft. Therefore, 1,312 ft was recommended by UGR LLC to be used as well spacing for future wells in the rest of analysis since it corresponds to a standard for the local area. A development spacing of 1,312 ft yields a recovery efficiency of 57%, which is below the 65% upper limit used by most reserves auditors. Later in Chapter 4, I used half of this well spacing (656 ft) as the maximum value that fracture half-length can take.

3.8 Design 300 Completion Cases for Economic Analysis

In this section, I define the completion cases for economic analysis. In the next section, I apply the predictive multivariable model (per-fluid) that was developed previously for the Town

field to predict B3 for these completion cases. Later in Chapter 5, the Town field production type curve is scaled by the ratio of predicted B3 to the type curve B3 to provide a production forecast for a specific completion design. The resulting production profiles, along with completion and drilling cost models, was used in an economic analysis to identify the economic optimum completion design.

Sand, lateral length and entry points were the critical variables in the per-fluid model in the previous section. Therefore, I defined 3 sets of values for these completion parameters: 6 values for lateral length, 5 values for sand intensity and 10 values for entry points. The combination of these parameter values results in 300 different cases (Table 3.11).

EP	LL, ft	Sand Intensity, lb/ft
10	**3,280**	**471**
25	**4,920**	**942**
50	**6,560**	1,413
100	8,200	2,019
150	9,840	2,688
200	13,120	
250		
350		
400		

Table 3.11—Completion parameters utilized in 300 completion designs

Some of these 300 designed sets fall inside the range of current completion practices in the industry (highlighted in Table 3.11); others fall outside current practices. In all the 300 designs, sand-to-fluid ratio is 52.3 $\frac{lb}{bbl}$. Table 3.12 shows the actual ranges of completion parameters for the 44 wells in the Town field.

	EP	LL, ft	Sand Intensity, lb/ft
Minimum	10	3,280	471
Average	24	4,838	712
Maximum	64	6,560	1,344

Table 3.12—Range of current completion designs in the Town field

I designed 300 completion cases that encompass both current and potential practices. For lateral length and sand-intensity parameters, the range starts from minimum values in the current completion parameters of the Town field and ends at two times the maximum value of these current completion parameters. For example, in the Town field, the minimum value for lateral length is 3,280 ft and the maximum value is 6,560 ft. Therefore, designed sets start from 3,280 ft and continue up to 13,120 ft, which is two times the maximum current practice in the field. Since in the 44-well dataset there is no well that is completed with the maximum values of sand intensity, LL, using two times the maximum values provide sufficient parameter space. To define the range for EP, UGR LLC recommended to design the number of stages between 10 to 50 as lower and upper values of number of stages (first column of Table 3.13). Then I calculated EP using relationship between number of entry points and number of stages (Eq. 28). For example, using 50 stages in Eq. 28, EP will be 400 and using 10 stages in the Eq. 28, EP will be 10.

$$Number\ of\ entry\ points = Number\ of\ stages \times 9.75 - 87.5 \quad (28)$$

Number of stages is important because it will be used for the economics later in Chapter 5. Number of stages and number of entry points are shown in Table 3.13 using Eq. 28. For 10

entry points, number of stages is 10 and there is a 1:1 ratio. For 400 entry points, the number of stages is 50 and there is 8:1 ratio. The linear relationship between number of entry points and number of stages is shown in Fig. 3.16.

Number of stages	EP
10	10
12	25
14	50
19	100
24	150
29	200
35	250
40	300
45	350

Table 3.13—Number of entry points and the number of stages

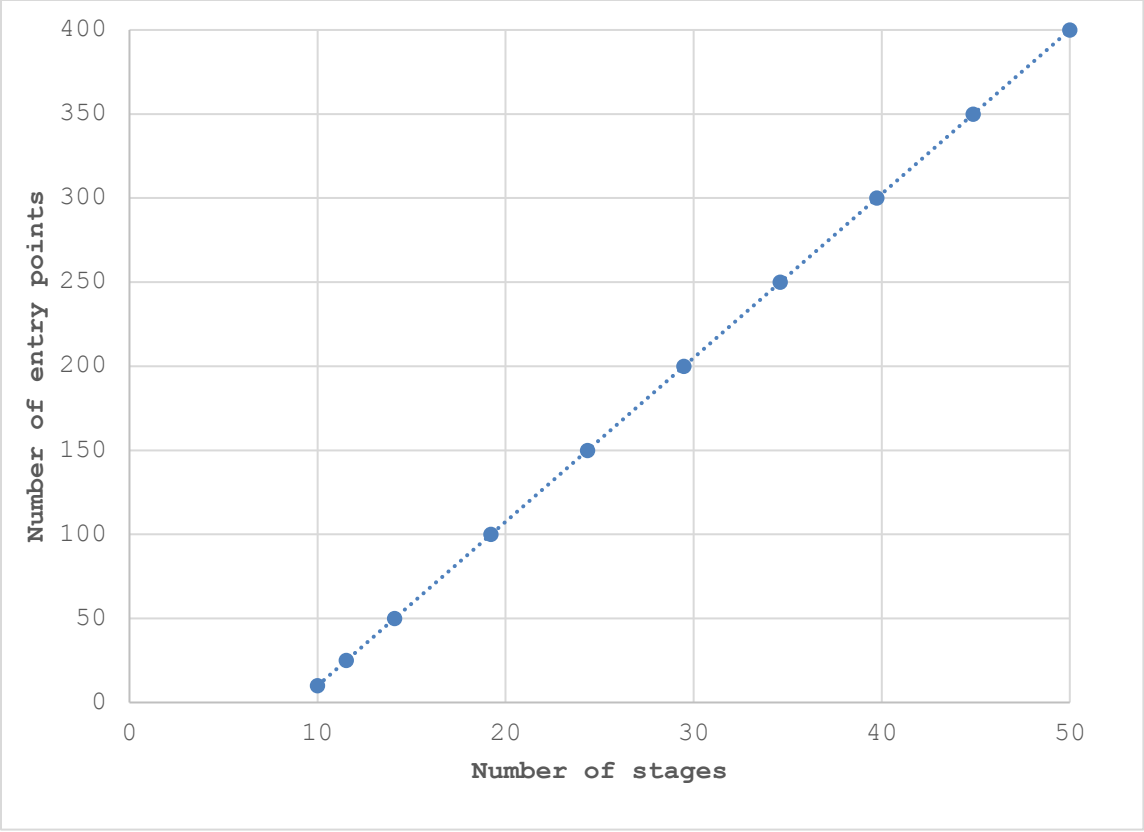

Fig. 3.16—Correlation between entry points and the number of stages

3.9 Predict Well Performance of 300 Completion Cases, Per-Fluid Model

In this section, I used the per-fluid model to predict B3 of the 300 cases defined in the previous section. In Table 3.14, column "B3(regressed)" is the calculated B3 from the per-fluid regression model in the Town field for minimum, mid-point, and maximum of current and potential completion practices in the 300 cases ("mid-point" was defined in terms of parameter values in SI units). The last column of Table 3.14 is the ratio of regressed B3 (calculated in the previous column) to the type curve B3 of the Town field. The B3 of the type curve in the Town field is a constant value of 3,039 Mcfed. The word "Inside" in Table 3.14 refers to completion designs defined in Section 3.8 that are inside the current practices in the industry. Similarly, the word "Outside" in Table 3.14 refers to potential completion designs defined in Section 3.8 that are outside of the current practices in the industry.

As shown in Table 3.14 for the average completion of 44 wells, the regression predicts B3 close to the type curve B3 of 44 wells (their ratio is 1.3). This ratio close to one is expected because the regression model is calibrated to the average well in the Town field and the type curve is also calculated from zero-time averaging of 44 wells in the town field.

The ratio of regressed B3 to the type curve B3 for the minimum completion of 10 entry points, 471 lb/ft of sand and 3,280 ft of lateral length is 0.7. As the completion parameters increase, this ratio increases. For the maximum completion of 400 entry points, 2,688 lb/ft of sand and 13,120 ft of lateral length the ratio is 8.2 and B3 is 25,024 Mcfed. As completion parameters get further outside the space of current completion parameters, the rate of increase of the ratio increases.

	EP	Sand Intensity, lb/ft	Lateral length, ft	B3(regressed), Mcfed	B3(regressed), Mcfed / B3, Mcfed (from type curve of 44 wells)
Minimum completion	10	471	3,280	2,127	0.7
Average completion from 44 wells	24	712	4,838	4,073	1.3
Mid-point completion-Inside	25	942	4,920	4,924	1.6
Maximum completion-Inside	50	942	6,560	6,064	2.0
Mid-point completion-Outside	200	1,413	6,560	8,649	2.8
Maximum completion-Outside	400	2,688	13,120	25,024	8.2

Table 3.14—B3 of minimum, mid–point, and maximum of current and potential completion practices in the 300 cases

Fig. 3.17 to Fig. 3.22 are cumulative production and gas rates of the 6 completion designs in Table 3.14. The red triangles in these figures are the actual data of gas rate and cumulative production that are calculated by zero-time averaging of actual data of 44 wells in the Town field, which represents average completion parameters of the Town field. The green lines in these figures are the original type curve in the Town field that was developed in the Section 3.8. The dark blue lines in these figures are the scaled type curve in the Town field using the scaling ratio calculated in the last column of Table 3.14. For example, for the minimum completion the scaling ratio is 0.7, which is 2,127 divided by 3,039. Therefore, all monthly gas rates of the original type curve are scaled by 0.7 (dark blue line) in the figure. Later in Chapter 5, I will use the scaled type curve to perform economic analysis.

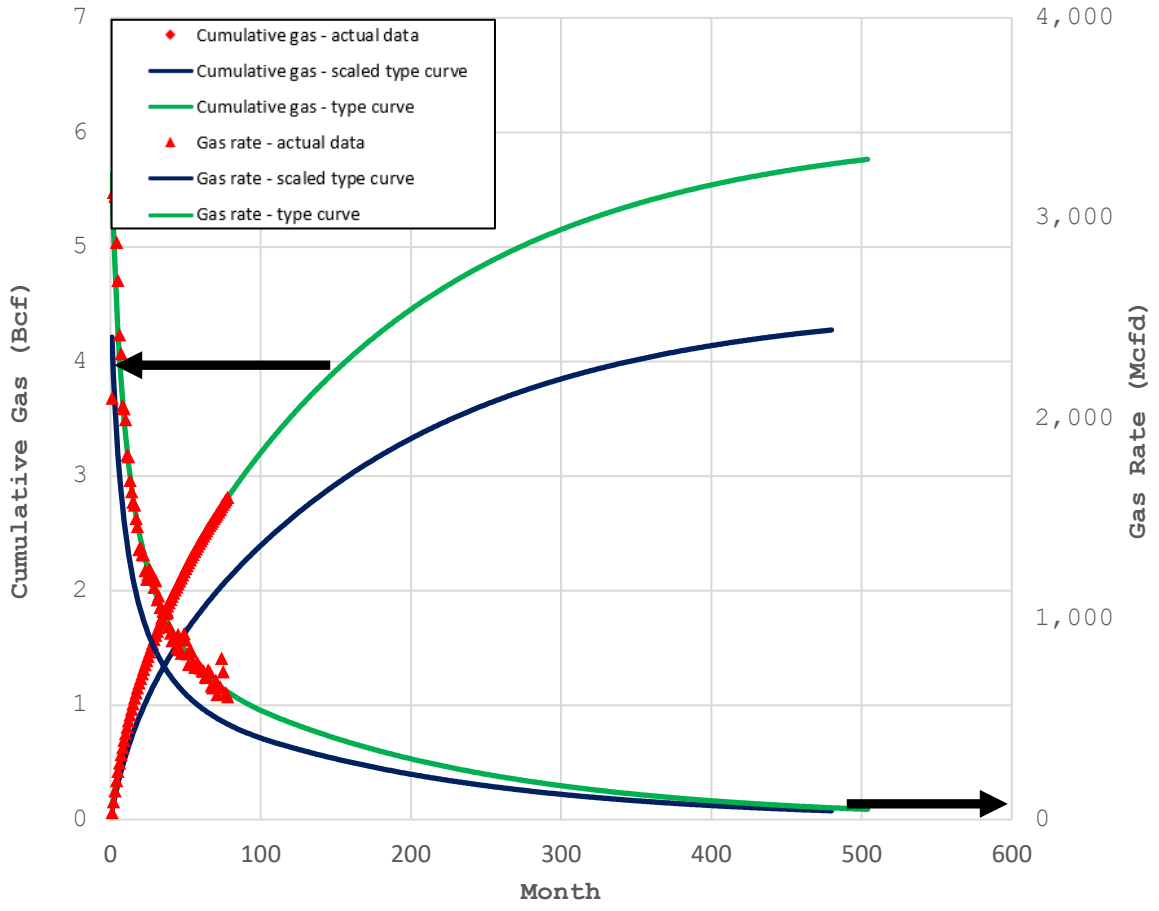

Fig. 3.17— Comparison of regressed typed curve vs. type curve and actual data for the minimum completion with 10 Entry Points, 471 lb/ft, 3,280 ft

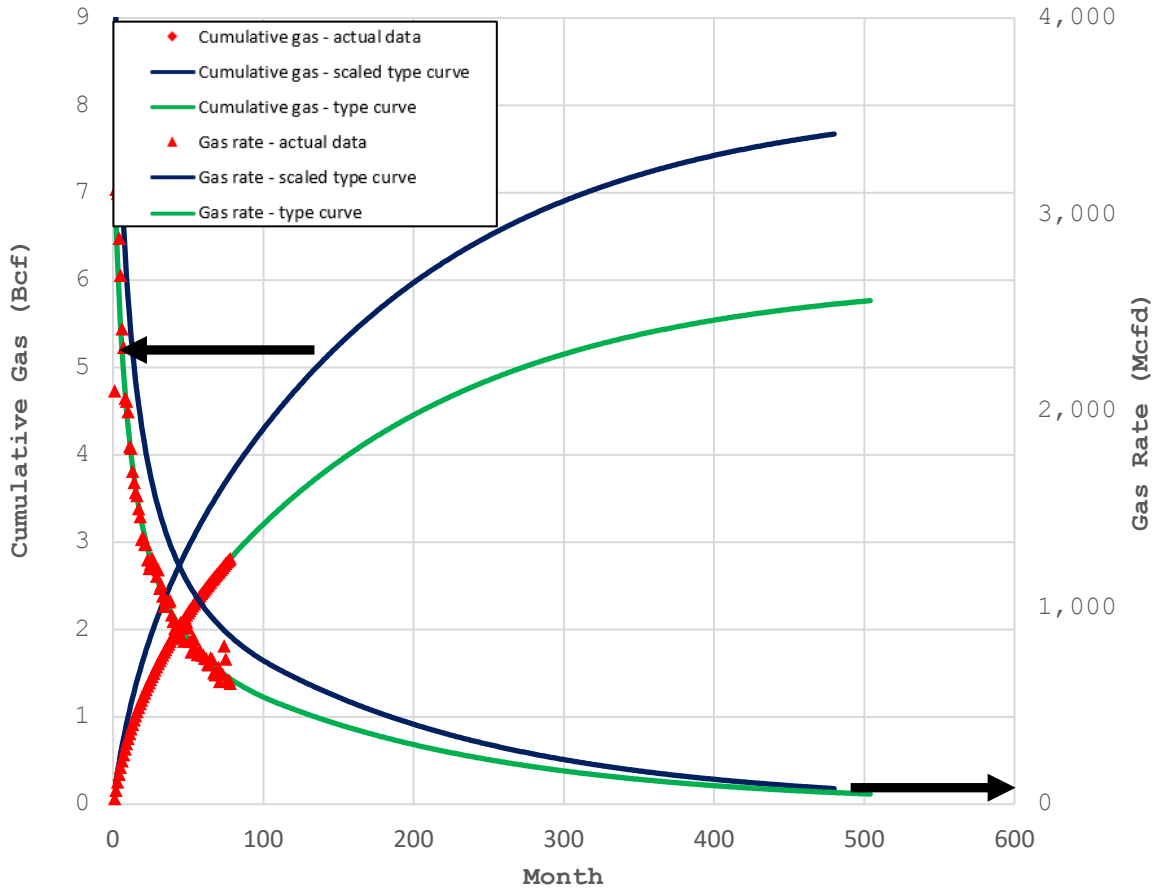

Fig. 3.18—Comparison of regressed typed curve vs. type curve and actual data for the average completion with 24 Entry Points, 712 lb/ft, 4,838 ft

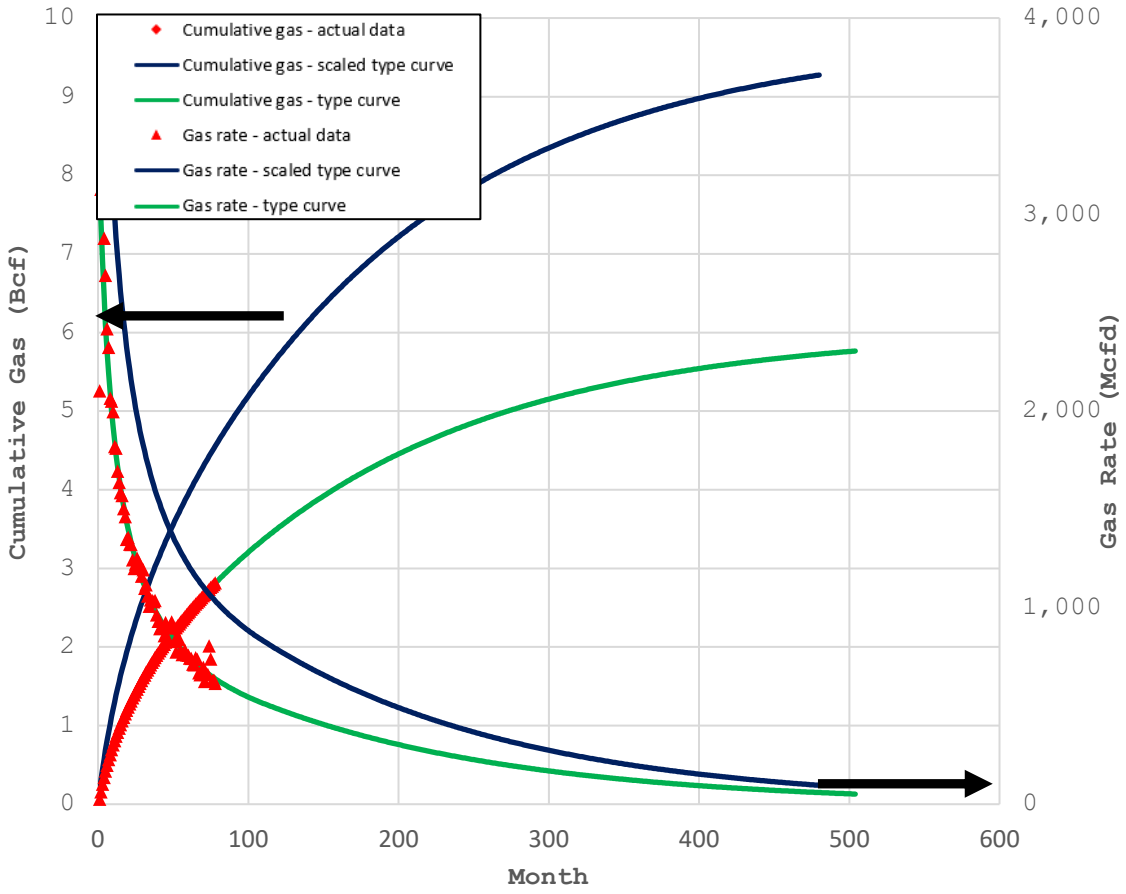

Fig. 3.19— Comparison of regressed typed curve vs. type curve and actual data for the mid-point completion with 25 Entry Points, 942 lb/ft, 4,920 ft

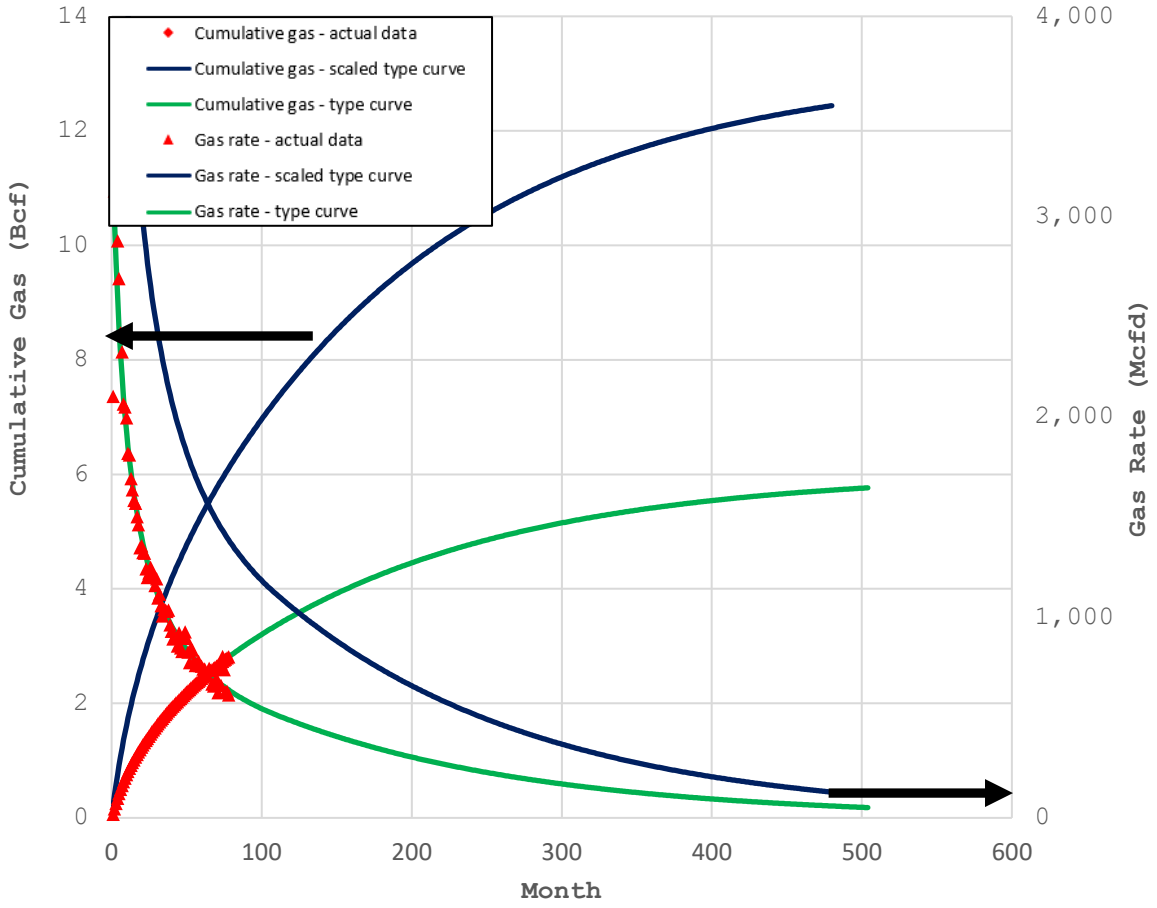

Fig. 3.20— Comparison of regressed typed curve vs. type curve and actual data for the maximum completion with 50 Entry Points, 942 lb/ft, 6,560 ft

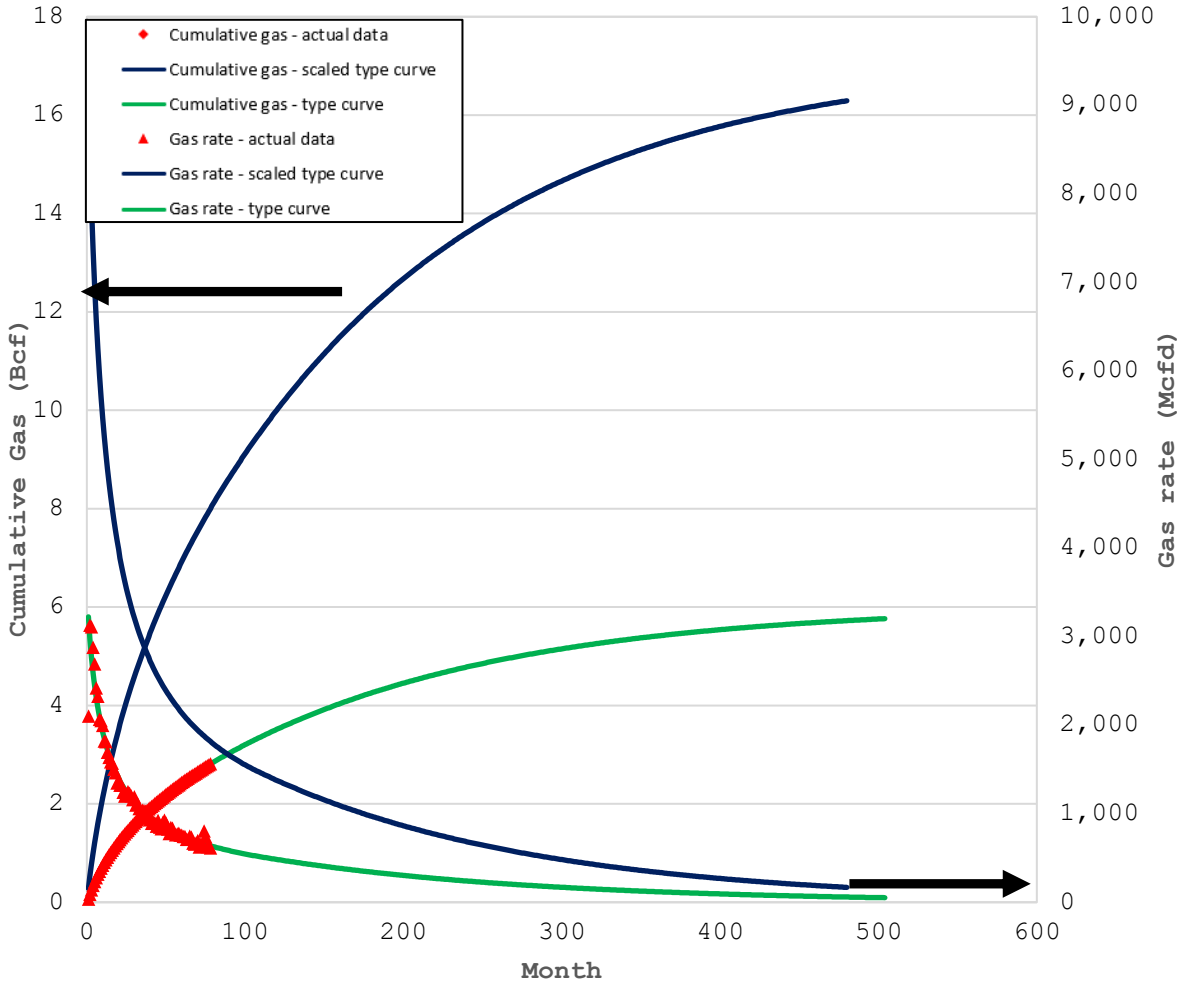

Fig. 3.21— Comparison of regressed typed curve vs. type curve and actual data for the mid-point completion with 200 Entry Points, 1,413 lb/ft, 6,560 ft

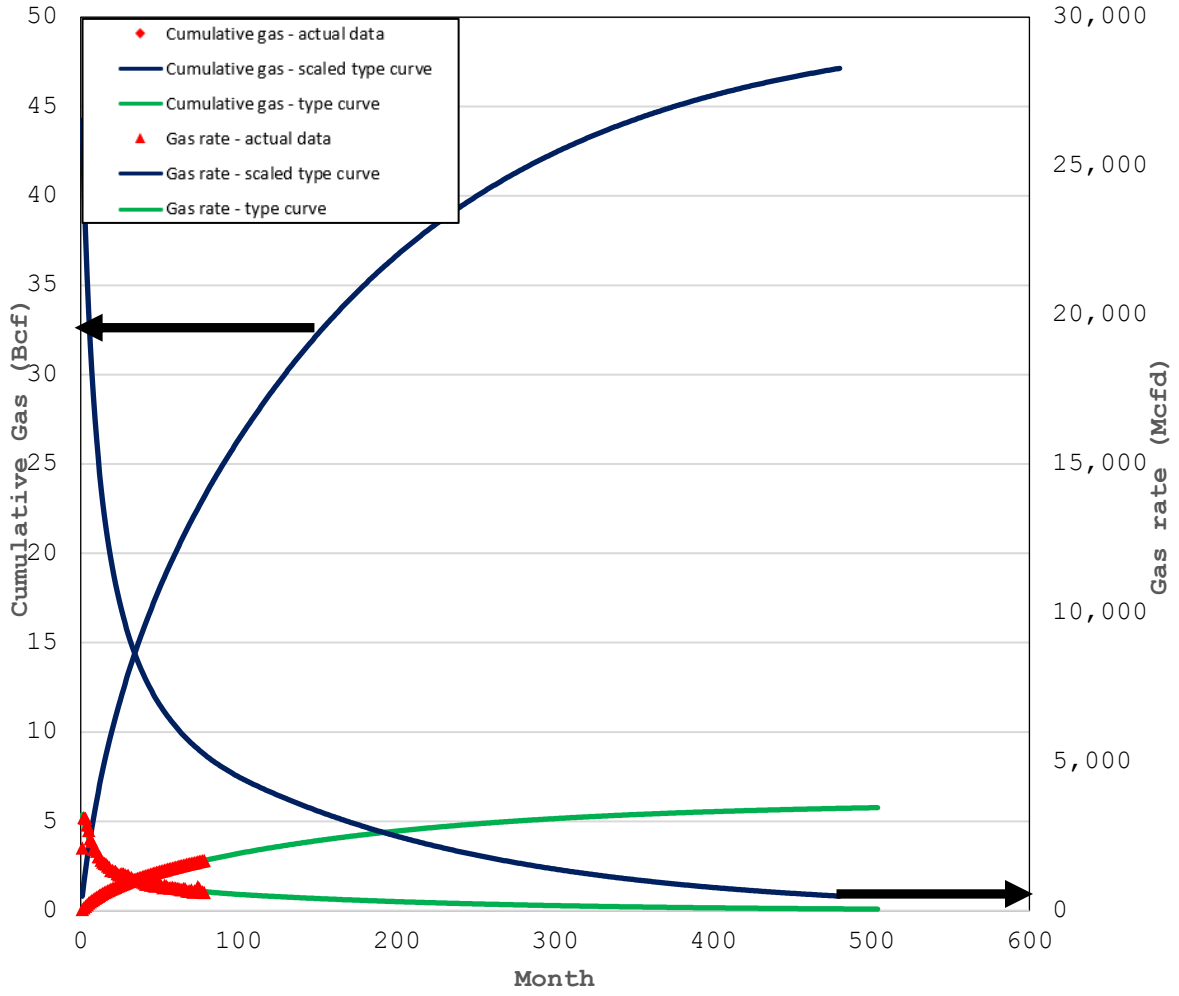

Fig. 3.22— Comparison of regressed typed curve vs. type curve and actual data for the maximum completion of with 400 Entry Points, 2,688 lb/ft, 13,120 ft

3.10 Limitation of Multivariable Regression

Multivariable regression was used to predict performance that is used later in this dissertation to perform the economic analysis under a wide range of completion designs. In this chapter, predictive analytics was used to relate short-term production data to completion parameters without the requirement to run a huge number of reservoir simulations and perform

history matching. However, the limitation of data analytics methods is that they are by construction interpolation models. Therefore, they should be used with great caution for extrapolation beyond the range of given data. Fig. 3.23 illustrates the large error that can result from using multivariable regression to extrapolate beyond a range of observed data. Assuming that the red line is the true function of blue dots in Fig. 3.23, extrapolating the blue line leads to large error in predictions.

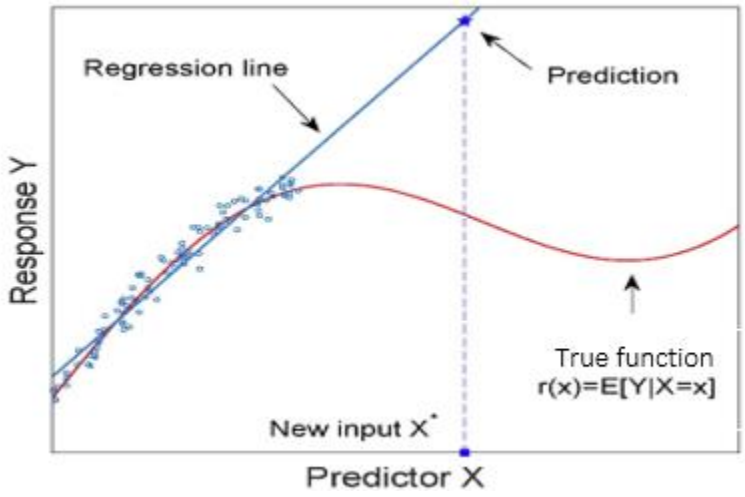

Fig. 3.23—Invalid extrapolation beyond the range of observed data with multivariable regression with assumption that red curve is the true function

CHAPTER 4 RESERVOIR SIMULATION MODELS

4.1 Introduction

In this chapter, my objective is to predict well performance for a specific completion design using a physics-based reservoir simulation model calibrated against production data. A physics-based model will still be uncertain outside the dataset used for calibration, and the uncertainty should be greater the further one gets away from the calibration dataset. However, because extrapolation outside the dataset with simulation is constrained by the laws of physics while extrapolation outside the data with data analytics is not constrained by the laws of physics, one would expect the uncertainty for extrapolation with simulation to be lower than that for data analytics.

I used a simulation model to predict production performance for the 300 completion designs described in the previous chapter (Table 3.11), which are inside and outside the range of current practices. To create a reservoir simulation model in the Town field, I used the production profile of the production type curve with terminal decline of 6% in the Town field developed in the previous chapter (Fig. 3.13). First, I performed a history match of 78 months of gas rates from the production type curve, as well as observed wellhead pressure data. Then I used the history-matched reservoir simulation model to calculate the B3 of the 300 completion designs. Next, I predicted 40-year production profiles for the 300 completion designs (Table 3.11) in the Town field that will be used in Chapter 5.

4.2 History Matching

History matching is a process to calibrate a reservoir simulation model so that the production and pressure data predicted by the model match the observed production rates and pressures. This is accomplished by trying many different combinations of reservoir and hydraulic-fracture properties and finding the combination of parameters that minimizes the differences between predicted and observed production and pressure data. History matching is necessary due to uncertainties in important subsurface properties such as formation permeability and fracture half-length.

In this study, I performed a history match of the production type curve with a multi-fractured horizontal lateral length of 4,838 ft, 24 entry points, 3,448,030 lb of sand and 712 lb/ft of sand intensity (Table 4.1), which are the average values of these parameters for the 44 wells in the Town field. Each entry point is assumed to have a single transverse fully-penetrating hydraulic fracture. Hydraulic fractures in this study are assumed identical and 100% effective, which means only one of them needs to be modeled in reservoir simulation, due to the symmetry of the drainage area.

I used the reservoir properties of the Town field provided by UGR to perform the history match (Table 4.2). The well spacing in Table 4.2 was calculated in Section 3.7. Entry point spacing in Table 4.2 is computed by dividing completed the lateral length of 4,838 ft by 23, which is number of spaces along the lateral. Since there are 24 entry points in the well, there are 23 spaces between entry points. I performed history matching on the 78 months of gas production and well pressure data. Since bottom-hole pressures are not available in this study, I used a common operating condition of 200 psi for the wellhead pressure (recommended by UGR) as a matching parameter.

Completed lateral length, ft	Total entry points	Total sand, lb	Sand intensity, lb/ft
4,838	24	3,448,030	712

Table 4.1—Summary of average well completion used in the history match

Porosity	0.031
Water saturation	0.25
Reservoir pressure, psi	3,647
Bottom-hole temperature, F	190
Well spacing, ft	1,312
Average depth, ft	6,038
Net pay, ft	262
Gas gravity	0.7
Entry point spacing, ft	211

Table 4.2—Reservoir and fluid properties

Fig. 4.1 is a schematic of the drainage area. In the figure, the well is in the green lines and fractures are in the blue lines. The red dashed line is the boundary of each fracture. The resulting single-fracture model does not properly model the fractures at each end of the well, but it does adequately model the interior fractures.

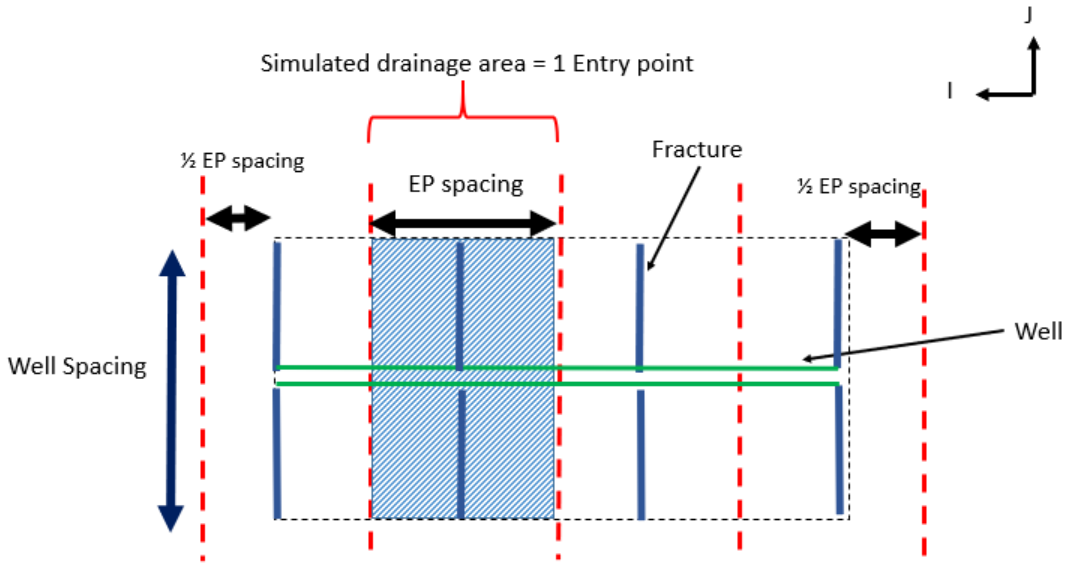

Fig. 4.1—Schematic of the drainage area

I modeled one fracture and used the symmetry of the drainage area to divide the well gas rates by the number of fractures (24) and calculate the production of one fracture. Therefore, to calculate the gas rate for the entire well length, the simulation results should be multiplied by the number of fractures. The original gas in place (OGIP) for the assumed drainage area (1 fracture) from the simulation model is 0.384 Bcf. Therefore, OGIP for the drainage area of the full wellbore (24 fractures) from the simulation model is 9.2 Bcf.

The horizontal well is in the *i* direction (red dot) and fracture is in *j* direction (yellow dash line) (Fig. 4.2). The fracture in the *j* direction is perpendicular to the wellbore in the *i* direction. The model has a single-porosity system with two phases—water and gas. There are 60,075 grids in the model—25 grids in *i* direction, 267 grids in the *j* direction and 9 layers in the *z* direction. I refined gridding near the wellbore logarithmically to capture large pressure drops. Since I simulated one fracture, the fracture spacing in the *i* direction is 211 ft. I assumed the well is not isolated (as discussed in the Section 3.7) and the fracture half-length can grow to the tips

of fractures in adjacent wells. The drainage distance calculated in Section 3.7 was 1,312 ft and was assumed to be the well spacing for future wells. Therefore, fracture half-length in the *j* direction can grow to half of the well spacing, which is 656 ft.

In the history matching process, it is possible to get matches in which fracture heights are significantly greater than total fracture length, which is not realistic. To prevent these history matching cases, I tested three different fracture heights with a constraint on total fracture lengths. The constraint was that total fracture length can be significantly greater than fracture height if there are sufficient barriers to vertical fracture growth, but it cannot be less than the fracture height. The first-case fracture height has reservoir net pay of 262 ft and total fracture length more than 262 ft. The second-case fracture height has 7/9 reservoir net pay, which is 204 ft, and total fracture length more than 204 ft. The third-case fracture height has 5/9 reservoir net pay, which is 145 ft, and total fracture length more than 145 ft.

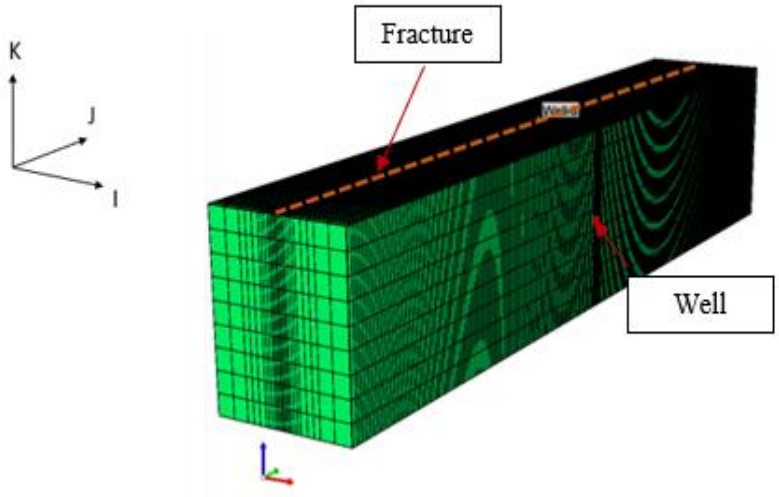

Fig. 4.2—Schematic of well and gridding

History match parameters are fracture permeability, matrix permeability and fracture half-length (Table 4.3). Fracture half-length has a uniform distribution, and all possible values from 5 ft to 656 ft for fracture half-length have an equal chance in the matching process. Permeabilities of the fracture and matrix have logarithmic distributions since permeability usually is lognormally distributed. Lognormal distributions are truncated by upper and lower bounds. The values for lower and upper bounds of the distributions were provided by UGR.

Parameters	Minimum	Maximum	Distribution
Permeability of matrix, md	1E-6	0.01	Lognormal
Permeability of fracture, md	1	1,500	Lognormal
Fracture half-length, ft	5	656	Uniform

Table 4.3— Prior distributions of history match parameters

Since bottom-hole pressure data are not available in this study, I used a common operating condition of 200 psi for the wellhead pressure (recommended by UGR). After I built the model, I performed history matching with one objective function that has 2 terms. The two terms are cumulative gas production and 200-psi wellhead pressure. The primary well constraint in the first three months of production is rate and the secondary constraint in the first three months of production is wellhead pressure of 200 psi. Starting in month four, wellhead pressure of 200 psi is the primary constraint.

As I mentioned earlier, I constrained fracture half-length. The constraint is that fracture half-length should be greater than half of the fracture height. For this purpose, I performed a history match on three different fracture-height cases with constrained fracture half-length (Table 4.4). In the table there is a percentage of error for matching cumulative gas and a percentage error for matching wellhead pressure with historical data. I averaged the percentage error of

these two terms of the objective function and selected the case with a minimum average percentage error. This table shows the best match is the second one with the minimum average percentage error of wellhead pressure and cumulative gas. The fracture half-length is 343 ft, the permeability of fractures is 2.51 md and the permeability of matrix is 112.2 nd (Table 4.4). I will use the second model in the table for further analysis in this chapter.

Case	Formation height, ft	Fracture height, ft	Constrained fracture half-length, ft	Error rate (Cumulative gas)	Error rate (WHP)	Average error rate for WHP and cumulative gas	Xf, ft	Permeability matrix, nd	Permeability fracture, md
1	262	262	> 131	84%	0.0000087 %	42%	393	60.2	1.86
2	262	204 (7/9 H formation)	> 102	66%	0%	33%	343	112.2	2.51
3	262	145 (5/9 H formation)	> 72	97%	0%	48%	583	79.4	3.46

Table 4.4—Results of the history match

In Fig. 4.3, Fig. 4.4 and Fig. 4.5 the blue circles show historical data for the 78 months, and the red line shows the predicted values from reservoir simulation for Case 2. The red line and blue circles align relatively closely, which indicates the reservoir simulation model is a good match.

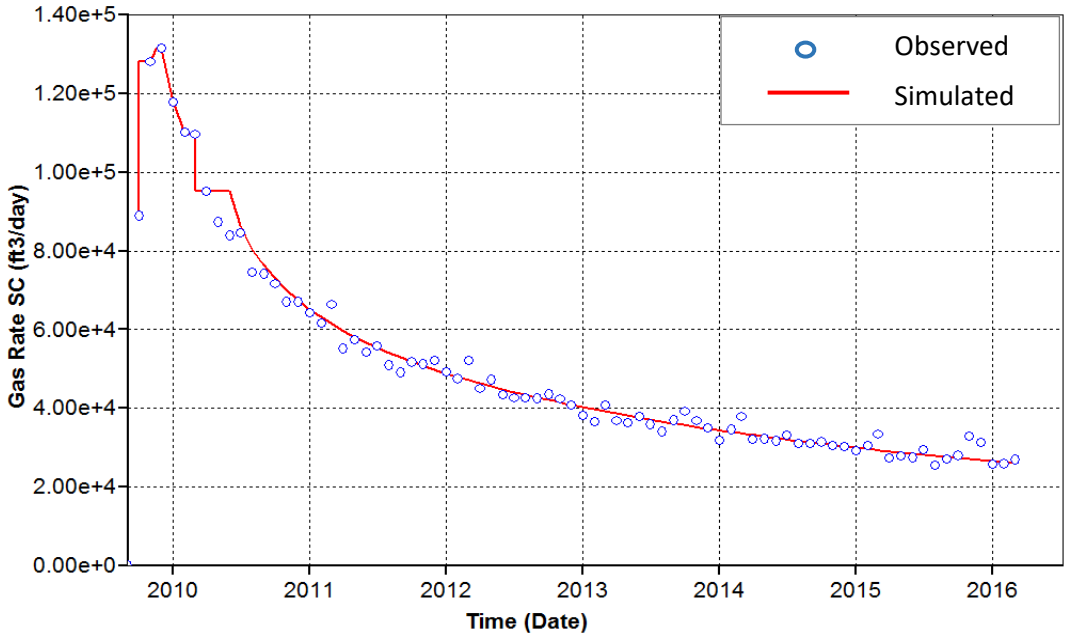

Fig. 4.3—History match of gas production rates - one entry point

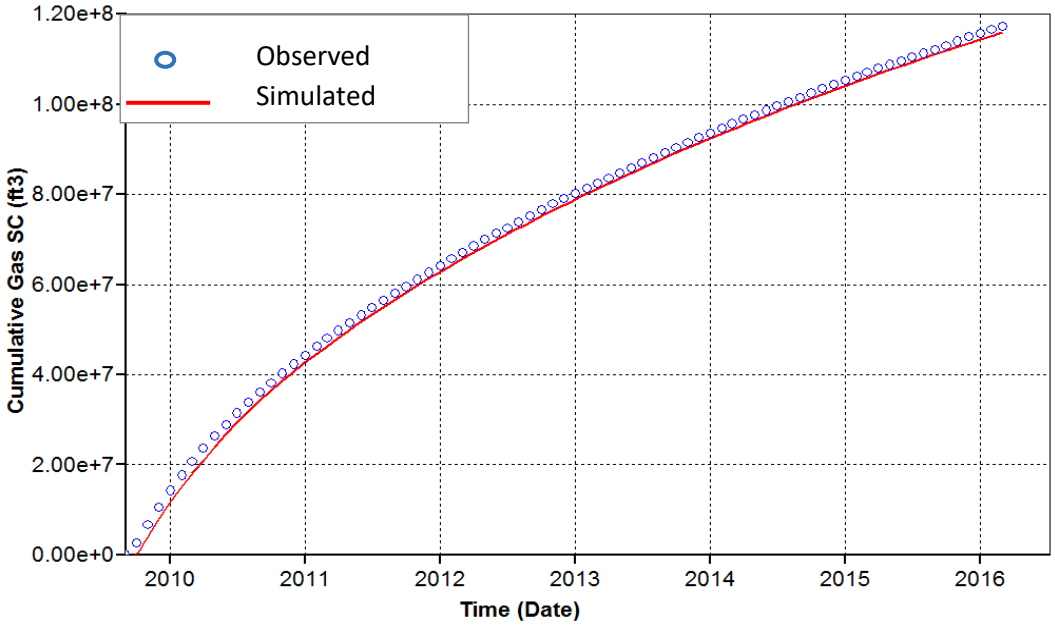

Fig. 4.4—History match of cumulative gas - one entry point

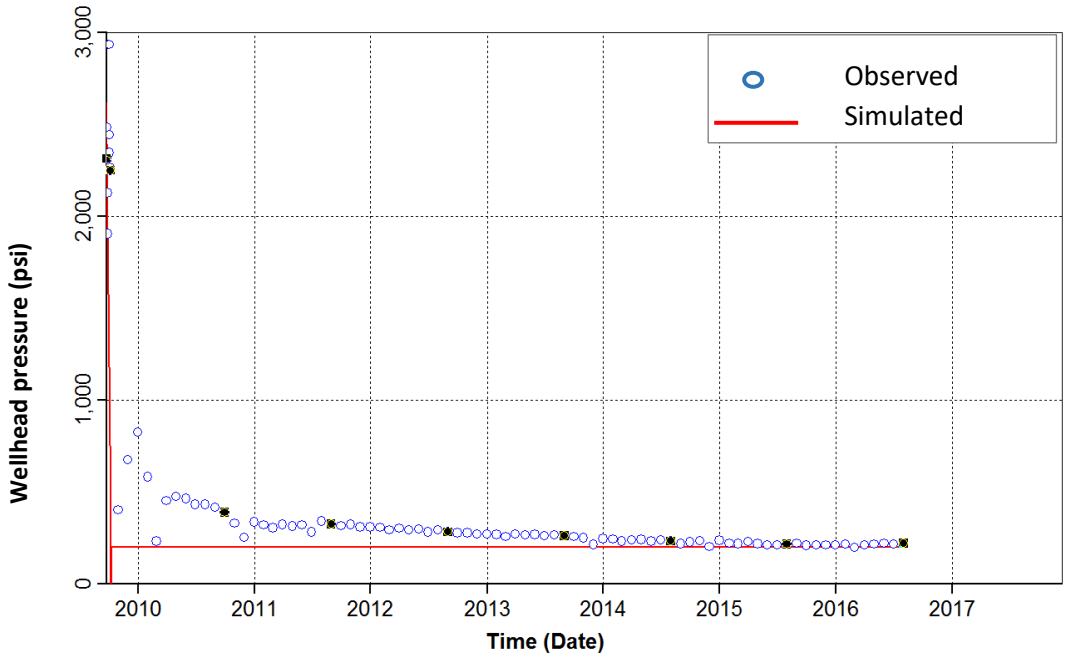

Fig. 4.5—History match of wellhead pressure - one entry point

4.3 Comparison between Predicted B3 per Fluid from Reservoir Simulation to the Actual B3 Per- Fluid of 44 Wells

In this section, I compared the predicted B3 from reservoir simulation developed in Section 4.2 to the actual B3 of the 44 wells. Fig. 4.6 is a 2-D plot of predicted B3 per fluid model using both reservoir simulation (blue dots) and the regression model (orange dots) on the y-axis and actual B3 per fluid of 44 wells in the Town field on the x-axis. The R^2 of the orange line for the regression model is 0.2 and R^2 of the blue line for the simulation model is 0.11, which shows there is more uncertainty in the simulation model for the 44 wells in the Town field. However, neither of the models do a good job in predicting individual wells. Furthermore, the orange line for the regression model is flatter (lower slope) compared to the blue line for the simulation

model. Thus, the simulation model does a better job in predicting the extremes than the regression model. However, neither model predicts well over the full range of B3-per-fluid values.

In summary, there is a trade-off between slope and R^2. The simulation model has a greater slope compared to regression model; as a result, it can better predict the extremes of B3 compared to the regression model. However, the simulation model has a smaller R^2 compared to the regression model and, thus, there is more uncertainty in the simulation model compared to the regression model.

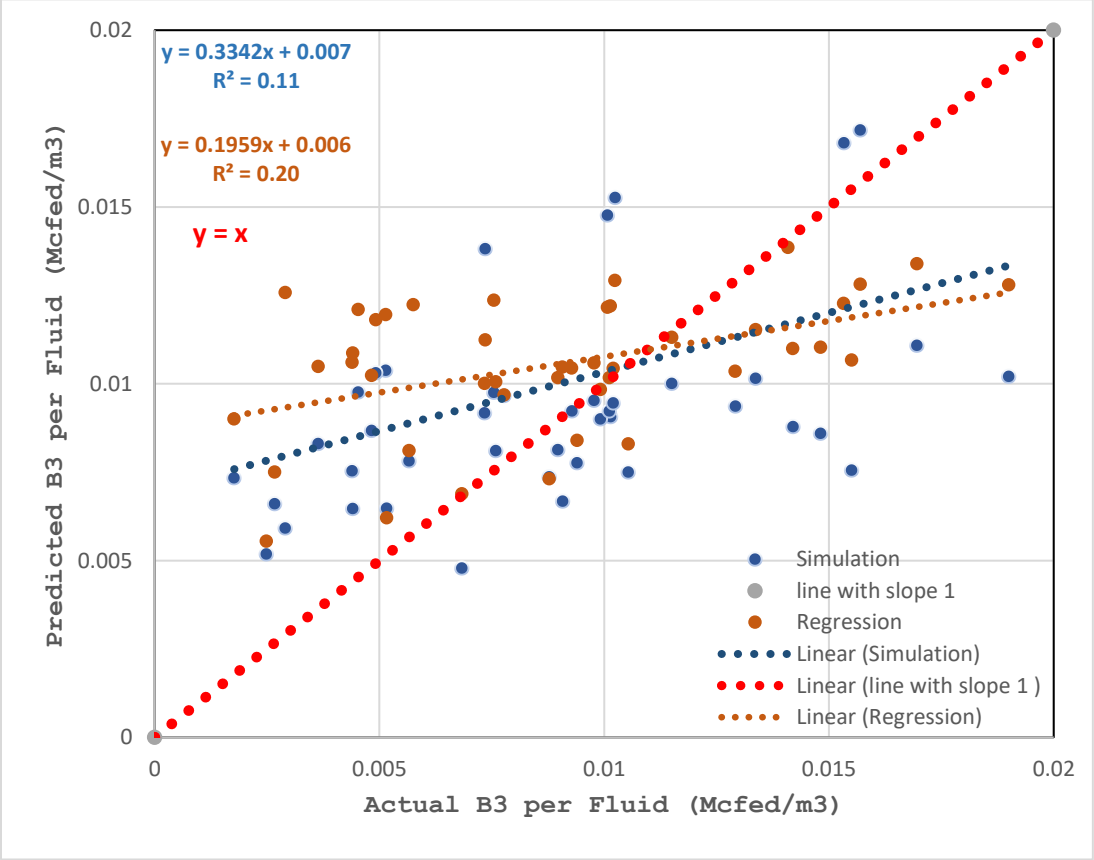

Fig. 4.6—2-D regression line of predicted vs. actual B3 per fluid, Mcfed/ft^3 values for 44 wells in the Town field

4.4 Predict Well Performance of 300 Completion Cases Using Simulation Model

In this section, I used the calibrated simulation model to predict B3 of the 300 cases defined in Section 3.8. Table 4.5 shows the B3 for the minimum, mid–point, and maximum of current and potential completion practices in the 300 cases that are predicted from reservoir simulation. The fifth column is predicted B3 from the reservoir simulation model, and the sixth column is the ratio of predicted B3 from reservoir simulation to the B3 of the 44-well type curve, 3,039 Mcfed. As the completion parameters increase, the ratio of simulation B3 to the type-curve B3 increases.

For the average completion of 44 wells, the reservoir simulation model predicts B3 close to the type-curve B3 of 44 wells (their ratio is 1:1). This ratio is expected because I developed a reservoir simulation model based on the type curve of the 44 wells and completion design of the average entry points, lateral length and sand intensity of the 44 wells. In 3.14, the value for the same ratio from the regression model is 1.3, which demonstrates that reservoir simulation does better in predicting B3 for the average well.

	Entry point	Sand Intensity, lb/ft	Lateral length, ft	B3, Mcfed (predicted from simulation model)	B3, Mcfed (predicted from simulation model)/ B3, Mcfed (from type curve of 44 wells)
Minimum completion	10	471	3,280	2,193	0.7
Average completion from 44 wells	24	712	4,838	3,485	1.1
Mid-point completion-Inside	25	942	4,920	4,644	1.5
Maximum completion-Inside	50	942	6,560	7,053	2.3
Mid-point completion-Outside	200	1,413	6,560	10,031	3.3
Maximum completion-Outside	400	2,688	13,120	15,508	5.1

Table 4.5—Reservoir-simulation-predicted B3 and its ratio to the type curve B3 of 44 wells for the minimum, mid–point and maximum of current and potential completion practices in the 300 cases

After performing the history match, I used the matched parameters in the reservoir simulation model to compute 40 years of gas production rates (from 2017 to 2057) for the 300 defined completion designs. Using these rates, I performed economic analysis in the next chapter.

Fig. 4.7 to Fig. 4.12 are cumulative production and gas rates of the 6 completion designs in Table 4.5. The red triangles in these figures are the actual data of gas rates and cumulative production that are calculated by zero-time averaging of production data from the 44 wells. The green lines in these figures are the original type curve and its cumulative production in the Town field that was developed in Section 3.6. The dark blue lines in these figures are gas rates and cumulative production from the reservoir simulation model. These figures show that as completion parameters increase, cumulative production (blue line) increases. However, the increase is bounded by physics of the simulation model such as reservoir size and friction, and it does not increase as much as for the regression model. For example, the cumulative production (blue line) in Fig. 4.10 is 8.8 Bcf after 480 months while cumulative production (blue line) in Fig. 3.20 for the same design in the regression model is 12.4 Bcf after 480 months.

In Fig. 4.7, simulated gas rates of the minimum completion design (blue line) are below actual gas rates and the Town field type curve (red and green lines). The ratio of the B3 from simulation to B3 of the type curve is 0.7.

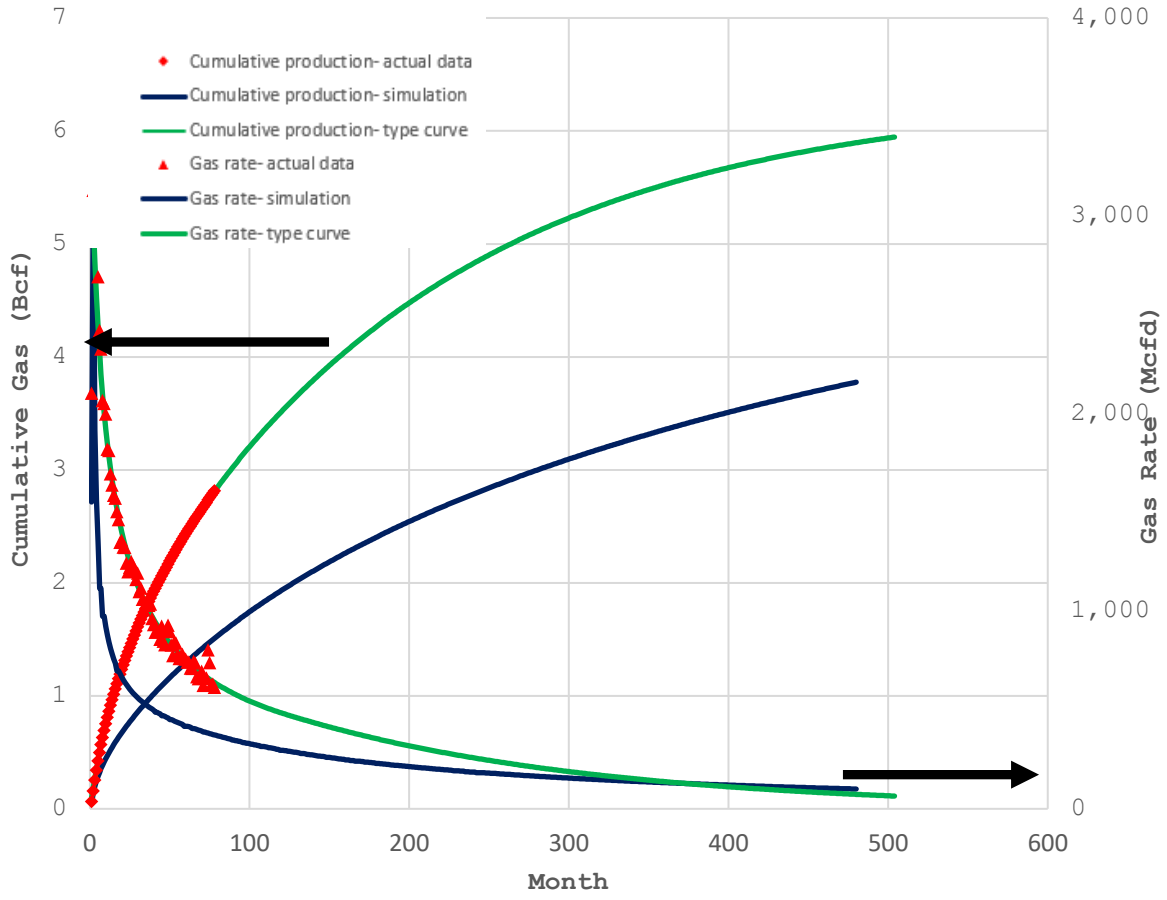

Fig. 4.7—Comparison of simulation gas rates vs. type curve and actual gas rates for the minimum completion with 10 Entry Points, 471 lb/ft, 3280 ft

In Fig. 4.8, simulated gas rates of the average completion design (blue line) are similar to actual gas rates and the type curve of Town field (red and green lines) as expected. The ratio of the B3 from simulation to B3 of the type curve is 1.1.

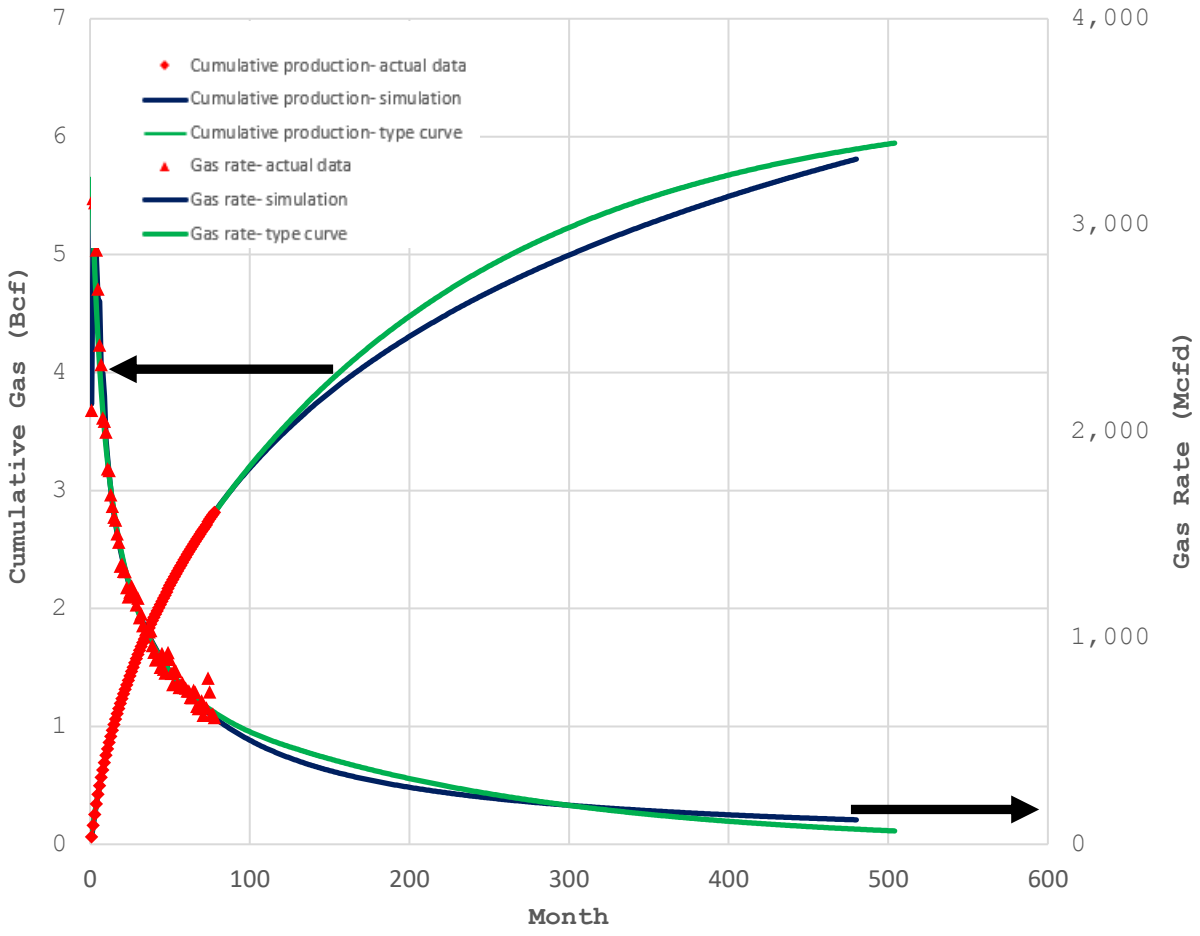

Fig. 4.8—Comparison of simulation gas rates vs. type curve and actual gas rates for the average completion with 24 Entry Points, 712 lb/ft, 4,838 ft

In Fig. 4.9, simulated gas rates of the mid-point completion design (blue line) are greater than actual gas rates and the type curve of Town field (red and green lines). The ratio of the B3 from simulation to B3 of the type curve is 1.5.

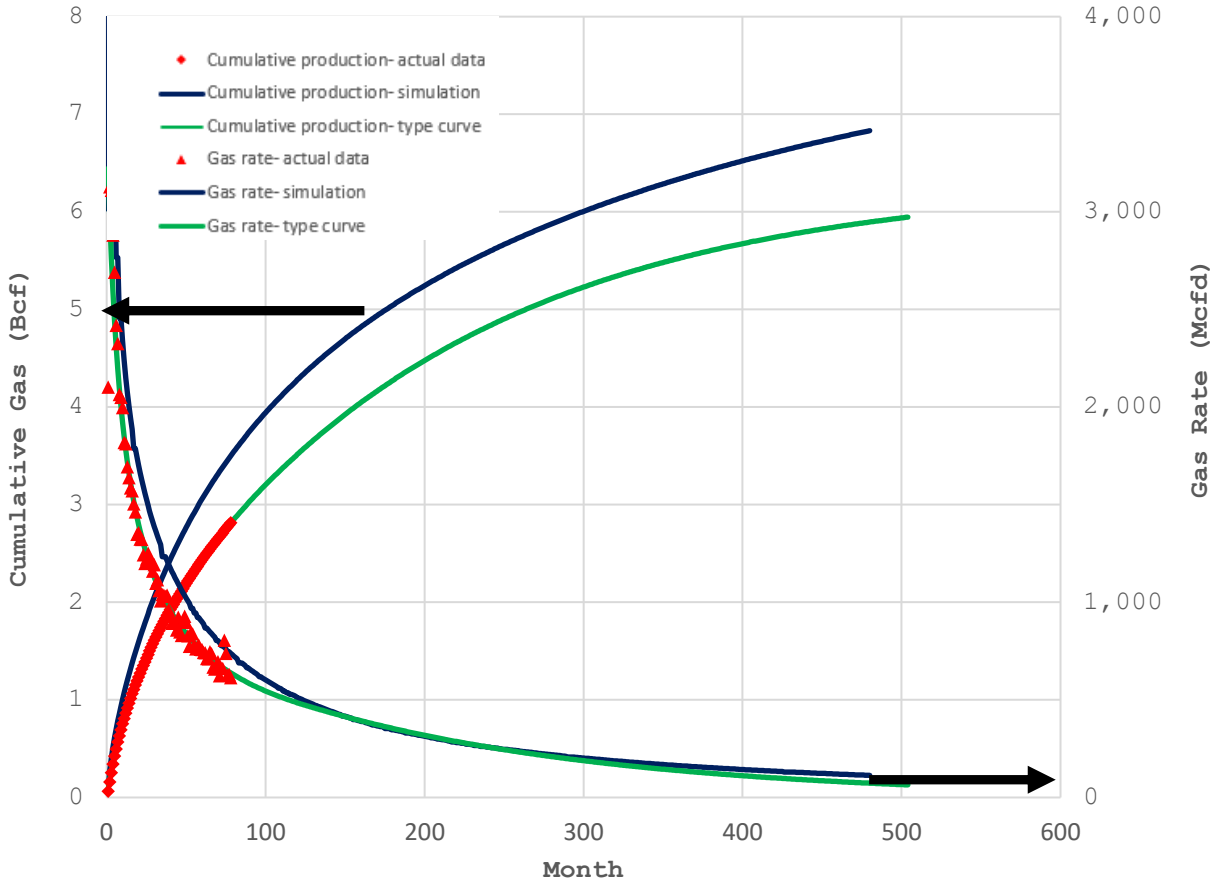

Fig. 4.9—Comparison of simulation gas rates vs. type curve and actual gas rates for the mid-point completion with 25 Entry Points, 942 lb/ft, 4,920 ft

In Fig. 4.10, simulated gas rates of the maximum completion design inside the current industry practices (blue line) are greater than actual gas rates and the type curve of Town field (red and green lines). The ratio of the B3 from simulation to B3 of the type curve is 2.3.

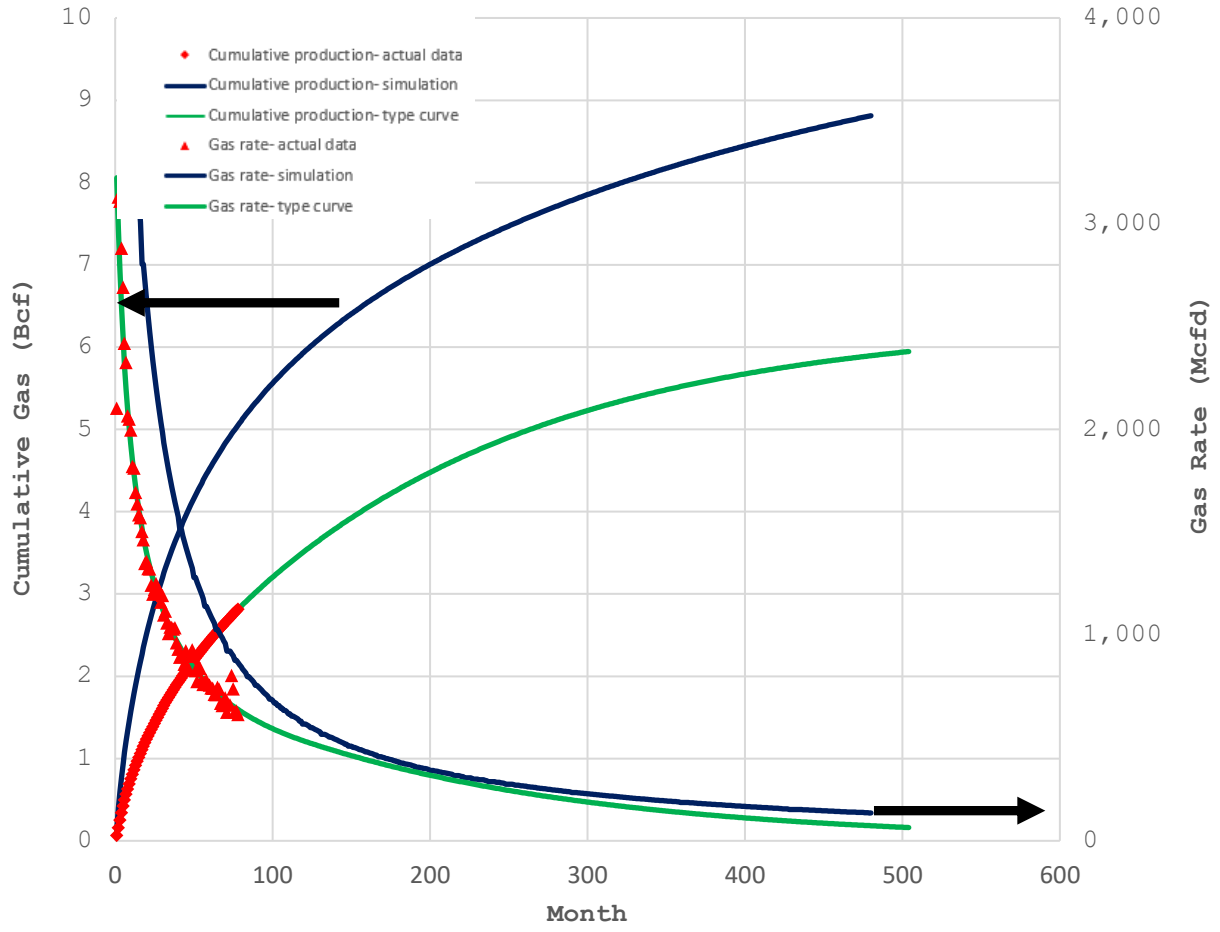

Fig. 4.10—Comparison of simulation gas rates vs. type curve and actual gas rates for the maximum completion with 50 Entry Points, 942 lb/ft, 6,560 ft

In Fig. 4.11, simulated gas rates of the mid-point completion design which is outside the space of current industry practices (blue line) are greater than actual gas rates and the type curve of Town field (red and green lines). The ratio of the B3 from simulation to B3 of the type curve is 3.3.

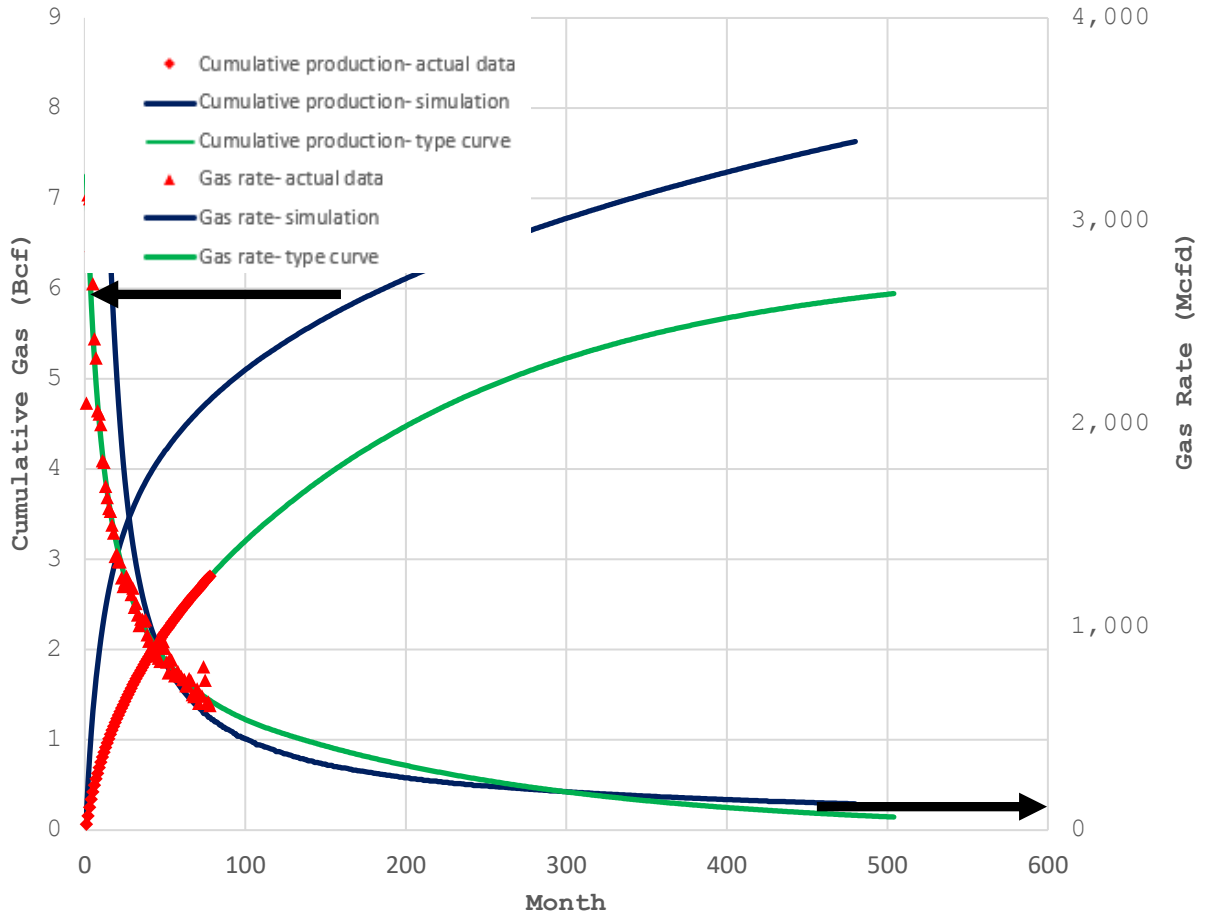

Fig. 4.11—Comparison of simulation gas rates vs. type curve and actual gas rates for the mid-point completion with 200 Entry Points, 1,413 lb/ft, 6,560 ft

In Fig. 4.12, simulated gas rates of the maximum completion design, which is outside the space of current industry practices (blue line), are greater than actual gas rates and the type curve of Town field (red and green lines). The ratio of the B3 from simulation to B3 of the type curve is 5.1.

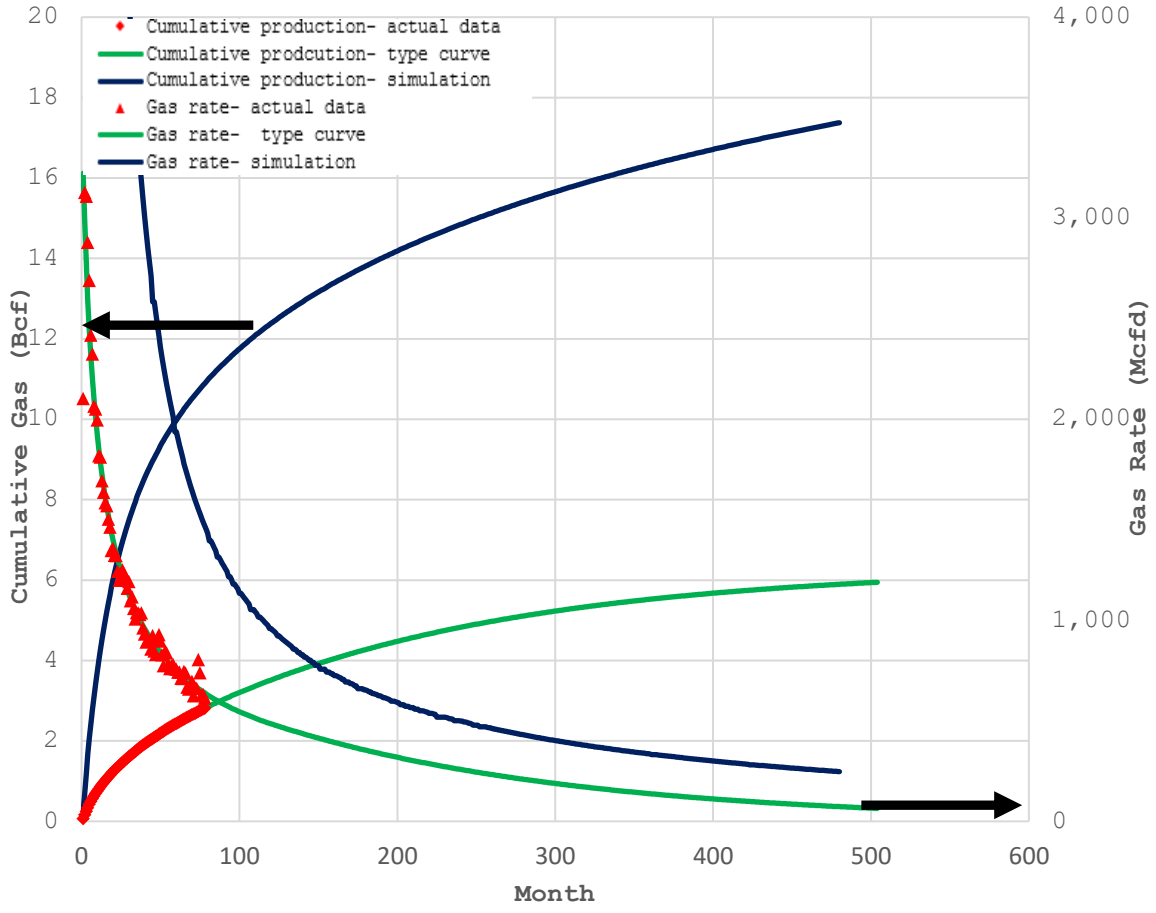

Fig. 4.12—Comparison of simulation gas rates vs. type curve and actual gas rates for the maximum completion with 400 Entry Points, 2,688 lb/ft, 13,12

CHAPTER 5 ECONOMIC ANALYSIS

In this chapter, the main objective is to identify an economic optimum completion for the upper Montney formation in the Town field in British Columbia, Canada. To perform the optimization a wide range of completion designs must be evaluated from cost, well performance and financial perspectives. I approximated the range of completion designs with 300 specific completion designs incorporating varying values of lateral length (3,280 to 13,120 ft), number of fracture entry points (10 to 400) and sand intensity (471 to 2,688 lb/ft). These ranges are defined in Chapter 2. In this chapter, I describe well-cost models for the completion and drilling costs that are applied to the 300 completion designs, resulting in well costs ranging from $3.5 to $14.6 MM for a commodity price of CAD$2/MMbtu. These well costs are combined with the predicted production performance calculated from the reservoir-simulation and multivariable-regression models to compute rate of return and present value to identify the economic optimum completion design. All monetary values are in CAD$ unless specifically noted otherwise.

5.1 Range of Completion Designs

The ranges of values for each completion design parameter as found in the existing wells in the Town field are shown in Table 3.11. This table lists the parameters used for the 300 completion designs evaluated in this study. There are 6 values for lateral length, 5 values for sand intensity and 10 values for fracture entry points. The completion technology in the 44 Town wells is ball-drop-sleeve. However, the completion technologies in the 300 cases in this chapter are a blend of plug-and-perf and ball-drop-sleeve technologies, since some of these cases have

400 entry points and it is not viable to complete a well with 400 entry points with ball-drop-sleeve technology.

The plug-and-perf system (Fig. 5.1) utilizes bridge plugs and perforation guns at specific intervals in a wellbore. This is the most common method of stimulating flow from low-permeability formations completed with horizontal wells in North America. The completion starts at the toe of the wellbore (the furthest end of the well), completing one stage at a time and moving from the toe towards the heel (where the wellbore begins to bend towards the vertical). Once the first stage is completed, a bridge plug is set inside the lateral to isolate the prior stage perforations from the about-to-be completed stage. Once the bridge plug is set, the perforation gun creates holes in the casing that penetrate the reservoir. Then hydraulic pressure is applied to the inside of wellbore, forcing fluid from the wellbore, through the perforations and into the rock. As the fluid is forced into the rock, the pressure builds until the rock fractures. As the fractures are created and extended by pumping additional fluid, proppant (sand or man-made sand-sized particles) is added to the fluid in order to fill and prop open the fractures in the rock. Once pumping stops, the fluid leaks off into the formation, leaving the propped fractures as conduits for flowing hydrocarbons from the formation to the wellbore. The propped fractures are much better conduits for flow than the unfractured formation. The bridge plug, perforation & fracturing process is then repeated for each stage until the entire lateral has been completed. Following the completion of the last stage, the plugs are drilled out to allow all stages to contribute to production.

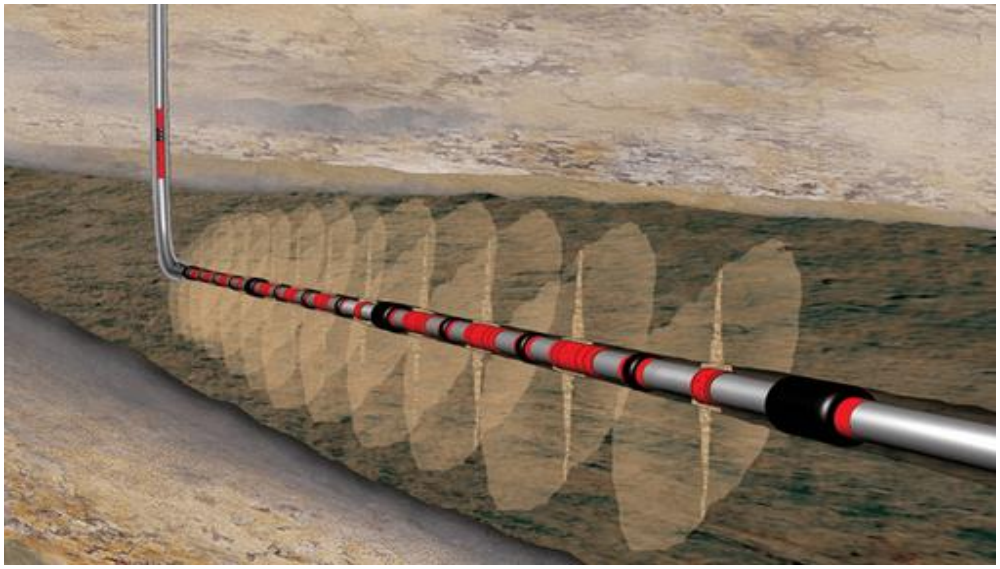

Fig. 5.1—Plug-and-perf system

The ball-drop-sleeve system (Fig. 5.2) uses balls that are dropped into the wellbore while pumping fluid to shift sliding sleeves in the lateral section, which allows communication with the reservoir at specific intervals. The balls are sized so that the stages are opened sequentially from toe to heel. This is a common completion practice in the Montney formation in Canada. To complete a single stage, a single ball of a specific size is pumped through the well until it seats in a restriction inside the wellbore that is sized specifically for that ball. When the ball seats, the wellbore is temporarily a closed system so hydraulic pressure builds until it is sufficient to shift the sleeve attached to the ball seat restriction. Shifting the sleeve exposes ports in the casing so that hydraulic pressure inside the well can push fluid through the ports and into the formation. Then the stage fluid and sand is pumped in the same manner as with a plug and perf stage. At the end of stage, a ball is pumped to seat and open the next sleeve. This is repeated until the entire lateral is completed. The balls dissolve with time and temperature. The advantage of the ball-drop-sleeve system is the elimination of running bridge plugs and perforation guns and the faster

completion times. The reduced cost of the completion with this system is roughly offset by the cost of the sleeves.

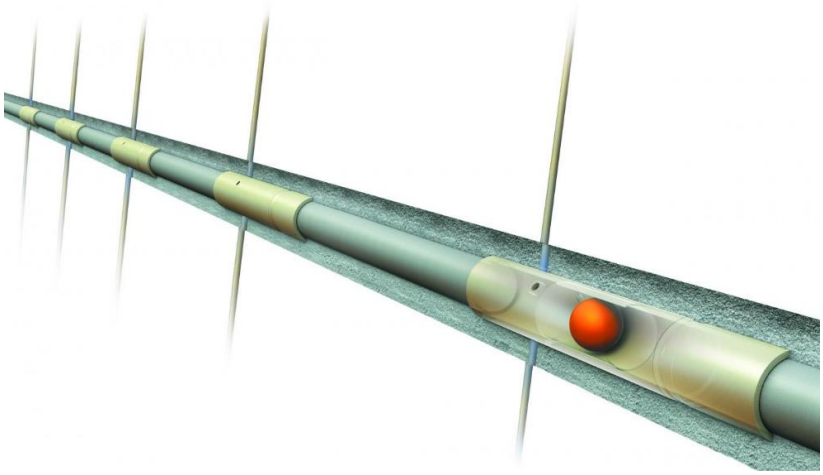

Fig. 5.2—Ball-drop-sleeve system

5.2 Drilling Costs Model

When considering the drilling operation and associated costs, it can conceptually be divided into several pieces to allow logical grouping of several operational and cost items:

1. The drilling of the wellbore segments: The vertical hole, the build segment where the inclination changes from vertical to horizontal and the lateral (horizontal) hole.
2. The hardware that is placed in the well (casing, sleeves, e.g.)
3. A variety of other costs that are independent of the actual drilling operation such as rig mobilization, logging, e.g.

In considering these groupings when creating a drilling cost model, two drilling-cost parameters that change with different completion designs are the lateral length and the number of completion stages. The lateral length dictates the time to drill the lateral, and the number of stages dictate the amount of stage-dependent hardware (sleeves and plugs) that will be utilized.

Thus, the model I used reflects those requirements. I do treat several items as constants that in practice are variables, such as the time to drill the vertical and build segments, rig mobilization, and de-mobilization cost, drilling day rates.

Due to the continuously-changing market for drilling, completion services and materials, one could find themselves in a never-ending cycle of attempting to stay current with local costs. Instead, I chose to fix those costs and let only the costs change that were due to specific changes in lateral length and stage count. Likewise, I assumed a single formation depth rather than model slightly different formation depths that would have had a small, but immaterial, impact on well cost.

The costs are positively correlated with commodity prices such that as commodity prices rise, the well costs also rise. For a 50% increase in the gas price, drilling and completion costs increase by 15%. CAD$2/MMbtu gas price is the commodity price associated with the stated costs in the various tables that showed the cost components in Section 5.1 and 5.2. Factor ComCost in the cost equations in section 5.1 and 5.2 represents the commodity price of gas. It is 1 for CAD$2/MMbtu, 1.15 for CAD$3/MMbtu and 1.30 for CAD$4/MMbtu.

The drilling cost model is comprised of four components as described below.

$$DrillCost = LatDrillCost + CasingCost + AddMatCost + MiscCost \quad (29)$$

where

$DrillCost = total\ drilling\ cost, \$$

$LatDrillCost = cost\ of\ drilling\ lateral, \$$

$CasingCost = cost\ of\ casing, \$$

$AddMatCost = \ cost\ of\ additional\ material, \$$

$MiscCost$

$= \ cost\ of\ misc\ (mobilization, demobalization, vertical\ \&\ build\ segements\ h$

$, cementing, logging, etc\ , \$$

The observed costs were provided by UGR and cost model was calibrated to local actual costs by UGR. The costs in Eq. 30 are calculated as follows:

1. Cost of drilling the lateral

$$LatDrillCost = \ LatDrillTime \ * \ DrillCostRate * ComCost, \quad (30)$$

where

$LatDrillCost \ = \ cost\ of\ drilling\ lateral, \$$

$LatDrillTime = \ number\ of\ days\ to\ drill\ lateral, day$

$DrillCostRate \ = daily\ drilling\ cost\ rate, \frac{\$}{day}$

$ComCost = commidity\ gas\ price\ factor, 1\ for\ CAD\$2/MMbtu$

I used a constant of $80,000 for the daily drilling rate. This daily rate includes the cost of the drilling rig, drilling mud, equipment rentals, manpower, fuel and numerous small consumables that are used during the drilling operation. The number of days to drill a lateral in the Town upper Montney is a nonlinear function of lateral length (Table 5.1).

Lateral length, ft	Drilling rate, ft/day	LatDrillTime, day
0-3,280	1,476	2.22
3,280-4,920	1,312	3.5
4,920-6,560	1,312	4.7
6,560-8,200	656	7.2
8,200-9,840	164	9.7
9,840-13,120	82	39.7

Table 5.1—Drilling pace in the lateral

Table 5.2 shows the cost to drill the lateral for the minimum, mid-point, and maximum completions. Cost of drilling lateral increases as the number of days to drill increase.

Completion parameters	DrillCostRate, $/day	LatDrillTime, day	LatDrillCost, $MM
Minimum Entry Points = 10 Sand Intensity = 471 lb/ft Lateral Length = 3,280 ft	80,000	2.22	0.18
Mid-point Entry Points = 200 Sand Intensity = 1,413 lb/ft Lateral Length =6,560 ft	80,000	4.7	0.37
Maximum Entry Points = 400 Sand Intensity = 2,688 lb/ft Lateral Length = 13,120 ft	80,000	39.7	3.17

Table 5.2—Cost of drilling lateral for the minimum, mid-point, and maximum completions for CAD$2/MMbtu

2. Cost of casing

The casing model presumes two sizes of casing are utilized in the well, 5-1/2” casing (large casing, internal diameter) to line the wellbore from surface to near the beginning of the horizontal section and 4-1/2” casing (small casing, internal diameter) that lines the wellbore from the end of the large casing to end of the lateral. The reason for using this casing arrangement is to reduce the well cost without creating an unacceptable amount of operational risk. The bigger the

hole, the easier it is to work in, but the more expensive it is to drill and case. Most operators in the Town field utilize this casing arrangement.

$$CasingCost = (SmallCasLen * UnitSmallCasCost + LargeCasLen * UnitLargeCasCost) * ComCost, \quad (31)$$

where

$CasingCost = cost\ of\ casing, \$$

$SmallCasLen = lateral\ length\ of\ small\ casing, ft$

$UnitSmallCasCost = cost\ of\ small\ casing, \frac{\$}{ft}$

$LargeCasLen = lateral\ length\ of\ large\ casing, ft$

$UnitLargeCasCost = cost\ of\ large\ casing, \frac{\$}{ft}$

$ComCost = commidity\ gas\ price\ factor, 1\ for\ CAD\$2/MMbtu$

In Eq. 31, I used a constant of 13.7 $/ft for the cost of small casing, a constant of 8,200 ft as an average estimated length of large casing, and a constant of 24.4 $/ft for the cost of the large casing. Table 5.3 shows the cost of the casing for the minimum, mid-point, and maximum completions.

Completion parameters	SmallCaseLen, ft	UnitSmallCasCos, $/ft	LargeCaseLen, ft	UnitLarge CasCost , $/ft	CasingCost, $MM
Minimum Entry Points = 10 Sand Intensity = 471 lb/ft Lateral Length = 3,280 ft	3,280	13.7	8,200	24.4	0.24
Mid-point Entry Points = 200 Sand Intensity = 1,413 lb/ft Lateral Length =6,560 ft	6,560	13.7	8,200	24.4	0.29
Maximum Entry Points = 400 Sand Intensity = 2,688 lb/ft Lateral Length = 13,120 ft	13,120	13.7	8,200	24.4	0.38

Table 5.3—Cost of casing for the minimum, mid-point, and maximum completions for CAD$2/MMbtu

3. Cost of additional material:

$$AddMatCost = NumStages * StageAddCost * ComCost, \quad (32)$$

where

$AddMatCost = cost\ of\ additional\ material, \$$

$NumStages = number\ of\ working\ stages\ in\ full\ lateral\ length$

$StageAddCost = cost\ of\ additional\ material\ per\ stage, \frac{\$}{stage}$

$ComCost = commidity\ gas\ price\ factor, 1\ for\ CAD\$2/MMbtu$

Eq. 32 calculates the cost of plugs used with the plug-and-perf technology or the cost of sleeves used in the ball-drop-sleeve technology. I used a constant of $10,000 per stage for the cost of these materials. The ball-drop-sleeves are run in the casing string at the time the well is cased while the plug-and-perf are run at the time of the completion. Many operators will include the cost of the plugs in the completion cost, but I choose to include them in the drilling costs so that the cost of wellbore-related hardware would appear in the same drilling category for the two technologies.

Table 5.4 shows the cost of additional material for the minimum, mid-point, and maximum completions.

Completion parameters	NumStages	StageAddCost, $/stage	AddMatCost, $MM
Minimum Entry Points = 10 Sand Intensity = 471 lb/ft Lateral Length = 3,280 ft	10	10,000	0.10
Mid-point Entry Points = 200 Sand Intensity = 1,413 lb/ft Lateral Length =6,560 ft	29	10,000	0.29
Maximum Entry Points = 400 Sand Intensity = 2,688 lb/ft Lateral Length = 13,120 ft	50	10,000	0.50

Table 5.4—Cost of additional material for the minimum, mid-point and maximum Completions for $CAD2/MMbtu

4. Cost of miscellaneous

$$MiscCost = (VertTime * DrillCostRate + MoveInRigUpCost) * ComCost \quad (33)$$

where

$MiscCost$
$= cost\ of\ miscellaneous(mobilization\ and\ demobilization\ , vertical\ hole\ costs), \$$
$VertTime = number\ of\ days\ for\ vertical, and\ build\ segmetn, day$
$DrillCostRate = daily\ drilling\ cost\ rate, \frac{\$}{day}$
$MoveInRigUpCost = move\ in\ and\ rig\ up\ cost, \$$
$ComCost = commidity\ gas\ price\ factor, 1\ for\ CAD\$2/MMbtu$

In Eq. 33, I used a constant of 15 days for the number of days in the Town field for the time to drill the vertical and build (the transition from the vertical to horizontal wellbore inclination) segments at an average daily cost rate of $74,667. This daily rate is less than the $80,000 per day used for the lateral drilling costs due to 4 of the 15 days being after total depth is

reached but before rig release where active drilling is not occurring and some rental equipment is not being used. I used a constant of $100,000 for the drilling rig move-in and rig-up costs and any other costs not included in this or other drilling categories. Table 5.5 **Table 5.5** shows the cost of miscellaneous items for the minimum, mid-point and maximum completions using the drilling cost model.

Completion parameters	VertTime, day	DrillCostRate, $/day	MiscCost, $MM
Minimum Entry Points = 10 Sand Intensity = 471 lb/ft Lateral Length = 3,280 ft	15	74,667	1.22
Mid-point Entry Points = 200 Sand Intensity = 1,413 lb/ft Lateral Length =6,560 ft	15	74,667	1.22
Maximum Entry Points = 400 Sand Intensity = 2,688 lb/ft Lateral Length = 13,120 ft	15	74,667	1.22

Table 5.5—Cost of miscellaneous for the minimum, mid-point, and maximum completions for CAD$2/MMbtu

The drilling-cost components, as well as total drilling costs, for the minimum, mid-point, and maximum completion parameters are presented in Table 5.6.

Completion parameters	LatDrillCost, $MM	CasingCost, $MM	AddMatCost, $MM	MiscCost, $MM	**DrillCost, $MM**
Minimum Entry Points = 10 Sand Intensity = 471 lb/ft Lateral Length = 3,280 ft	0.18	0.24	0.10	1.22	**1.74**
Mid-point Entry Points = 200 Sand Intensity = 1,413 lb/ft Lateral Length =6,560 ft	0.37	0.29	0.29	1.22	**2.17**
Maximum Entry Points = 400 Sand Intensity = 2,688 lb/ft Lateral Length = 13,120 ft	3.17	0.38	0.50	1.22	**5.27**

Table 5.6—Drilling cost components for the minimum, mid-point, and maximum completions for CAD$2/MMbtu

Table 5.7 and Fig. 5.3 present the drilling costs and total well costs (which are the sum of completion and drilling costs) for the minimum, mid-point, and maximum of completion designs parameters. The drilling costs increase as the completion parameters increase, as expected.

Completion parameters	Drilling cost, $MM	Total well cost, $MM
<u>Minimum</u> Entry Points = 10 Sand Intensity = 471 lb/ft Lateral Length = 3,280 ft	$1.74	$3.44
<u>Mid-point</u> Entry Points = 200 Sand Intensity = 1,413 lb/ft Lateral Length =6,560 ft	$2.17	$5.68
<u>Maximum</u> Entry Points = 400 Sand Intensity = 2,688 lb/ft Lateral Length = 13,120 ft	$5.27	$14.62

Table 5.7—Drilling and total costs for the minimum, mid-point and maximum, completions for CAD$2/MMbtu

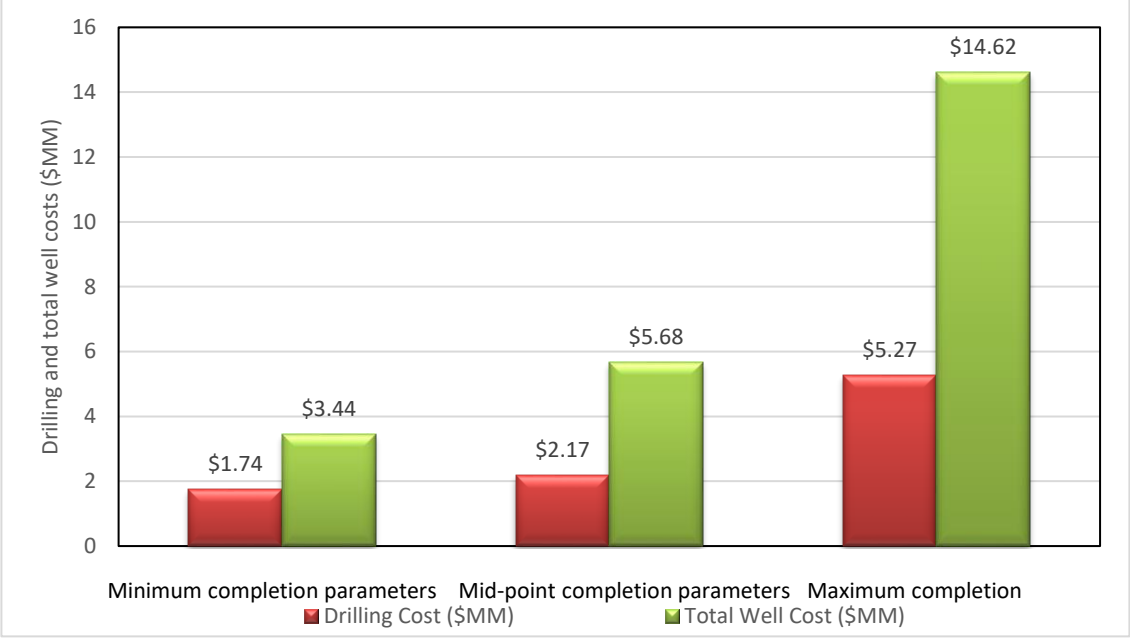

Fig. 5.3—Drilling and total well costs for CAD$2/MMbtu gas price

5.3 Completion Cost Model

The completion operation is performed on a stage-by-stage basis after the drilling rig has been removed from the well site. There are numerous cost items in a completion operation, but the largest individual items are the pumping charges and cost of chemicals, sand and water. There are also a variety of sand sieve sizes used in typical fracture treatment, and the use of resin-coated sand is common.

As the completion design changes, it usually manifests itself as changes to the number of stages and the amount of chemicals, sand, and water pumped into the well. The combination of number of stages and volume of sand and water will dictate how much time is required to complete the well. Since pumping charges are often based on hourly and/or day rates, one must compute the estimated number of days to complete the well in order to compute those pumping charges. Since chemicals, sand and water are sold on a volume basis; their cost can be easily computed from the volume times the unit cost.

As with the drilling cost model, the completion cost model treats a number of inputs as constant, such as the unit's costs for chemical, sand, and water, despite the business reality that those costs change on a regular basis. As such the completion cost model only provides for cost changes related to the time duration of the completion process and the volume of materials used in operation. There are several small cost items that are included in a miscellaneous category which also includes the pumping charges which is a large cost item by itself.

The completion cost model consists of five components as described below.

$$CompCost = WaterCost + ChemCost + 40/70Cost + 50/140ResCost + MiscCost \quad (34)$$

where

$CompCost = total\ completion\ cost, \$$

$WaterCost = cost\ of\ water, \$$

$ChemCost = cost\ of\ chemicals, \$$

$40/70Cost = cost\ of\ 40/70\ sand, \$$

$50/140ResCost = cost\ of\ 50/140\ and\ resin\ sand, \$$

$MiscCost$

$= cost\ of\ miscellaneous\ (not\ fracturing\ cost, equipment\ charges), \$$

The observed completion costs were provided by UGR, and the cost model was calibrated to local actual cost by UGR. The formula for each component in Eq. 34 is as follows:

1. Cost of water

$$WaterCost = NumStages * StageWatVol * UnitWatCost * ComCost, \quad (35)$$

where

$WaterCost = cost\ of\ water, \$$

$NumStages = number\ of\ working\ stages\ in\ full\ lateral\ length$

$StageWaterVol = volume\ of\ water\ per\ stages, \frac{bbl}{stage}$

$UnitWatCost = costs\ to\ source\ and\ truck\ water\ to\ well, \frac{\$}{bbl}$

$ComCost = commidity\ gas\ price\ factor, 1\ for\ CAD\$2/MMbtu$

In Eq. 35, the costs to source and truck water to a well in the Town field are $4.77/bbl. Table 5.8 shows costs of water for the minimum, mid-point, and maximum completions.

Completion parameters	NumStages	StageWaterVol, bbl/stage	WaterVol, bbl	UnitWatCost, $/bbl	WaterCost, $MM
Minimum Entry Points = 10 Sand Intensity = 471 lb/ft, Lateral Length = 3,280 ft	10	3,082	30,820	4.77	0.15
Mid-point Entry Points = 200 Sand Intensity = 1,413 lb/ft, Lateral Length =6,560 ft	29	6,376	184,904	4.77	0.88
Maximum Entry Points = 400 Sand Intensity = 2,688 lb/ft, Lateral Length = 13,120 ft	50	14,088	704,399	4.77	3.36

Table 5.8—Cost to source and truck water for the minimum, mid-point, and maximum completion for CAD$2/MMbtu

2. Cost of chemicals

$$ChemCost = NumStages * SatgeWaterVol * UnitChemCost * ComCost, \quad (36)$$

where

$ChemCost = cost\ of\ chemicals, \$$

$NumStages = number\ of\ working\ stages\ in\ full\ lateral\ length$

$StageWaterVol = volume\ of\ water\ per\ stages, \frac{bbl}{stage}$

$UnitChemCost = cost\ of\ chemicals\ to\ treat\ water, \frac{\$}{bbl}$

$ComCost = commidity\ gas\ price\ factor, 1\ for\ CAD\$2/MMbtu$

In Eq. 36, I used a constant cost of $1.79 per barrel of fracturing water for the cost of chemicals to treat the water. Those chemicals include biocides to kill bacteria and friction reducers to reduce friction losses in the tubular while pumping. Lower friction losses equate to lower surface pumping pressures which equate to lower pumping charges. Table 5.9 shows chemical costs for the minimum, mid-point and maximum completions.

Completion parameters	NumStages	StageWaterVol, bbl/stage	WaterVol, bbl	UnitChemCost, $/bbl	ChemCost, $MM
Minimum Entry Points = 10 Sand Intensity = 471 lb/ft, Lateral Length = 3,280 ft	10	3,082	30,820	1.79	0.05
Mid-point Entry Points = 200 Sand Intensity = 1,413 lb/ft, Lateral Length =6,560 ft	29	6,376	184,904	1.79	0.33
Maximum Entry Points = 400 Sand Intensity = 2,688 lb/ft, Lateral Length = 13,120 ft	50	14,088	704,399	1.79	1.25

Table 5.9—Cost of chemicals for the minimum, mid-point, and maximum completions for CAD$2/MMbtu

3. Cost of 40/70 sand

The 40/70 sieve size sand constitutes the majority of the sand used in the fracturing treatment. The completion cost model used for this work presumes each fracturing stage will also use 5 tonnes of 50/140 sand and 10 tonnes of resin-coated sand which is often 30/50 mesh size. When designing a completion, the overall design methodology only considers the total tonnage of sand, usually thought of as the sand intensity (lb/ft) multiplied by the completed lateral length (ft). As a result, a given completion design only specifies the total sand tonnage and the cost model then imposes the 50/140 and resin-coated sand assumptions. Therefore, the cost model starts with the total sand tonnage and subtracts the tonnage of 50/140 and resin-coated sand to determine the amount of 40/70 sand. The model also includes $150,000 miscellaneous costs which are related to sand trucking and sand storage equipment.

$$40/70Cost = \Big([StageTotalSandMass - Stage50/140SandMass - StageResSandMass] * NumStages * \frac{Unit40}{70Cost} + MiscTruckCost\Big) * ComCost, \quad (37)$$

where

$40/70Cost = cost\ of\ 40/70\ sand, \$$

$StageTotalSandMass = volume\ of\ sand\ per\ stage, \frac{lb}{stage}$

$Stage50/140SandMass = volume\ of\ 50/140\ sand\ per\ stage, \frac{lb}{stage}$

$StageResSandMass = volume\ of\ resin\ sand\ per\ stage, \frac{lb}{stage}$

$NumStages = number\ of\ working\ stages\ in\ full\ lateral\ length$

$$Unit40/70Cost = cost\ of\ 40/70\ sand, \frac{\$}{lb}$$

$$MiscTruckCost = cost\ of\ trucking\ and\ storage\ of\ sand, \$$$

$$ComCost = commidity\ gas\ price\ factor, 1\ for\ CAD\$2/MMbtu$$

In Eq. 37, volume of 50/140 sand is 11,023 lb/stage (5 tonnes/stage) and the volume of resin sand is 22,046 lb/stage (10 tonnes/stage). The cost of the 40/70 sand is $165/tonne which converts to $0.748/lb. I used a constant of $150,000 for miscellaneous cost which is for sand trucking and storage. Table 5.10 shows costs of 40/70 sand for the minimum, mid-point, and maximum completions.

Completion parameters	NumStages	StageTotSand Mass, lb/stage	TotSandMass, lb	Stage 50/140Sand Mass, lb/stage	50/140 SandMass, lb	Stage ResSand Mass, lb/stage
Minimum Entry Points = 10 Sand Intensity = 471 lb/ft, Lateral Length = 3,280 ft	10	154,324	1,543,240	11,023	110,230	22,046
Mid-point Entry Points = 200 Sand Intensity = 1,413 lb/ft, Lateral Length =6,560 ft	29	319,670	9,270,430	11,023	319,667	22,046
Maximum Entry Points = 400 Sand Intensity = 2,688 lb/ft, Lateral Length = 13,120 ft	50	705,479	35,273,950	11,023	551,150	22,046

Table 5.10—Cost of 40/70 sand for minimum, mid-point and maximum completions for CAD$2/MMbtu

Table 5.10 Continued.

Completion parameters	ResSandMass, lb	Stage40/70 Mass, lb/stage	40/70Mass, lb	Unit40/70 Cost, $/lb	MiscTruck Cost, $	**40/70 Cost, $MM**
Minimum Entry Points = 10 Sand Intensity = 471 lb/ft, Lateral Length = 3,280 ft	220,460	121,255	1,212,550	0.075	150,000	**0.24**
Mid-point Entry Points = 200 Sand Intensity = 1,413 lb/ft, Lateral Length =6,560 ft	639,334	286,601	8,311,429	0.075	150,000	**0.77**
Maximum Entry Points = 400 Sand Intensity = 2,688 lb/ft, Lateral Length = 13,120 ft	1,102,300	672,410	33.620,500	0.075	150,000	**2.67**

4. Cost of resin and 50/140 sand

$$50/140ResCost = NumStages * (Stage50/140SandMass + StageResSandMass) * Unit50/140ResSandCost * ComCost, \quad (38)$$

where

$$50/140ResCost = cost\ of\ resin\ and\ 50/140\ sand, \$$$

$$NumStages\ =\ number\ of\ working\ stages\ in\ the\ full\ lateral$$

$$Stage50/140SandMass = volume\ of\ 50/140\ sand\ per\ stage, \frac{lb}{stage}$$

$$StageResSandMass\ = volume\ of\ resin\ sand\ per\ stage, \frac{lb}{stage}$$

$$\frac{Unit50}{140ResSandCost} = cost\ of\ \frac{50}{140} sand\ and\ resin\ sand, \frac{\$}{lb}$$

$$ComCost = commidity\ gas\ price\ factor, 1\ for\ CAD\$2/MMbtu$$

In Eq. 38, volume of 50/140 sand is 11,023 lb/stage (5 tonnes/stage) and the volume of resin sand is 22,046 lb/stage (10 tonnes/stage). I used a constant of 0.184 $/lb for the cost of resin and 50/140 sand. Table 5.11 shows the costs of other sand for the minimum, mid-point, and maximum completions.

Completion parameters	Num Stages	Stage 50/140SandMass, lb/stage	StageRes SandMass, lb/stage	Unit50/140 ResSandCost, $/lb	50/140 ResSandCost, $MM
<u>Minimum</u> Entry Points = 10 Sand Intensity = 471 lb/ft, Lateral Length = 3,280 ft	10	11,023	22,046	0.184	0.06
<u>Mid-point</u> Entry Points = 200 Sand Intensity = 1,413 lb/ft, Lateral Length =6,560 ft	29	11,023	22,046	0.184	0.18
<u>Maximum</u> Entry Points = 400 Sand Intensity = 2,688 lb/ft, Lateral Length = 13,120 ft	50	11,023	22,046	0.184	0.30

Table 5.11—Cost of 50/140 and resin sand for minimum, mid-point and maximum completions for CAD$2/MMbtu

5. Cost of miscellaneous elements

Miscellaneous cost is variety of costs that happens during the days that all stages of a completion design are being completed. Therefore, to calculate miscellaneous cost, I should calculate the number of days that it takes to complete all stages in a completion design. To calculate the number of days to complete all stages in a completion design, first, I calculated the number of minutes that takes to complete one stage using slurry volume and injection rate. Second, I calculated the number of stages that can be completed in one day given the fact that completion and fracturing equipment is available 12 hours per day. Third, I calculated the number of days that it takes for all stages to be completed in one completion design. For example, for minimum completion design with 10 entry points, slurry volume of 3,390 bbl and injection rate of 53.4 bbl/min, it takes 123 minutes to complete one stage. Given that the completion and fracturing equipment is only available 12 hours a day, 5.8 stages can be completed per day. Therefore, to complete all 10 stages in this design, it takes 1.7 days. With 1.7 days that it takes to complete a well with minimum completion design and miscellaneous daily rate of $25,264$, it costs $42,948, which will be add up to $1,151,600 cost of truck and rental and result in MM$1.19.

To calculate miscellaneous cost, first I calculate the number of minutes it takes to complete one stage using equation 39:

$$StageTime = \left(\frac{StageSlurryVolume}{InjRate}\right) + BetStageTime, \quad (39)$$

where

$$StageTime =$$

$$calculated\ number\ of\ minutes\ required\ for\ each\ stage, min/stage$$

$$StageSlurryVolume\ = volume\ of\ slurry, \frac{bbl}{stage}$$

$$InjRate\ = number\ of\ minutes\ between\ stages, min$$

Number of minutes between stages is 60 minutes. To calculate slurry volume, I multiplied the volume of water per stage by a constant of 1.1. The injection rate is a constant of 53.4 bbl/min. Calculated number of minutes per stage for minimum, mid-point n and maximum completion designs is in Table 5.12 is derived from Eq. 39.

Completion parameters	StageWaterVolume, bbl/stage	VolSlurry, bbl	InjRate, bbl/min	StageTime, min/stage
Minimum Entry Points = 10 Sand Intensity = 471 lb/ft, Lateral Length = 3,280 ft	3,082	3,390	53.4	123
Mid-point Entry Points = 200 Sand Intensity = 1,413 lb/ft, Lateral Length =6,560 ft	6,376	7,013	53.4	191
Maximum Entry Points = 400 Sand Intensity = 2,688 lb/ft, Lateral Length = 13,120 ft	14,088	15,497	53.4	350

Table 5.12—Calculated minutes per stage for the minimum, mid-point, and maximum completions for CAD$2/MMbtu

After calculating number of minutes that takes to complete one stage, I calculated the number of stages that can be completed in one day, given that completion and fracturing equipment is available for 12 hours a day.

$$StageCompRate = \frac{EquipAvailFrac}{StageTime} \quad (40)$$

where

$$StageCompRate = completed\ number\ of\ stages\ per\ day, stage/day$$

$$EquipAvailFrac = fracturing\ equipment\ availability, hr/day$$

$$StageTime = calculated\ number\ of\ minutes\ required\ for\ each\ stage, min/stage$$

Number of hours that fracturing equipment is available per day is 12 and calculated minutes per stage was computed in Table 5.12. Number of stages that can be completed in a day for minimum, mid-point and maximum completion design is in Table 5.13 using Eq. 40.

Completion parameters	EquipAvailFrac, Hr/day	StageTime, Min/stage	StageCompRate, stage/day
<u>Minimum</u> Entry Points = 10 Sand Intensity = 471 lb/ft, Lateral Length = 3,280 ft	12	123	5.80
<u>Mid-point</u> Entry Points = 200 Sand Intensity = 1,413 lb/ft, Lateral Length =6,560 ft	12	191	3.80
<u>Maximum</u> Entry Points = 400 Sand Intensity = 2,688 lb/ft, Lateral Length = 13,120 ft	12	350	2.06

Table 5.13— Calculated number of stages per day and number of fracturing days for the minimum, mid-point, and maximum completions for CAD$2/MMbtu

Then I calculated the number of days that it takes to fracture all stages in a completion design by using Eq. 41.

$$FracCompTime = \frac{NumStages}{StageCompRate} \quad (41)$$

where

$$FracCompTime$$

$$= \ calculated\ number\ of\ days\ takes\ to\ fracture\ and\ complete\ a\ well, day$$

$$StageCompRate = \ completed\ number\ of\ stages\ per\ day, stage/day$$

$$NumStages \ = \ number\ of\ working\ stages\ in\ the\ full\ lateral$$

Number of days that takes to complete all stages for minimum, mid-point and maximum are in Table 5.14. Completed number of stages per day was computed in Table 5.13.

Completion parameters	NumStages	StageCompRate, Stage/day	FracCompTime, day
<u>Minimum</u> Entry Points = 10 Sand Intensity = 471 lb/ft, Lateral Length = 3,280 ft	10	5.80	1.7
<u>Mid-point</u> Entry Points = 200 Sand Intensity = 1,413 lb/ft, Lateral Length =6,560 ft	29	3.80	7.70
<u>Maximum</u> Entry Points = 400 Sand Intensity = 2,688 lb/ft, Lateral Length = 13,120 ft	50	2.06	24.30

Table 5.14— Calculated number of stages per day and number of fracturing days for the minimum, mid-point, and maximum completions for CAD$2/MMbtu

Finally, miscellaneous cost is calculated using number of days to fracture all stages in a completion design from Table 5.14 as well as miscellaneous daily rate and cost of trucking and rental.

$$MiscCost = (MiscCostRate * FracCompTime \ + \ RentCost) * ComCost\ , \qquad (42)$$

where

$MiscCost = cost\ of\ miscellaneous, \$$

$MiscCostRate = miscellaneous\ daily\ rate, \frac{\$}{day}$

$FracCompTime$

$= \ calculated\ number\ of\ days\ takes\ to\ fracture\ and\ complete\ a\ well, day$

$RentCost = cost\ of\ rental\ and\ testing, \$$

$ComCost = commidity\ gas\ price\ factor, 1\ for\ CAD\$2/MMbtu$

In Eq. 42, I used a constant of 25,264 $/day for miscellaneous daily rate and a constant of 1,151,600 $ for trucking, rental and testing costs. Table 5.15 shows costs of miscellaneous for the minimum, mid-point, and maximum completions.

Completion parameters	FracCompTime, day	MiscCostRate, $/day	RentCost, $	MiscCost, $MM
<u>Minimum</u> Entry Points = 10 Sand Intensity = 471 lb/ft, Lateral Length = 3,280 ft	1.70	25,264	1,151,600	1.19
<u>Mid-point</u> Entry Points = 200 Sand Intensity = 1,413 lb/ft, Lateral Length =6,560 ft	7.70	25,264	1,151,600	1.35
<u>Maximum</u> Entry Points = 400 Sand Intensity = 2,688 lb/ft, Lateral Length = 13,120 ft	24.30	25,264	1,151,600	1.77

Table 5.15—Cost of miscellaneous for the minimum, mid-point, and maximum completions for CAD$2/MMbtu

Table 5.16 shows completion component costs as well as total completion cost.

Completion parameters	WaterCost, $MM	ChemicalCost, $MM	40/70 Cost, $MM	50/140ResCost, $MM	MiscCost, $MM	CompCost, $MM
Minimum Entry Points = 10 Sand Intensity = 471 lb/ft, Lateral Length = 3,280 ft	0.15	0.05	0.25	0.06	1.19	**1.70**
Mid-point Entry Points = 200 Sand Intensity = 1,413 lb/ft, Lateral Length =6,560 ft	0.88	0.33	0.77	0.18	1.35	**3.51**
Maximum Entry Points = 400 Sand Intensity = 2,688 lb/ft, Lateral Length = 13,120 ft	3.36	1.25	2.67	0.30	1.77	**9.35**

Table 5.16—Completion components for the minimum, mid-point and maximum completions for CAD$2/MMbtu gas price

Table 5.17 and Fig. 5.4 present the completion costs for the minimum, mid-point and maximum completion parameters used in the range of designs that were evaluated. The completion costs increase as the completion parameters increase.

Completion parameters	Completion cost, $MM	Total well cost, $MM
<u>Minimum</u> Entry Points = 10 Sand Intensity = 471 lb/ft Lateral Length = 3,280 ft	1.70	3.44
<u>Mid-point</u> Entry Points = 200 Sand Intensity = 1,413 lb/ft Lateral Length =6,560 ft	3.51	5.68
<u>Maximum</u> Entry Points = 400 Sand Intensity = 2,688 lb/ft Lateral Length = 13,120 ft	9.35	14.62

Table 5.17—Completion and total well costs for CAD$2/MMbtu gas price

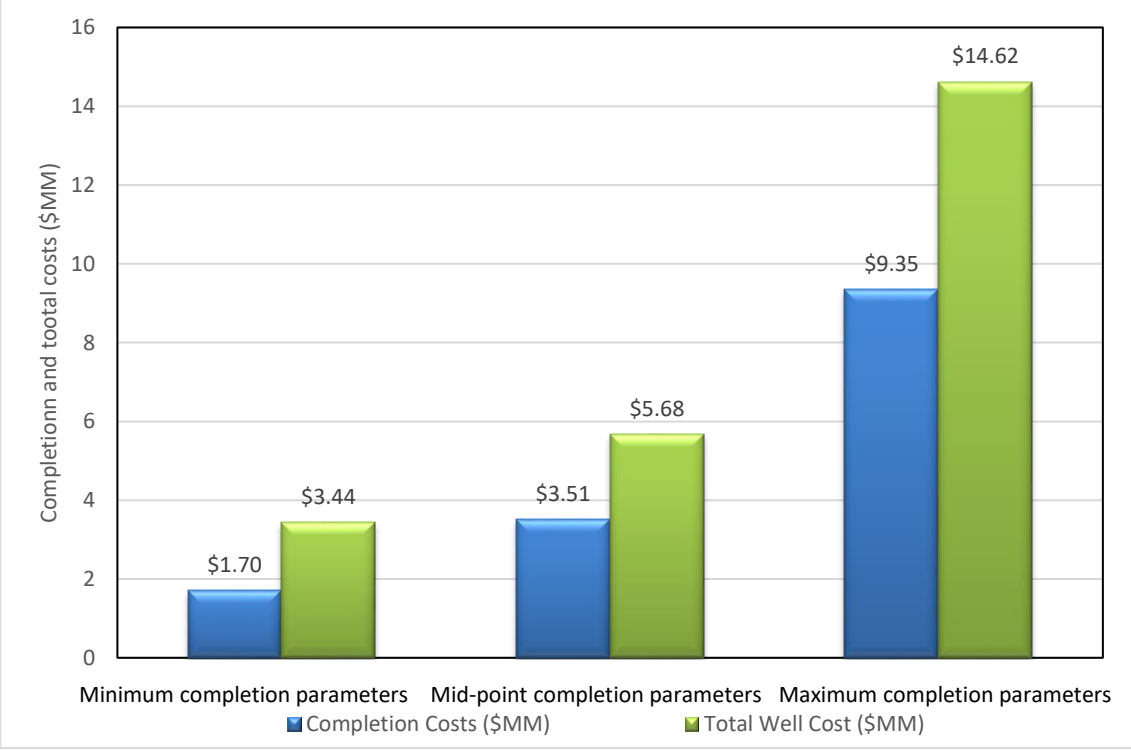

Fig. 5.4—Completion and total well cost for CAD$2/MMbtu gas price

The summary of drilling and completion costs for the minimum, mid-point, and maximum completions are in Fig. 5.5 and Table 5.18.

Completion parameters	Completion cost, $MM	Drilling cost, $MM	Total well cost, $MM
Minimum Entry Points = 10 Sand Intensity = 471 lb/ft Lateral Length = 3,280 ft	1.70	1.74	3.44
Mid-point Entry Points = 200 Sand Intensity = 1,413 lb/ft Lateral Length =6,560 ft	3.51	2.17	5.68
Maximum Entry Points = 400 Sand Intensity = 2,688 lb/ft Lateral Length = 13,120 ft	9.35	5.27	14.62

Table 5.18—Completion, drilling and total well costs for CAD$2/MMbtu gas price

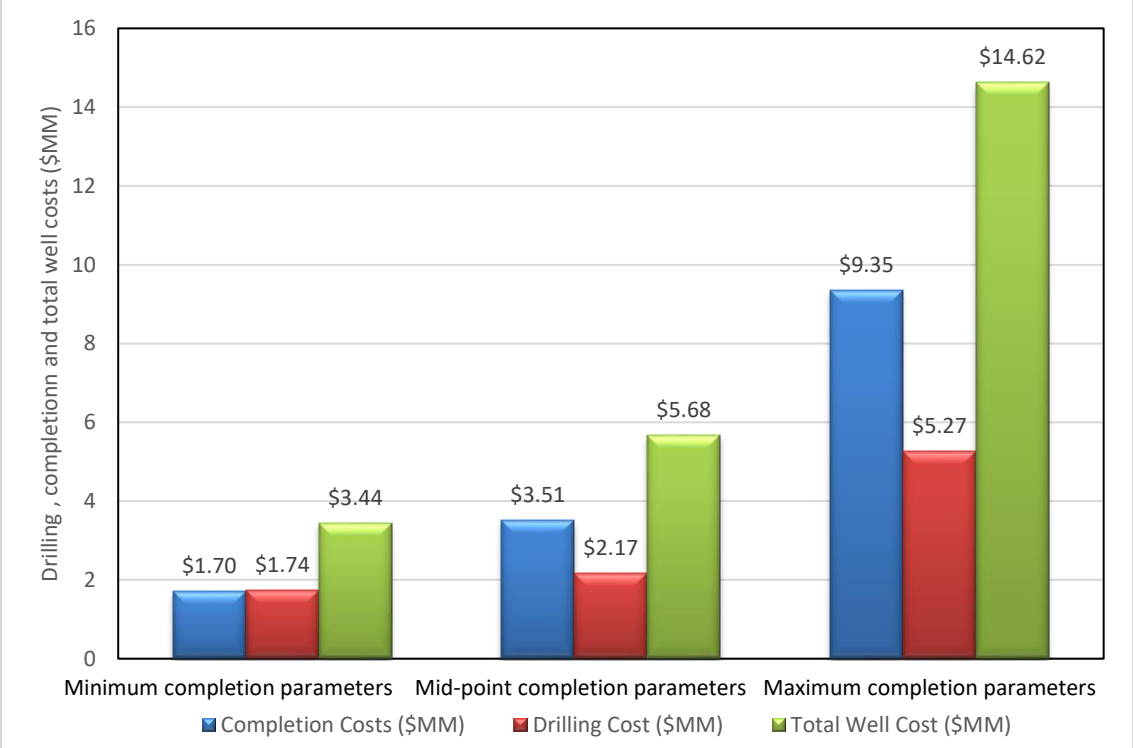

Fig. 5.5—Completion, drilling and total well costs for CAD$2/MMbtu gas price

The total well costs for different lateral lengths and entry points are shown in Fig. 5.6 and Fig. 5.7 with the sand intensity of 2,688 lb/ft. The total well costs are the same for reservoir simulation and regression methods.

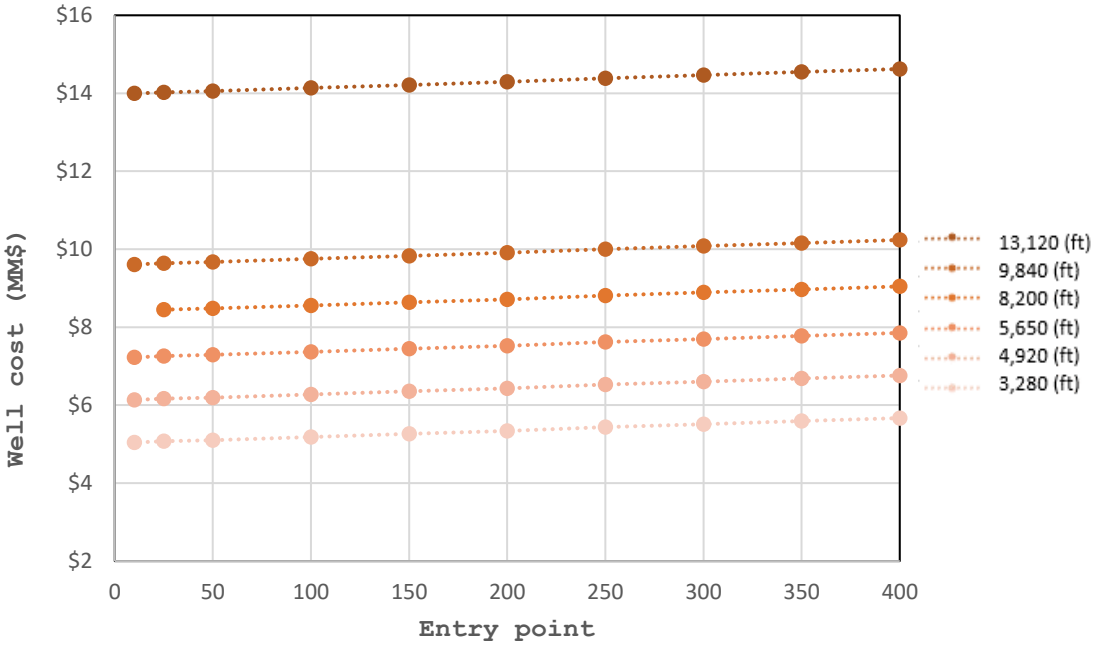

Fig. 5.6—Total well cost vs. entry points for different lateral lengths for CAD$2/MMbtu

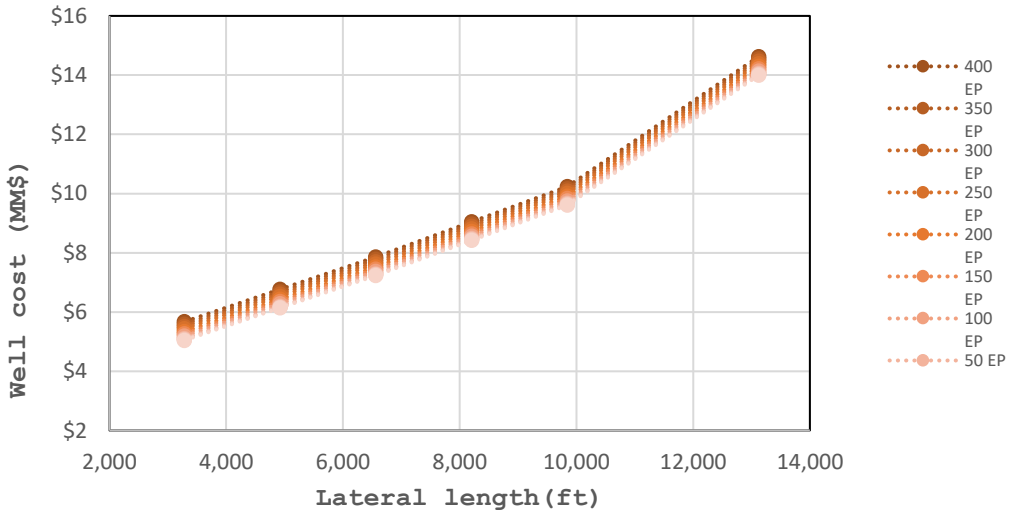

Fig. 5.7—Total well cost vs. lateral length for different entry points for CAD$2/MMbtu

Table 5.19 includes all the other economic inputs, such as variable operating costs, for calculating PV10 and ROR. The inputs were obtained from UGR. The economic analyses use July 1, 2018, as an effective date. The stated commodity prices are adjusted to AECO hub prices. AECO stands for Alberta Energy Company and is a Canadian hub. In this analysis, gas prices are CAD$2/MMbtu, CAD$3/MMbtu or CAD$4/MMbtu; the oil price is CAD$81.25/STB, and the condensate price is CAD$87.5/bbl. The fixed operating cost is CAD$6,500 well/month, working interest is 100%, and royalty before and after payout is 8%. A tie-in cost of CAD$400,000 per well is included in the economic analysis. The 10% royalty rate is used to approximate the sliding-scale royalties in British Columbia that vary as a function of commodity prices, production rates and eligible royalty holidays (royalty reductions that wells in Town should qualify). Actual royalties will be lower than 10% in the early life of the well, higher than 10% later in the well life and should average roughly 10% over the well life for completion designs typical of the historic completion in the Town field.

ECONOMIC INPUTS

AECO HUB GAS PRICES

Effective Date	
Starting Year	2018
starting Month	7
Gas Shrinkage	8.0%

Operating Costs (CAD)		
Fixed	$6,500	/Well/Month
Variable Gas	$1.00	/Mcf
Variable Oil	$0.00	/STB
Variable Cond	$0.00	/bbl
Water Disposal	$1.00	/bbl

Product Prices (CAD)		
Gas	$2.00	/MMbtu
Oil	$81.25	/STB
Cond/NGL	$87.50	/bbl

Price Escalation Rate: 0.000% /year 1.00000

Capital Costs (CAD)		
Drilling and Completion	$3,440,858	/well
Tie-In	$400,000	/well
Abandonment	$50,000	/well
Facilities	$0	

Gas Content	1.10	MMbtu/Mcf
Oil Gravity Price Adjustment	$0.00	/STB

Basis Differential (CAD)		
Gas	-$0.30	/MMbtu
Oil	$0.00	/STB
Cond/NGL	-$15.00	/bbl

Ownership		
	Before Pay Out	After Pay Out
WI	100.00%	100.00%
Royalty	10.00%	10.00%
Override	0.00%	0.00%

1 Boe = 6 Mcfe

Wellhead Prices (CAD)		
Gas	$3.70	/MMbtu
Cond/NGL	$72.50	/bbl

Table 5.19—Economic inputs

5.4 Economic Analysis Using the Regression Analysis-Based Production Forecast

In this section, I used the production forecast model derived from the regression analysis found in Chapter 3 as an input for economic analysis on the 300 completion designed sets. To conduct the economic analysis, I first calculated a B3 for each of the 300 different completion

designs using the equation shown in (Table 5.20). Thus, each completion design had an associated B3 value from which a production forecast was constructed. This equation was derived using multivariable regression as described in Chapter 3.

Per fluid model	$(B3.Fluid)^{(1.1)} = 2.8 * Sand.Fluid^{1.38} + 0.81 * LL.Fluid^{0.33} + 0.11 * EP.Fluid^{0.33} - 0.28$

Table 5.20—Per-fluid model from regression

Then I converted the B3 to a 40-year monthly production forecast by scaling the Town Field production type curve (Fig. 5.8). The scaling is performed by multiplying the monthly production values by a scale ratio, where the scale ratio is calculated as follows:

$$Scale\ Ratio = \frac{B3\ (calculated\ from\ multivariable\ regression)}{B3\left(Production\ type\ curve\ in\ the\ Town\ field, \frac{Mcf}{day}\right)} \quad (43)$$

The B3 in the denominator of Eq. 43 is the best three consecutive months of type curve production in the Town field (3,039, Mcfed). The impact of the scaling process is illustrated in Fig. 5.8. The scaling factor for the graph is shown in Eq. 44.

$$Scale\ Ratio = \frac{6{,}080\ Mcfed}{3{,}039\ Mcfed} = 2 \quad (44)$$

In Fig. 5.8, the red line is the initial type curve with B3 of 3,039 Mcfed, and the blue line is the scaled type curve with B3 of 6,080 Mcfed. The scaled factor which is shown with the red arrow is 2.

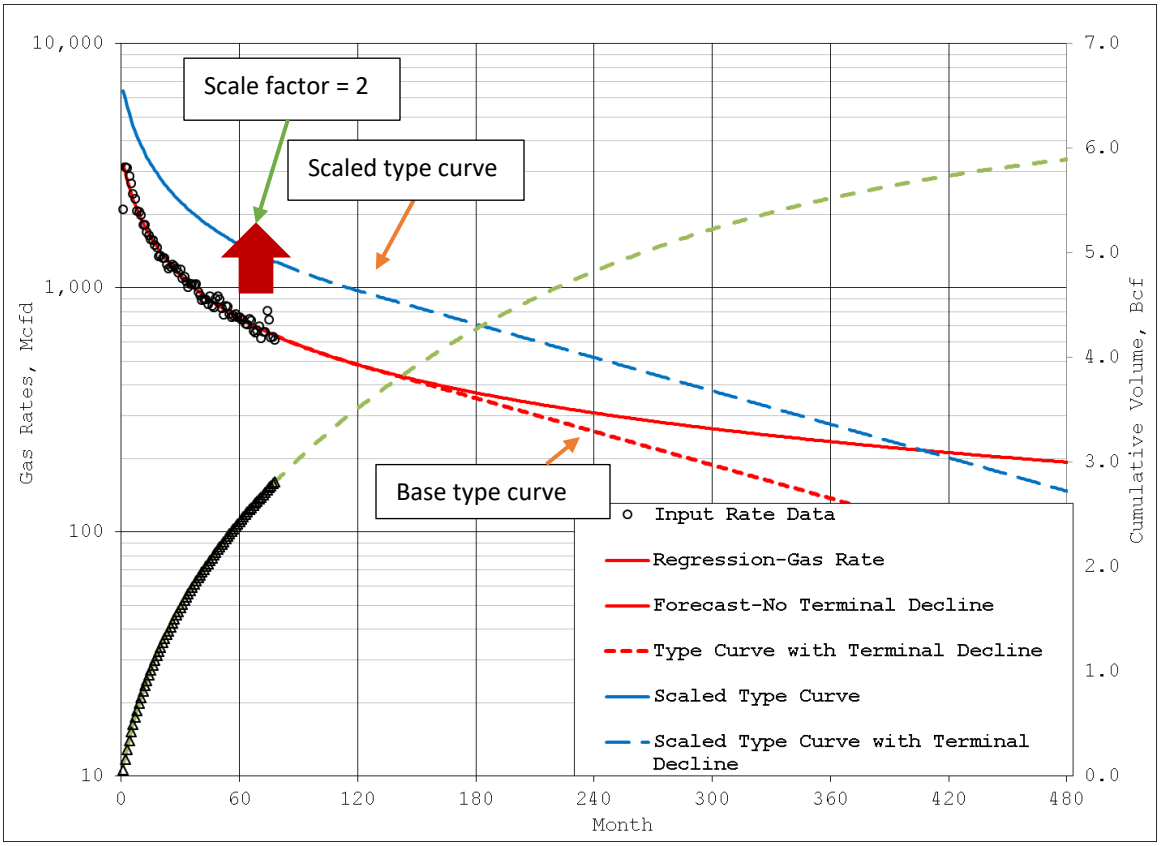

Fig. 5.8—Decline of production type curve in the Town field

The scaling ratios of the B3 from regression to the B3 from the Town field production type curve for the minimum, mid-point, and maximum completions parameters for regression methodology are in Fig. 5.9.

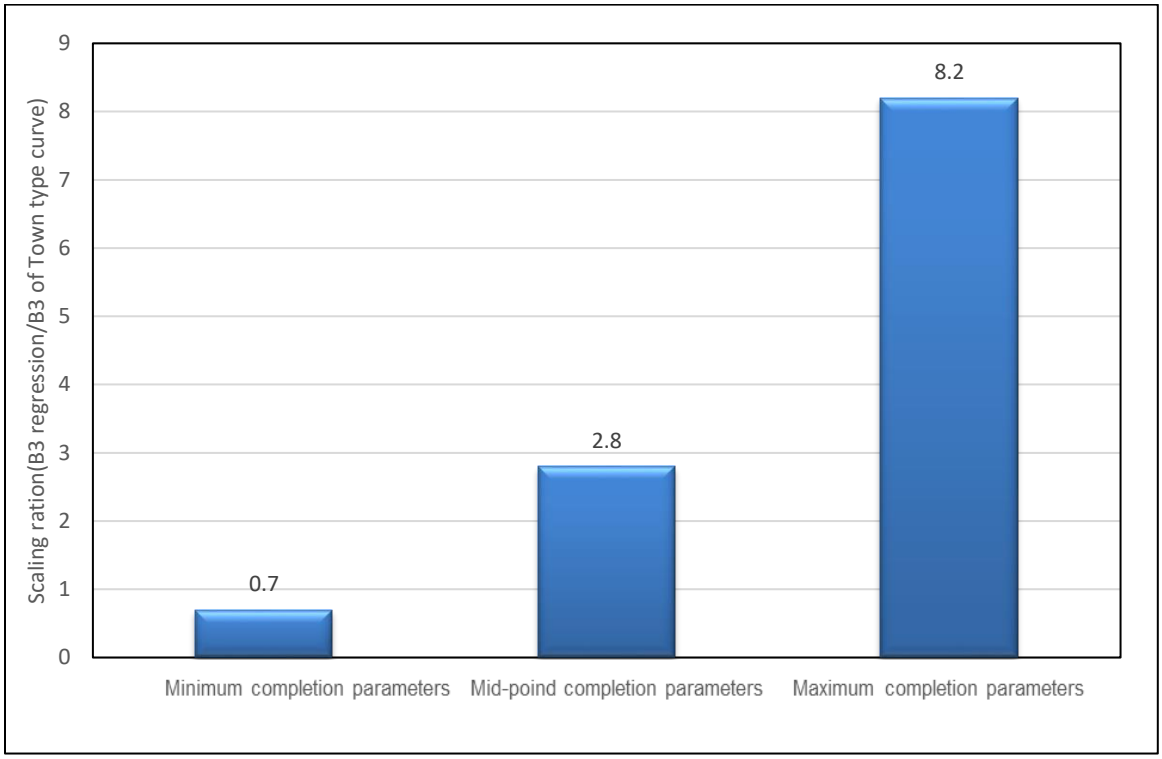

Fig. 5.9—The scaling ratio of the B3 from regression to the B3 from type curve for the minimum, mid-point and maximum completions parameters

The production type curve for the Town field was scaled for each of the 300 different completion designs as discussed above, generating a 40-year monthly production forecast of the gas phase for each completion design. I then used the 40-year monthly production forecasts with the specific completion design well costs for the economic analysis of each of the 300 completion designs. I computed the rate of return and PV10 of 300 completions and identified the one that yields the highest rate of return and PV10.

5.5 Economic Analysis Using Reservoir Simulation Model

Section 5.4 used multivariable regression to determine the B3 and scaled monthly production forecast to be input into the economic analysis. In this section, I used a reservoir simulation model to determine the monthly production forecast for use in the economic optimization assessment. To generate monthly production forecasts from the simulation model, I first calculated the estimated propped fracture half-length created by each of the 300 completion designs. This was performed by using a series of equations that computed the fracture surface area, fracture width and propped fracture half-length from the pumped vs. slurry volume as shown in Eq. 45, Eq. 46, Eq. 47 and Eq. 48. These equations were derived from regression analysis of a matrix of FracPro runs provided by UGR that modeled fracture dimensions as a function of slurry for the Upper Montney in the Town field.

With the known slurry volume per stage (Vs, ft) and number of entry points per stage (PC), the propped fracture width (w) is computed with equation 40 below. Equations were provided by UGR.

$$w = aVs^{b}PC^{C} \tag{45}$$

Constants a, b and c in are:

a = 0.0091
b = 0.1735
c = -0.415

Then I calculated fluid efficiency (FE) as a function of Vs, PC, and constants a, b and c:

$$FE = (aVs + b) * \frac{PC^{c}}{100}, \tag{46}$$

where

a = -0.0008
b = 93.223
c = -0.06

I next calculated the total propped surface area of all fracture(s) per stage, A_f, ft^2. A_f is calculated using fluid efficiency, total slurry volume and propped fracture width:

$$A_f = FE * \frac{Total\ Slurry\ Volume\ (Vs,ft3)}{Propped\ Fracture\ Width\ (w,ft)} \quad (47)$$

The assumption is $\frac{H}{L}$ = 0.75 where H is fracture height and L is propped fracture half-length. This assumption is provided by UGR. Propped fracture half-length is calculated as the following:

$$Propped\ Fracture\ Half-length = \frac{Af}{2 * 2 * PC * H} \quad (48)$$

In Eq. 48, we divide the total propped area by 2*2 to account for the fracture having two faces and being propped in two directions from the wellbore. Table 5.21 shows fracture parameters for the minimum, mid-point, and maximum of completion parameters.

Completion parameters	Slurry volume per stage (Vs), bbl/stage	Entry point per stage (PC)	Slurry volume per entry point, bbl/PC	Sand per entry point, lb/PC	Propped width, ft	Fluid efficiency (FE)	Propped surface area (Af), ft^2	Propped half-length, ft
Minimum Entry Points = 10 Sand Intensity = 471 lb/ft Lateral Length = 3,280 ft	3,117	1	3,117	70,000	0.03	0.90	4,321,906	380
Mid-point Entry Points = 200 Sand Intensity = 1,413 lb/ft Lateral Length =6,560 ft	6,450	6	1,075	21,000	0.02	0.78	44,035,761	271
Maximum Entry Points = 400 Sand Intensity = 2,688 lb/ft Lateral Length = 13,120 ft	14,251	8	1,781	40,000	0.05	0.82	68,438,882	345

Table 5.21—Fracture parameters for minimum, mid-point, and maximum completion parameters

With the calculated propped fracture half-length and fracture width, I ran the simulation model described in Chapter 4 on the different 300 completion designs in CMOST (reservoir simulation software). By selecting the grid size in both *i* and *j* directions, the desired fracture half-length and fracture width are made for each completion design. The grid size dimension is based on well spacing of 1,312 ft and initial entry point spacing of 211 ft. Maximum fracture half-length is half of the well spacing since I assumed there is no communication between two neighbor wells.

I performed the economic analysis using the calculated 40-year monthly production volumes of gas from the simulation-based model for each of the 300 completion designs with their completion and drilling costs. The maximum completion has shorter propped fracture half-lengths than the minimum completion since there is less sand per entry point in the maximum completion design.

5.6 Economic Analysis and Optimum Completion

I performed the economic analysis using CAD$2/MMbtu, CAD$3/MMbtu and CAD$4/MMbtu per MMbtu gas prices twice: once using monthly production forecasts derived from the multivariable regression and again using forecasts from the reservoir simulation process. I identified the completion design that has the highest rate of return or PV10 out of the 300 completion designs using economic analysis. Optimization was done with an assumed well spacing of 1,312 ft for all cases.

The tables below present summaries of completion design that maximize rate of return or PV10 using multivariable regression and reservoir simulation process for existing completion practices in the industry as well as those beyond the past observed practices. Below are eight

tables presenting the twenty-four combinations of completion parameters that have optimum ROR and PV10.

The completion designs maximizing rate of return from the multivariable regression process within the range of past observed completion practices are shown in Table 5.22.

Gas Price, (CAD)/MMbtu	Lateral length, ft	Sand intensity, lb/ft	Entry point	B3, Mcfed	EUR, Bcf	ROR
$2	6,560	942	50	6,604	11.0	13%
$3	6,560	942	50	6,604	11.0	43%
$4	6,560	942	50	6,604	11.0	74%

Table 5.22—Completion designs with optimum ROR using multivariable regression, current practices for a well spacing of 1,312 ft

The completion designs maximizing rate of return from the multivariable regression process over the entire range of 300 completion designs (which extend well beyond the past observed completion practices) are shown in Table 5.23.

Gas Price, (CAD)/MMbtu	Lateral length, ft	Sand intensity lb/ft	Entry point	B3, Mcfed	EUR, Bcf	ROR
$2	9,840	2,688	150	18,454	31.9	31%
$3	9,840	2,688	150	18,454	31.9	86%
$4	9,840	2,688	150	18,454	31.9	148%

Table 5.23—Completion designs with optimum ROR using multivariable regression, potential practices for a well spacing of 1,312 ft

The completion designs maximizing rate of return from the reservoir simulation process within the range of past observed completion practices are shown in Table 5.24.

Gas Price, (CAD)/MMbtu	Lateral length, ft	Sand intensity lb/ft	Entry point	B3, Mcfed	EUR, Bcf	ROR
$2	6,560	942	50	6,587	7.3	4%
$3	6,560	942	50	6,587	7.3	31%
$4	6,560	942	50	6,587	7.3	60%

Table 5.24—Completion designs with optimum ROR using reservoir simulation, current practices for a well spacing of 1,312 ft

The completion designs maximizing rate of return from the reservoir simulation process over the entire range of 300 completion designs (which extend well beyond the past observed completion practices) are shown in Table 5.25.

Gas Price, (CAD)/MMbtu	Lateral length, ft	Sand intensity, lb/ft	Entry point	B3, Mcfed	EUR, Bcf	ROR
$2	9,840	942	100	9,715	11.4	12%
$3	9,840	471	150	10,214	9.2	57%
$4	9,840	471	150	10,214	9.2	118%

Table 5.25—Completion designs with optimum ROR using reservoir simulation, potential practices for a well spacing of 1,312 ft

The completion design maximizing PV10 from the multivariable regression process within the range of past observed completion practices are shown in Table 5.26.

Gas Price, (CAD)/MMbtu	Lateral length, ft	Sand intensity, lb/ft	Entry point	B3, Mcfed	EUR, Bcf	PV10 (MM$)
$2	6,560	942	50	6,604	11.0	0.54
$3	6,560	942	50	6,604	11.0	5.73
$4	6,560	942	50	6,604	11.0	10.92

Table 5.26—Completion designs with optimum PV10 using multivariable regression, current practices for a well spacing of 1,312 ft

The completion designs maximizing PV10 from the multivariable regression process over the entire range of 300 completion designs (which extend well beyond the past observed completion practices) are shown in Table 5.27.

Gas Price, (CAD)/MMbtu	Lateral length, ft	Sand intensity, lb/ft	Entry point	B3, Mcfed	EUR, Bcf	PV10 (MM$)
$2	13,120	2,688	400	25,024	43.3	8.84
$3	13,120	2,688	400	25,024	43.3	29.03
$4	13,120	2,688	400	25,024	43.3	49.27

Table 5.27—Completion designs with optimum PV10 using multivariable regression, potential practices for a well spacing of 1,312 ft

The completion designs maximizing PV10 from the reservoir simulation process within the range of past observed completion practices are shown in Table 5.28.

Gas Price, (CAD)/MMbtu	Lateral length, ft	Sand intensity, lb/ft	Entry point	B3, Mcfed	EUR, Bcf	PV10 (MM$)
$2	6,560	942	50	6,587	7.3	-0.89
$3	6,560	942	50	6,587	7.3	2.96
$4	6,560	942	50	6,587	7.3	6.84

Table 5.28—Completion designs with optimum PV10 using reservoir simulation, current practices for a well spacing of 1,312 ft

The completion designs maximizing PV10 from the reservoir simulation process over the entire range of 300 completion designs (which extend well beyond the past observed completion practices) are shown in Table 5.29.

Gas Price, (CAD)/MMbtu	Lateral length, ft	Sand intensity, lb/ft	Entry point	B3, Mcfed	EUR, Bcf	PV10 ($)
$2	9,840	942	100	10,679	11.4	0.29
$3	13,120	1,413	100	12,364	17.3	7.27
$4	13,120	1,413	100	12,364	17.3	15.45

Table 5.29— Completion designs with optimum PV10 using reservoir simulation, potential practices for a well spacing of 1,312 ft

Fig. 5.10 to Fig. 5.17 are 2-D graphs of lateral lengths and entry points for different economics metrics PV10, ROR using multivariable regression and reservoir simulation for the sand intensity of 2,688 lb/ft. I chose this sand intensity because it was the maximum sand intensity in the defined range of the sand intensity parameter. The gas price used in these figures is CAD$2/MMbtu.

In Fig. 5.10, which optimizes for ROR using the regression method, the optimum designs occur in the range of 50 to 100 entry points regardless of different lateral lengths. This is because the lateral length is not as important in short term production in the regression model. ROR decreases after 100 entry points, but the rate of decline is not substantial.

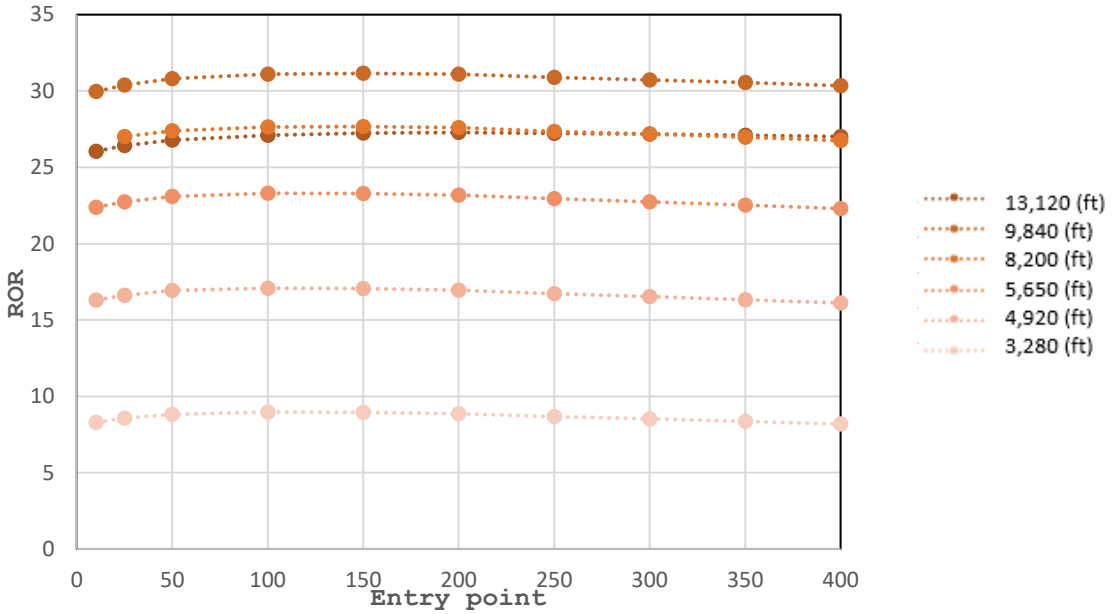

Fig. 5.10—ROR vs. entry point for different lateral lengths for the sand intensity of 2,688 lb/ft - regression

In Fig. 5.11, which optimizes for ROR using the simulation method, the optimum designs occur in the range of 25 to 100 entry points for different lateral lengths. ROR starts decreasing after 100 entry points. The optimum design is a function of lateral length. For example, in the below graph, for the 8,200 ft lateral length optimal design correlates roughly to 50 entry points and entry point spacings of 164 feet. With longer laterals, the optimum designs have more entry points, this is because the incremental cost of increasing the lateral length and adding entry points is being smaller than the incremental production gain.

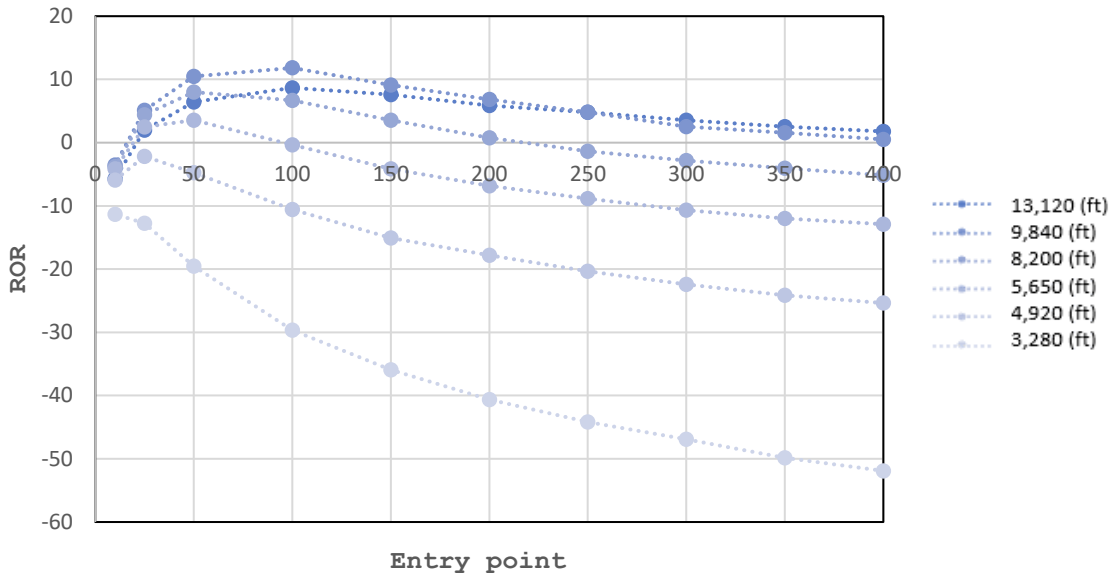

Fig. 5.11—ROR vs. entry point for different lateral lengths for the sand intensity of 2,688 lb/ft - simulation

In Fig. 5.12, which optimizes for ROR using the regression method, the optimum designs happen around 10,000 ft of lateral for all range of entry points as it has maximum ROR. Then ROR decreases after 10,000 ft. This is because, after 10,000 ft of lateral, the cost of drilling increased dramatically.

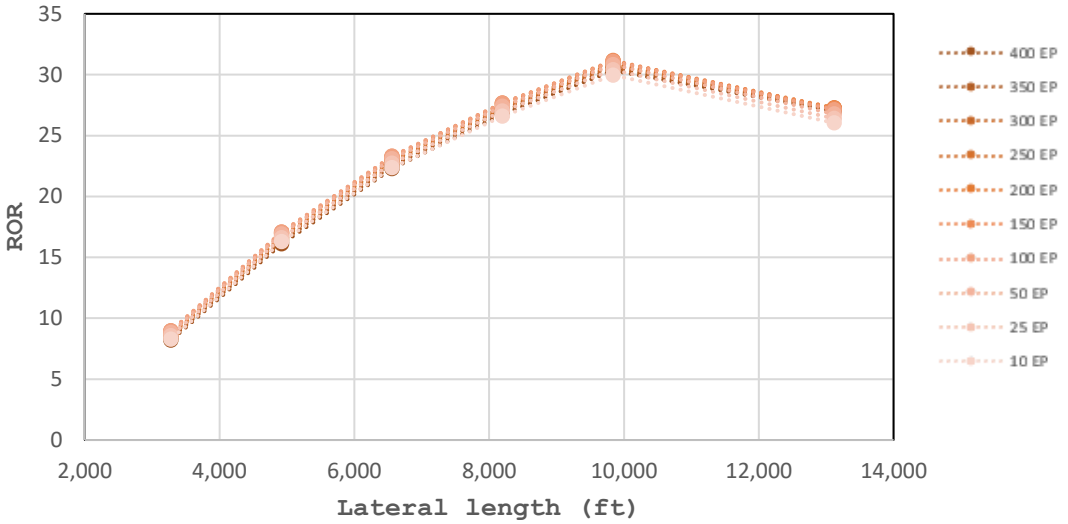

Fig. 5.12—ROR vs. lateral length for different entry points for the sand intensity of 2,688 lb/ft - regression

In Fig. 5.13, which optimizes for ROR using the simulation method, the ROR increases by increasing lateral length for the entire range of entry points. The optimum designs happen around 10,000 ft of lateral then ROR levels off or decrease after 10,000 ft for different entry points. This is because lateral length does not contribute to short-term well performance which significantly influences ROR. Also, the cost of drilling lateral increase significantly after 10,000 ft.

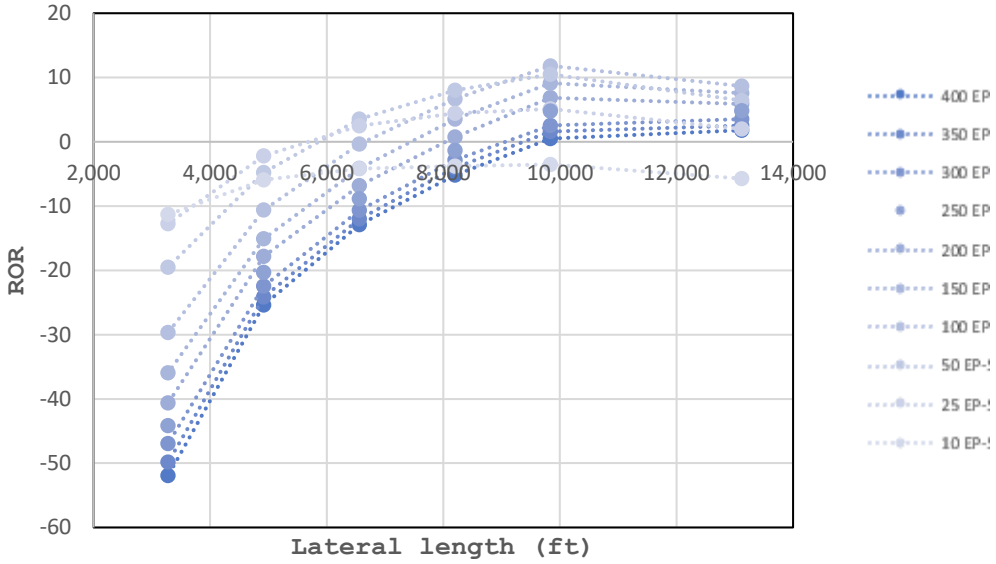

Fig. 5.13—ROR vs. lateral length for different entry points for the sand intensity of 2,688 lb/ft - simulation

In Fig. 5.14, which optimizes for PV10 using the regression method, PV10 increase by increasing entry points for all range of lateral length but the incremental increase in PV10 after 50 entry point is not substantial. This can be because the number of entry points do not contribute substantially to long-term well performance which materially influences PV10.

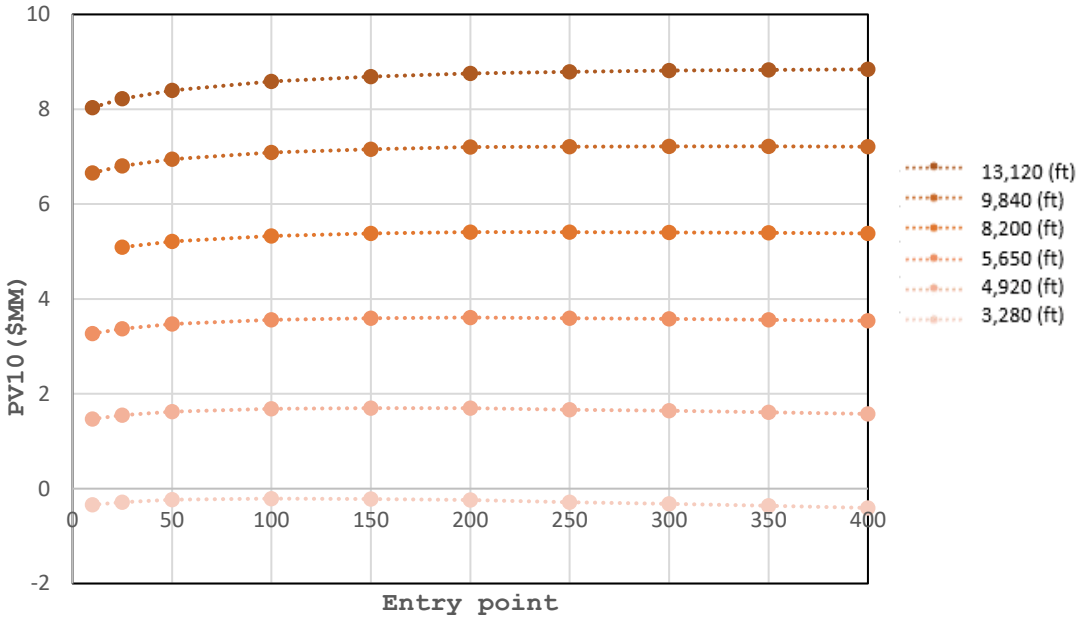

Fig. 5.14—PV10 vs. entry points for different lateral lengths for the sand intensity of 2,688 lb/ft - regression

In Fig. 5.15, which optimizes for PV10 using the simulation method, PV10 increases as number of entry points increase till range of 50 to 100 entry points and then starts decreasing for all range of lateral length. Optimum design is a function of lateral length. As the lateral length increases, the number of entry points in the optimum designs increases. This can be because of as the lateral length increases, more entry points per unit of lateral length are required to drain the reservoir. Number of entry points and later length in the optimum designs are the balance between draining more fluid out of the reservoir due to a bigger contact area with reservoir while keeping the friction losses in the tubular system as well costs at a minimum.

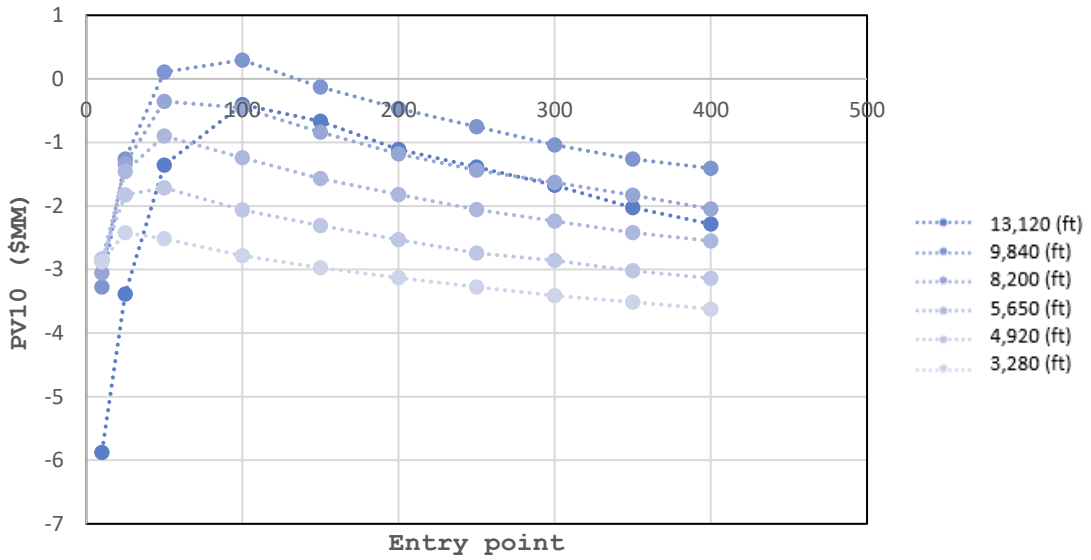

Fig. 5.15—PV10 vs. entry points for different lateral lengths for the sand intensity of 2,688 lb/ft - simulation

In Fig. 5.16, which optimizes for PV10 using the regression method, PV10 increases as lateral length increases. Optimum design happens in the 14,000 ft which is the largest lateral length for all range of entry point. This is because the regression model is not constrained to the limitation of drainage size. Therefore, as the lateral length increase, the regression model assumes the drainage area increases and cannot put a limitation on the size of it. As a result, PV10 increases as lateral length increase.

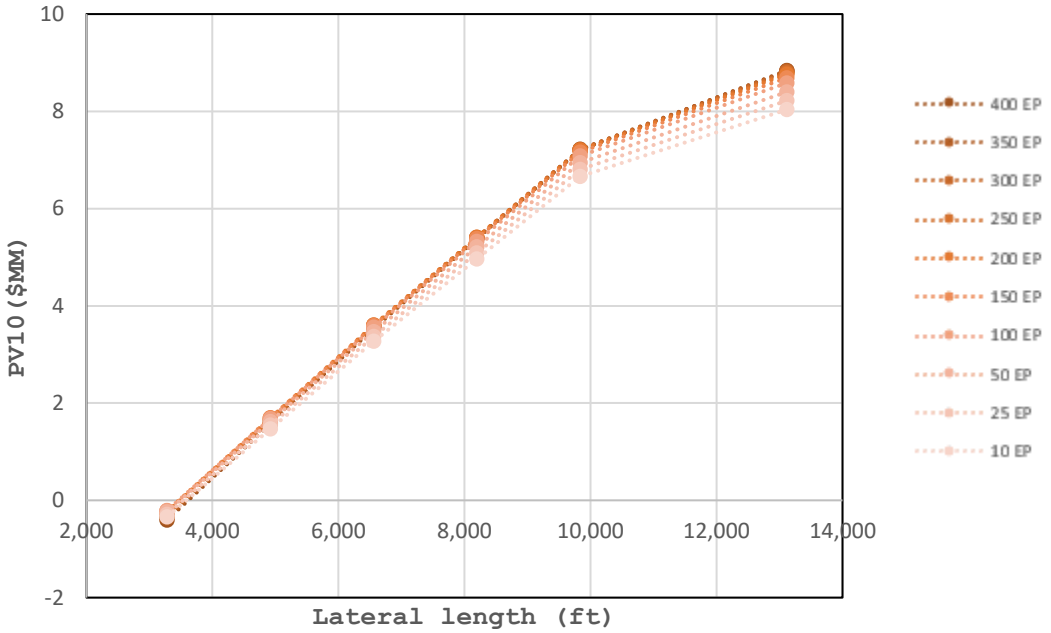

Fig. 5.16—PV10 vs. lateral length for different entry points for the sand intensity of 2,688 lb/ft – regression

In Fig. 5.17, which optimizes for PV10 using the simulation method, PV10 increases as the lateral length increases up to 10,000 ft. In 10,000 lateral length, optimum completions happen for a different range of entry points. PV10 starts decreasing after 10,000 ft for all range of entry points because the drilling cost starts increasing dramatically after this lateral length.

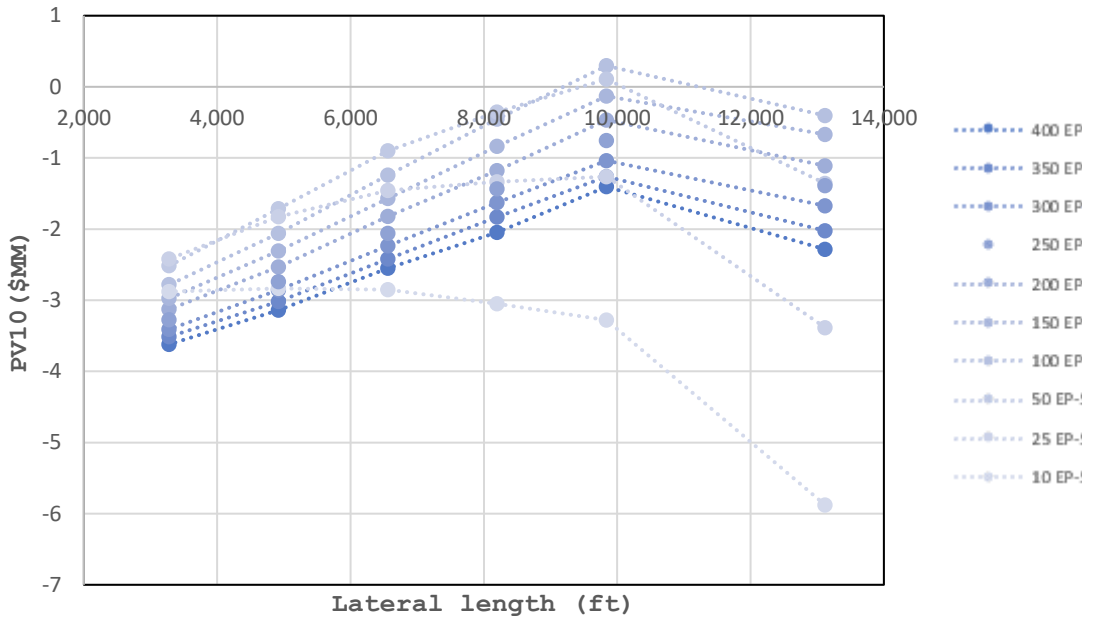

Fig. 5.17—PV10 vs. lateral length for different entry points for the sand intensity of 2,688 lb/ft – simulation

5.7 Comparison of Regression and Simulation Models

The multivariable regression method predicts higher ROR and PV10 compared to the reservoir simulation method. This is because the regression method forecasts higher short and long-term production (B3 and EUR) compared to the reservoir simulation method. The reason the regression methodology forecasts higher B3 in completion designs beyond what has tried in the field is that the regression methodology does not directly incorporate the physics of wellbore friction losses which can lead to higher forecast of production rates. Likewise, the regression methodology may predict higher EUR because it does not consider a limitation on drainage-area size, which may not have been manifested in the regression dataset. However, reservoir simulation method honors the physics of material balance, friction losses and pressure drop in the tubular, transient flow and constraints production by the limitation of reservoir size, drainage

area and capacity of the wellbore. Therefore, with the simulation methodology, long-term production is directly tied to the drainage volume (material balance) and production rates are limited to physics-based computations of the flow capacity of pipe and flowing pressures at the surface and at the formation. As a result, reservoir simulation production forecast is more realistic compared to the regression method forecast.

The regression technique can generate production volumes that exceed the drainage area. For example, for a completion design of 6,560 ft of lateral length, 25 entry points and 942 lb/ft of sand intensity, the regression model in the Town field predicts a B3 of 6,541 Mcfed and EUR of 10.9 Bcf which is 118% of initial OGIP (9.2 Bcf). The reservoir simulation-based model Town for the same completion results in B3 of 5,344 Mcfed and EUR of 7.8 Bcf which is 84% of initial OGIP (9.2 Bcf). A similar completion design in one of the 44 wells in the Town field has 6,080 ft of lateral length, 33 entry points and 680 lb/ft of sand intensity with the B3 of 4,426 Mcfed, so even the simulation-based method may appear optimistic at times even though it is the more conservative of the two methodologies. This maybe because there is an uncertainty in the underlying assumptions in the reservoir simulation model. Despite the possibility of optimistic B3 & EUR projections for the regression method, the likelihood of those optimistic projections diminishes when completion designs are considered that are inside the range of values in the observed dataset. Also, in terms of generating an optimized completion design, when inside the range of current completion practices both multivariable regression and reservoir simulation methods point out to the same completion design as the optimum one. However, outside the range of current industry practices multivariable regression and reservoir simulation method select different completion designs as the optimum. Due to problems for incorporating physics such as reservoir size, wellbore capacity and friction losses inside the tubular in the regression

model, multivariable regression is not recommended for optimizing completions that fall outside the range of completion designs in the observed dataset that was used to train the regression model.

On the other hand, the multivariable regression method is fast to implement compared to reservoir simulation method which is time-consuming and skill demanding (it takes more time to implement the physics of the reservoir such as frictions in the pipe, reservoir size and fluid properties in the model). Therefore, when inside the range of current completion practices, regression method can be a fast and reliable tool, but when the purpose is to explore outside the range of current practices, reservoir simulation method is recommended.

Both regression and reservoir simulation models are calibrated to the mean of observed data, regression by virtue of the regression analysis and simulation through history matching of the type curve. Fig. 5.18 (which is the same as Fig. 4.6) shows 2-D regression lines of predicted vs. actual B3-per-fluid values for 44 wells in the Town field for the regression model in orange dots and the simulation model in blue dots. The regressed line for predicted B3 per fluid from the regression model has higher R^2 but smaller slope. The regressed line for predicted B3 per fluid from the simulation model has lower R^2 but larger slope. There is trade-off between slope and R^2. The regression model with higher R^2 and smaller slope indicates that there is less uncertainty in the model due to missing information such as rock properties, but the model cannot reproduce the extremes as well. On the other hand, the simulation model with smaller R^2 and greater slope indicates that there is more uncertainty in the model, but the model does a better job in predicting the extreme values. Therefore, as completion parameters go toward the boundary of current-practices space, the simulation model does a better job in predicting the performance. However,

for the completion parameters that are inside the boundary of current practice and toward the average designs, the regression model has less uncertainty and is more suitable.

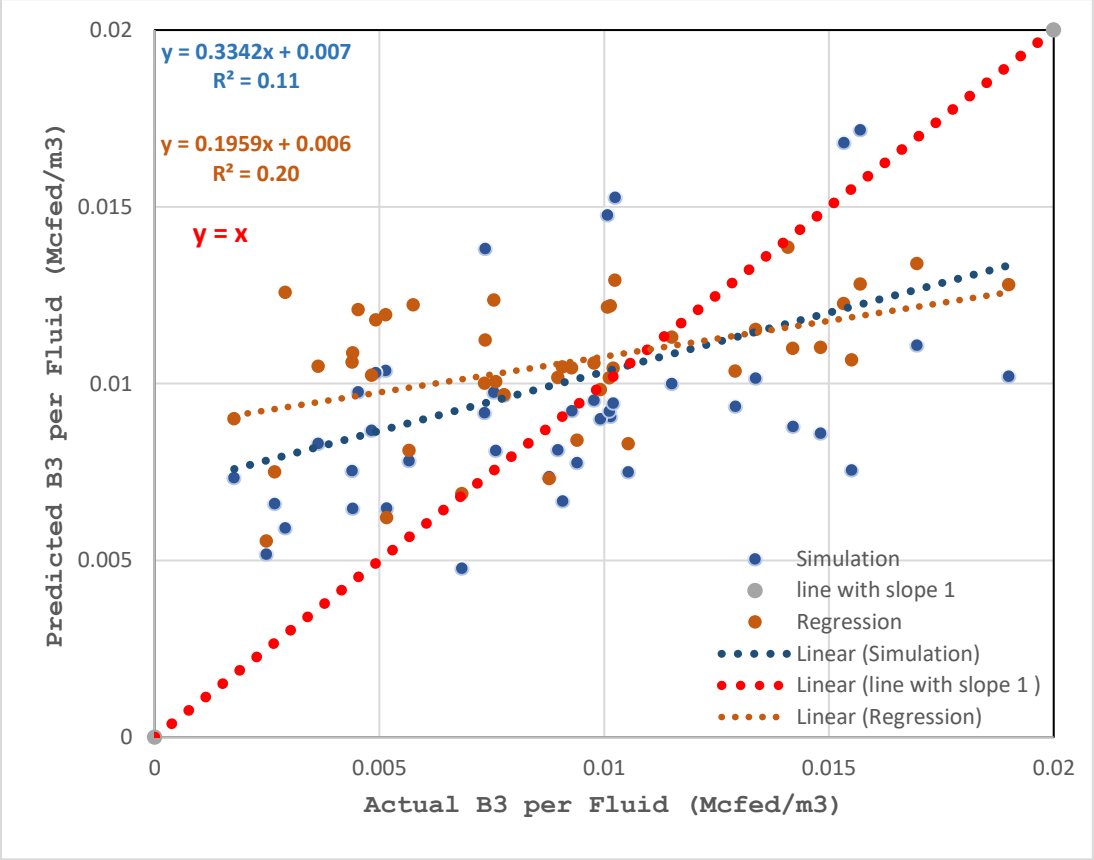

Fig. 5.18—2-D regression line of predicted vs. actual B3 per fluid, Mcfed/ft^3 values for 44 wells in the Town field

5.8 2-D Graphs of Economics for CAD$2/MMbtu

Below are 2-D graphs of lateral lengths and entry points vs. different economics metrics (B3, well life, EUR,) using multivariable regression and reservoir simulation for the sand intensity of 2,688 lb/ft (Fig. 5.19 to Fig. 5.30).

In Fig. 5.19, B3 increases as number of entry points increase because there are more connections between wellbore and reservoir. However, the incremental changes of B3 to number of entry points are not substantial. In Fig. 5.10, ROR vs. entry points showed a similar trend to

B3 vs. entry points since B3 and ROR correlate. The maximum B3 in the 44 wells in the Town field is 6,700 Mcfed, and the tubular capacity is 15,000 Mcfed which is far below some of the regression prediction range.

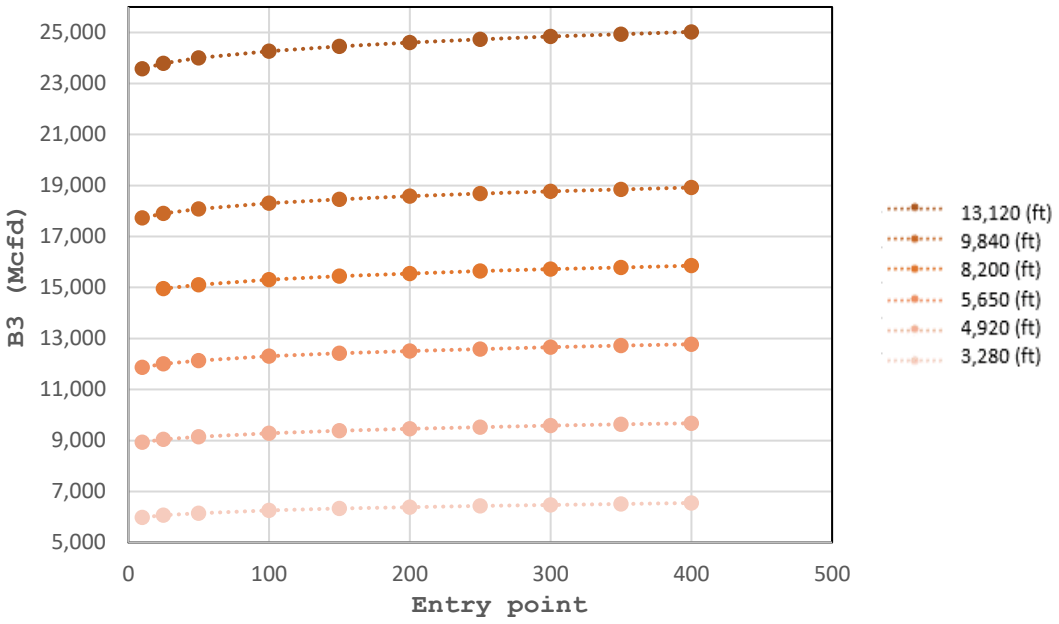

Fig. 5.19—B3 vs. entry point for different lateral lengths for the sand intensity of 2,688 lb/ft – regression

In Fig. 5.20, B3 increases as the number of entry points increase since the number of connections between reservoir and wellbore go up. However, after 200 entry points, B3 will level off because of reservoir size and friction in the wellbore as well as a limitation of tubular size that have been applied in the simulation method.

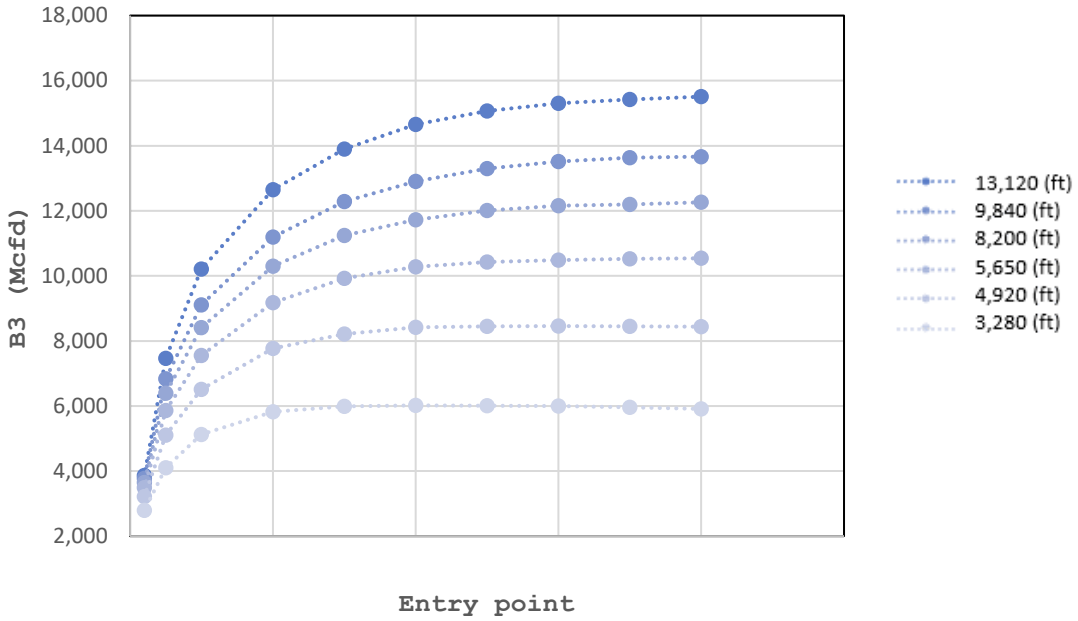

Fig. 5.20—B3 vs. entry point for different lateral lengths for the sand intensity of 2,688 lb/ft - simulation

In Fig. 5.21, B3 increases as the lateral length increases using the regression method because of additional reservoir being contacted via the longer lateral. However, since regression method does not incorporate any constraints on reservoir size or wellbore capacity, the trend of increasing B3 with lateral length continues growing. The B3 doubles when lateral length doubles, which indicates that as the lateral length doubles, therefore number of entry points doubles. As a result, the regression model predicts that B3 doubles, which is not physically reasonable. This is due to friction losses and fluid competition in tubular that increases when there is more fluid in the wellbore.

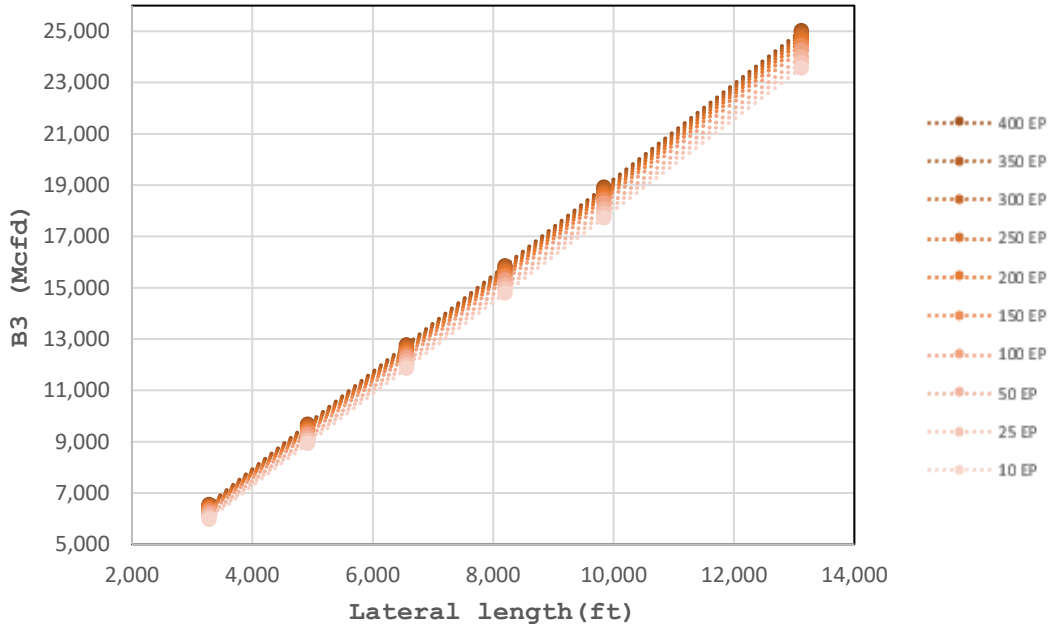

Fig. 5.21—B3 vs. lateral length for different entry points for the sand intensity of 2,688 lb/ft - regression

In Fig. 5.22, B3 increases as lateral length increases, however, the slope of growth in B3 to lateral lengths decreases as lateral length increase for different entry points. This is because of the hydraulic friction; reservoir size and wellbore capacity have been incorporated in the simulation method and the slope of change of B3 vs. lateral length decreases when lateral length increases.

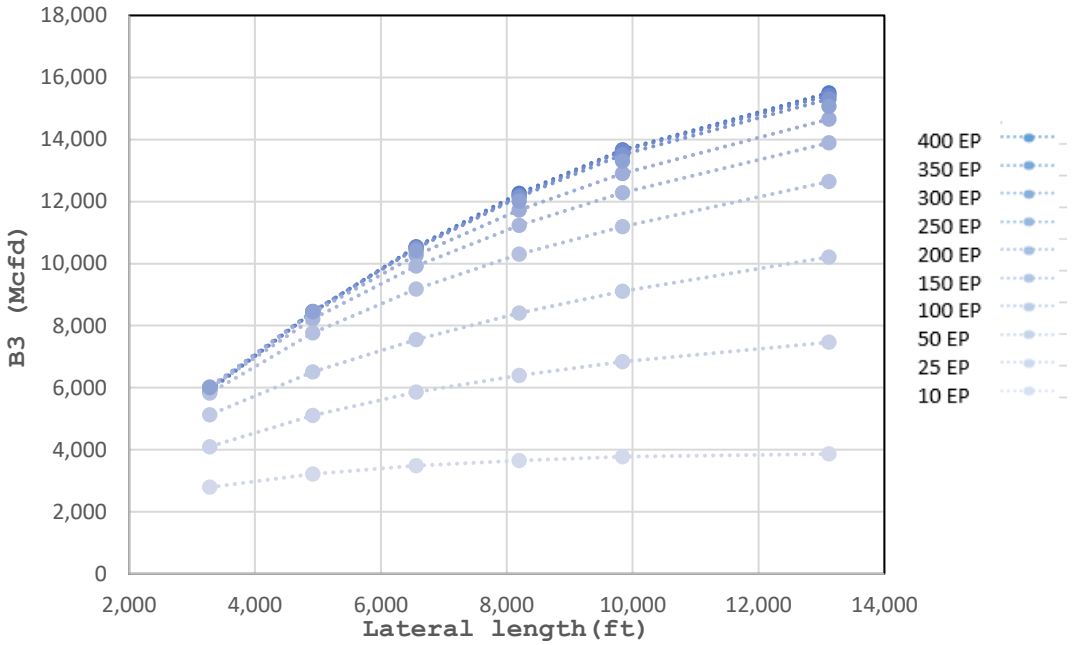

Fig. 5.22—B3 vs. lateral length for different entry points for the sand intensity of 2,688 lb/ft - simulation

In Fig. 5.23, EUR increases slightly as the number of entry points increase using the regression method. EUR is correlated to long-term production and number of entry points usually corresponds to short-term production. Therefore increasing the number of entry points does not increase EUR significantly.

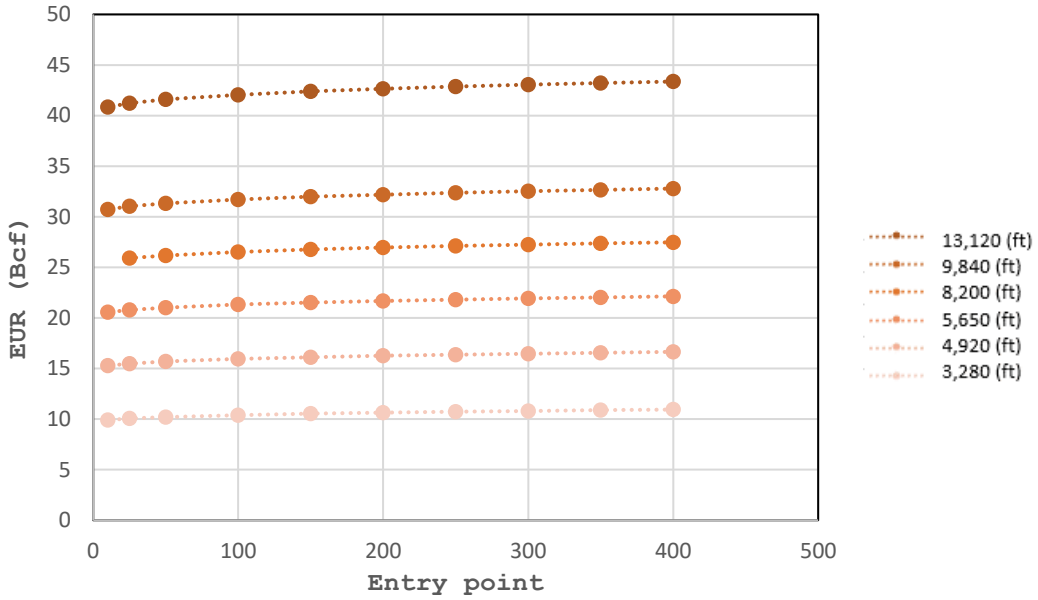

Fig. 5.23—EUR vs. entry point for different lateral lengths for the sand intensity of 2,688 lb/ft – regression

In Fig. 5.24, EUR increases in the range of 10 to 100 entry points for different lateral lengths. However, EUR goes down after 100 entry points in the simulation method. This is due to the increase in hydraulic frictions and fluid completion when there is a rise in number of connections and fluid in the wellbore. Fig. 5.15 (PV10 vs. entry points) shows a similar trend since they are both indicator of long-term production and long-term economic gains.

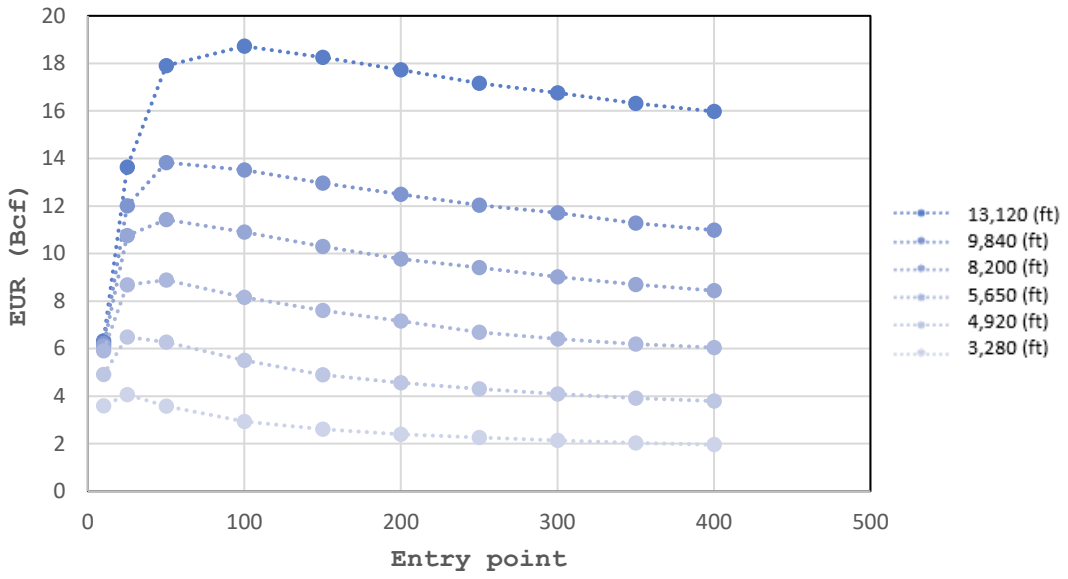

Fig. 5.24—EUR vs. entry point for different lateral lengths for the sand intensity of 2,688 lb/ft – simulation

In Fig. 5.25, EUR increases as lateral length increases using the regression method due to the additional reservoir being contacted. This trend is similar to the B3 vs. lateral length in Fig. 5.21. As the lateral length doubles, EUR approximately doubles in the regression model which not physically possible due to friction losses in tubular. This is due to the fact that regression method is not constraint by reservoir size and friction losses in the tubular of the problem.

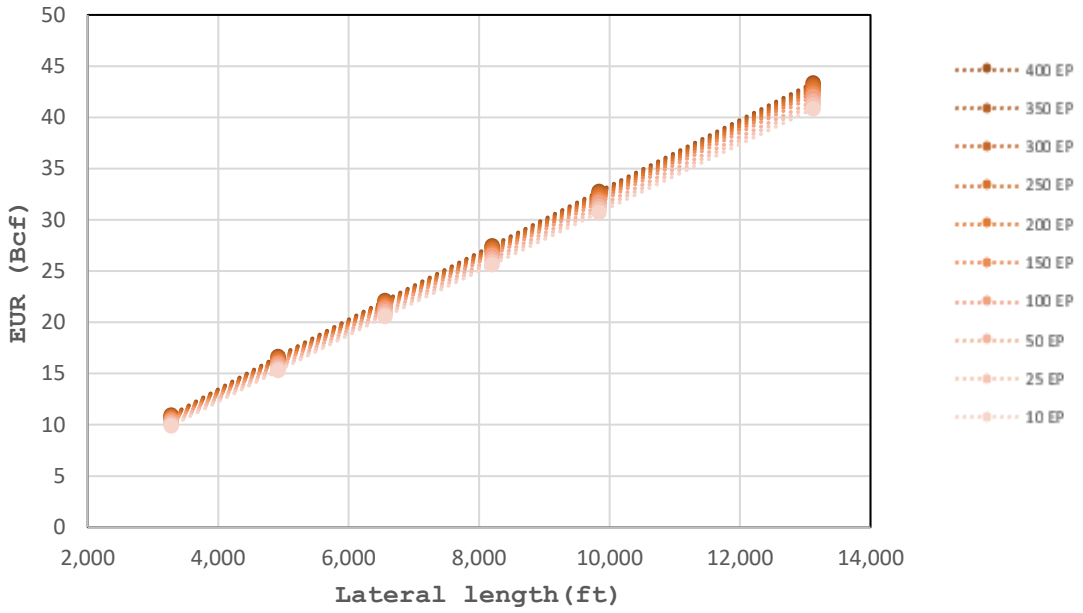

Fig. 5.25—EUR vs. lateral length for different entry points for the sand intensity of 2,688 lb/ft - regression

In Fig. 5.26, EUR increases as lateral length increases in the simulation method, but the range of EUR in simulation method (2 Bcf to 18 Bcf) is not as high as the regression method (9 Bcf to 42 Bcf). This is because in the reservoir simulation I considered the size of tubular and limit the flow when it exceeds more than tubular size.

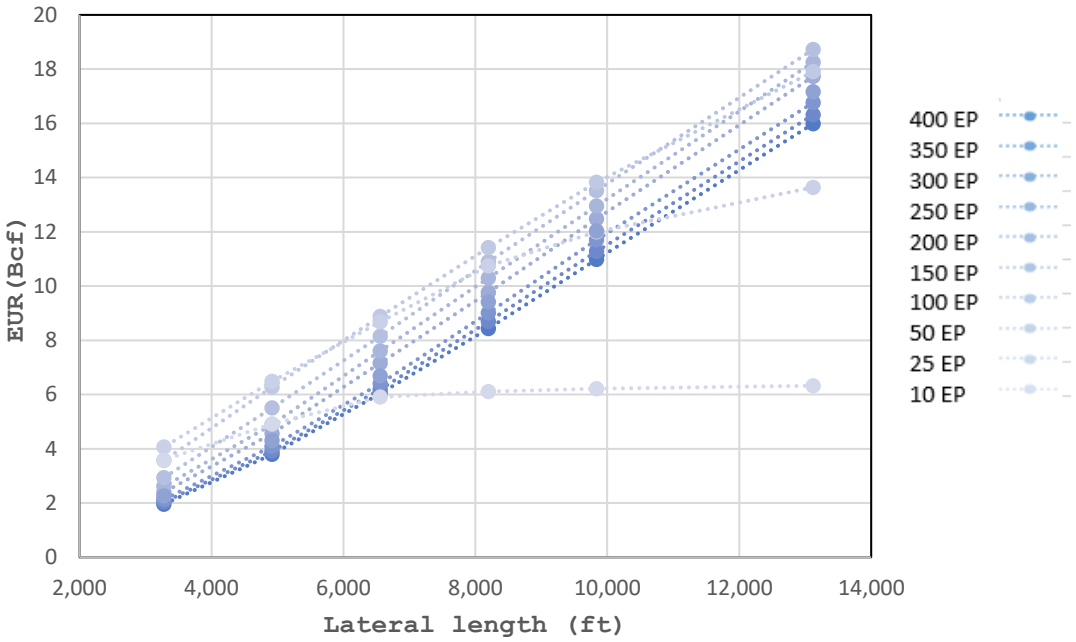

Fig. 5.26—EUR vs. lateral length for different entry points for the sand intensity of 2,688 lb/ft – simulation

In Fig. 5.27, as number of entry points increase, the well life increases slightly. As the number of entry points increase, there is more connection between reservoir and wellbore, however, number of entry point corresponds to short-term production at the early life of the well. Therefore increasing number of entry points does not have significant effect on the well life.

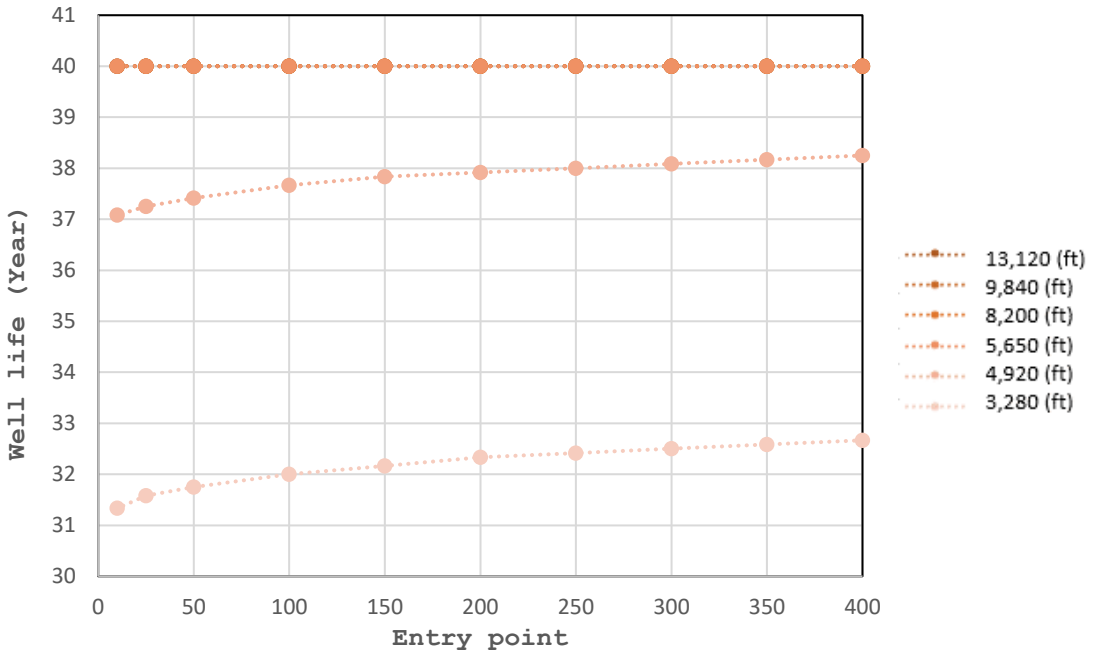

Fig. 5.27—Well life vs. entry points for different lateral lengths for the sand intensity of 2,688 lb/ft - regression

As presented by Fig. 5.28, lateral length has a significant impact on well life. Longer laterals generate much longer well lives. This is due to the combination of the additional reservoir being contacted via the longer lateral and the greater number of entry points that can be cost-effectively placed in the longer lateral. These parameters provide higher long-term total-wellbore production rates that when combined with the fixed operating costs cause the well to remain above the economic limit for a longer period of time than a well with a shorter lateral and/or fewer entry points. Well life does decrease modestly as the number of entry points increase as more entry points for a given lateral length will deplete the reservoir in less time.

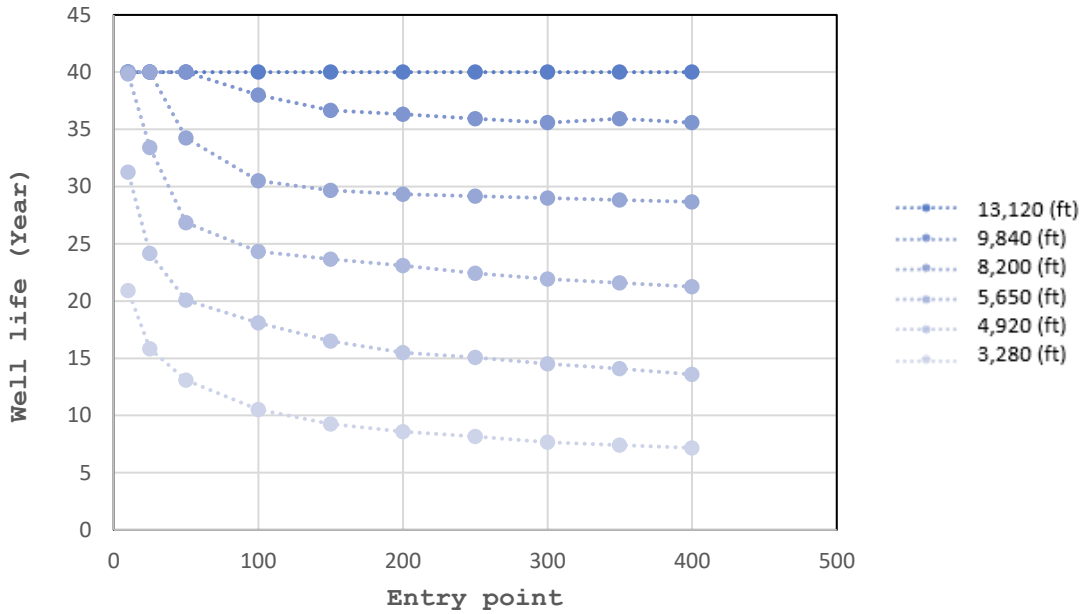

Fig. 5.28—Well life vs. entry point for different lateral lengths for the sand intensity of 2,688 lb/ft - simulation

In Fig. 5.29 and Fig. 5.30, well life increases as the lateral length increases. As the lateral length increases, more reservoir being contacted via the longer lateral, therefore the well life goes up both in the regression and simulation methods.

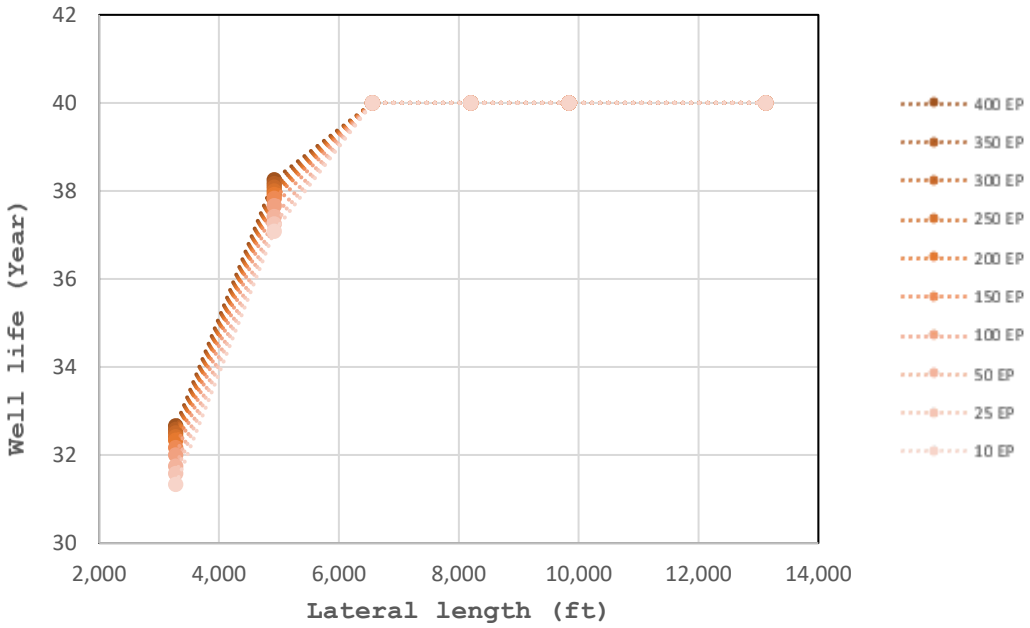

Fig. 5.29—Well life vs. lateral length for different entry points for the sand intensity of 2,688 lb/ft - regression

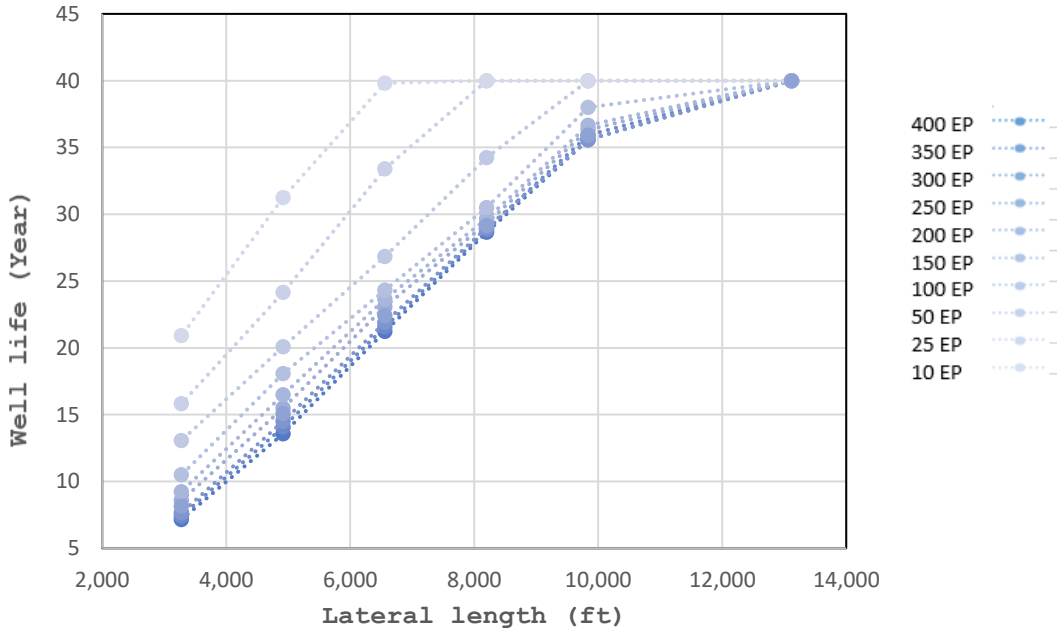

Fig. 5.30—Well life vs. lateral length for different entry points for the sand intensity of 2,688 lb/ft - simulation

Table 5.30 consists of different metrics I calculated in this chapter using simulation and regression methods for minimum, mid-point and maximum completion parameters.

Completion parameters	Regression B3, Mcfed	Simulation B3, Mcfed	Regression EUR, Bcf	Simulation EUR, Bcf	Regression, Well life, years	Simulation, Well life, years	Well cost, $MM	Regression, ROR	Simulation, ROR	Regression, PV10, $MM	Simulation, PV10
Minimum Entry Points = 10 Sand Intensity = 471 lb/ft, Lateral Length = 3,280 ft	2,127	2,193	2.86	2.34	17	17	3.44	-14%	-19%	-2.48	-2.90
Mid-point Entry Points = 200 Sand Intensity = 1,413 lb/ft, Lateral Length =6,560 ft	8,649	10,031	14.77	5.99	37	21	5.68	17%	-7%	1.64	-2.12
Maximum Entry Points = 400 Sand Intensity = 2,688 lb/ft, Lateral Length = 13,120 ft	25,024	15,508	43.36	15.98	40	40	14.62	27%	-1%	8.84	-5.16

Table 5.30—Comparison between regression and simulation methodologies

Fig. 5.31 to Fig. 5.35 illustrate B3, EUR, well life, ROR and PV10 of minimum, mid-point and maximum completions of regression and simulation methodologies as bar charts. These figures illustrate the overall impact of the regression and simulation-based methodologies on expected well performance and financial value of various completion designs.

As shown in Fig. 5.31, for the minimum completion parameters the regression and simulation B3 are close to each other. However, for the maximum completion parameters B3 from regression is about 60% greater than the simulation B3. This is due to the lack of physics constraints such as friction losses in the tubular, reservoir size and tubular size in the regression model. Thus, at the aggressive completions, which are beyond the range of observed field data, the regression analysis method will yield significantly optimistic B3's and therefore will likely yield incorrect optimal completion designs.

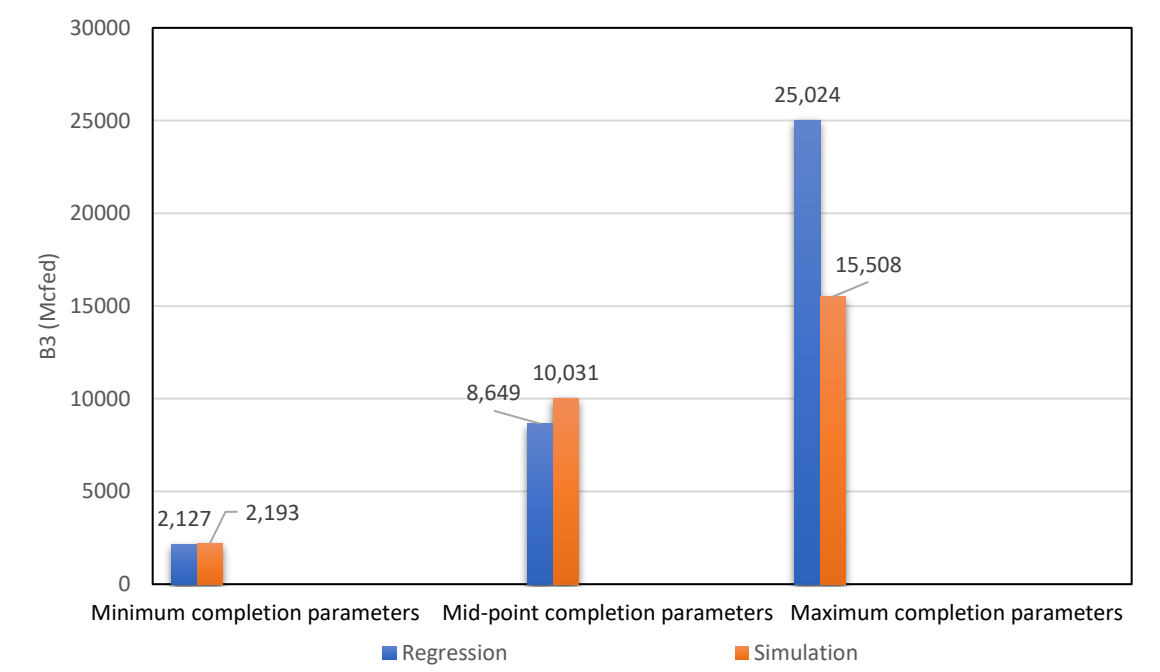

Fig. 5.31—B3 (Mcfed) of regression and simulation methodologies for the minimum, mid-point, and maximum completions

In Fig. 5.32, for the minimum completion parameters the regression and simulation EUR are close to each other. However, for the mid-point and maximum completion parameters EUR from regression is 146% and 186% greater than simulation EUR. This is again due to the lack of physics-based constraints such as friction losses in the tubular and reservoir size limitation in the regression model that manifests more severely in the long-term production. Thus, at the aggressive completions, which are beyond the range of observed field data, the regression analysis method will yield significantly optimistic EUR's and therefore will likely yield incorrect optimal completion designs.

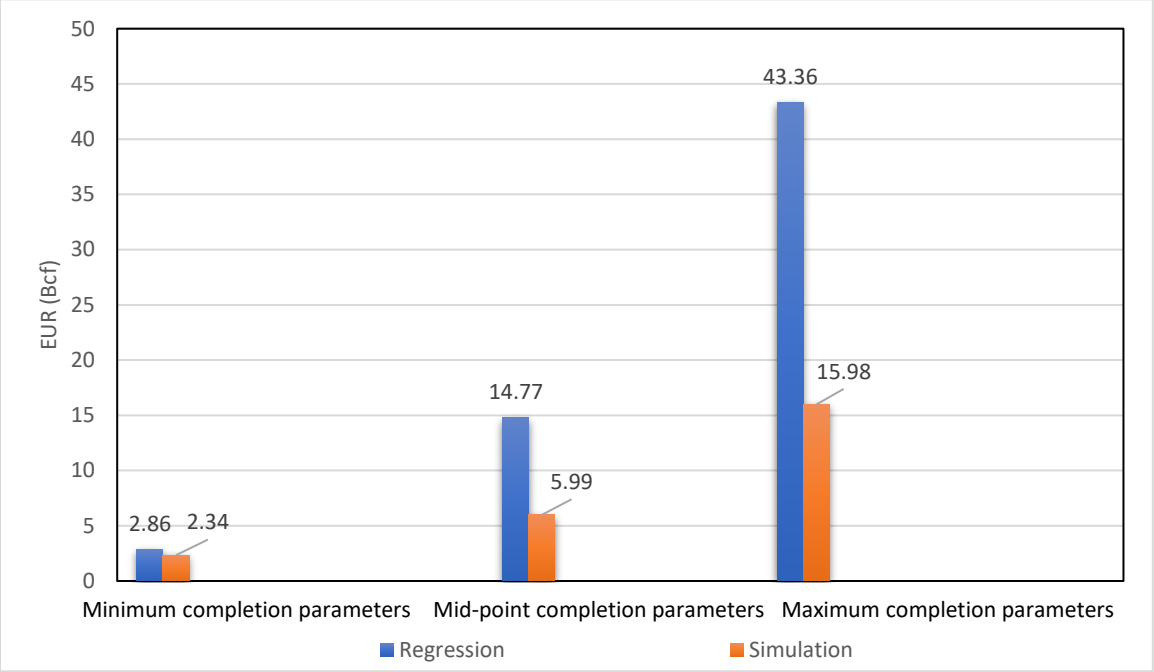

Fig. 5.32—EUR (Bcf) of regression and simulation methodologies for the minimum, mid-point, and maximum completions

In Fig. 5.33, for the minimum completion parameters the regression and simulation well-life are the same since in both methodologies they predict similar EUR. However, for the mid-point completion parameters well-life from regression is bigger than well-life in simulation

because regression predicts a higher EUR than simulation. For the maximum completion parameters, the well life of both methodologies is 40 years, this is because 40 years was the maximum well life incorporated in the economic model.

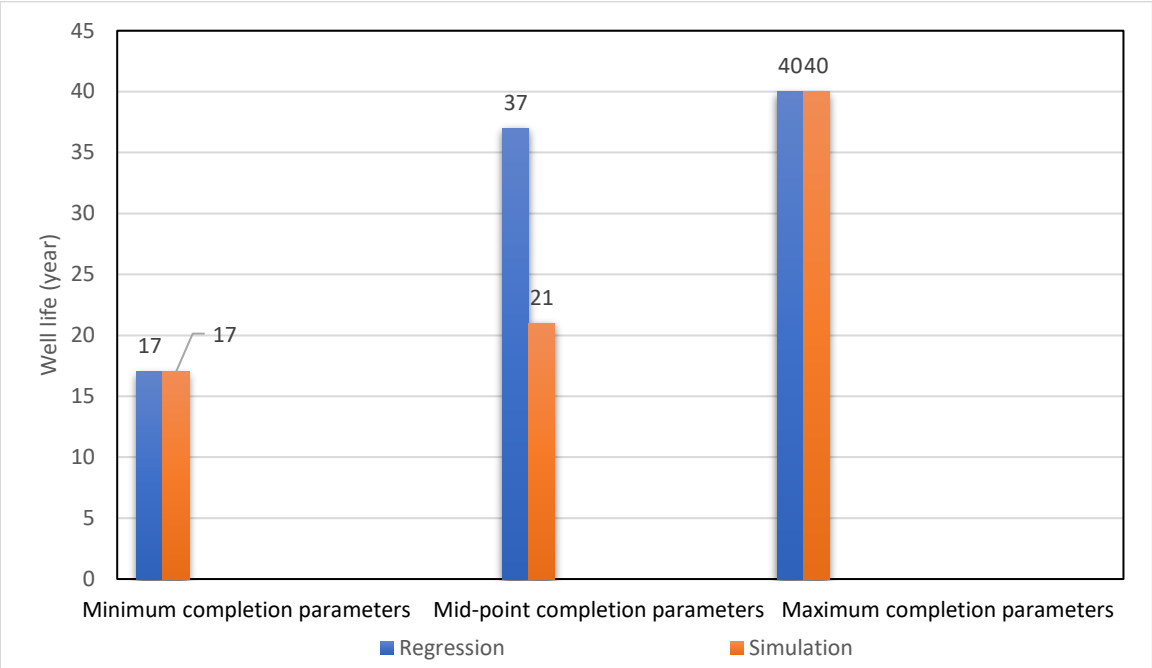

Fig. 5.33—Well life(year) of regression and simulation methodologies for the minimum, mid-point, and maximum completions

In Fig. 5.34 and Fig. 5.35, both ROR and PV10 for the minimum, mid-point and maximum completion parameters using simulation method is more conservative than the similar values in regression method. This is mainly because regression method predicts greater short and long-term production compared to the simulation method and is not bounded by physics such as limitations on reservoir size, tubular capacity and friction losses in tubular As a result, the predicted short-term and long-term economic gains in regression method are higher than simulation method with the same well costs in the economic model. Therefore, at the aggressive completions, which are beyond the range of observed field data, the regression analysis method

will yield significantly optimistic ROR's and PV10's and therefore will likely yield incorrect optimal completion designs. For example, for the minimum completion design the difference between optimum ROR from regression and simulation is 5%, for mid-point completion design this difference is 24% and for the maximum completion design the difference is 28%. Similarly, for the minimum completion design the difference between optimum PV10 from regression and simulation is $0.4MM, for mid-point completion design this difference is $3.76 MM and for the maximum completion design the difference is $14MM.

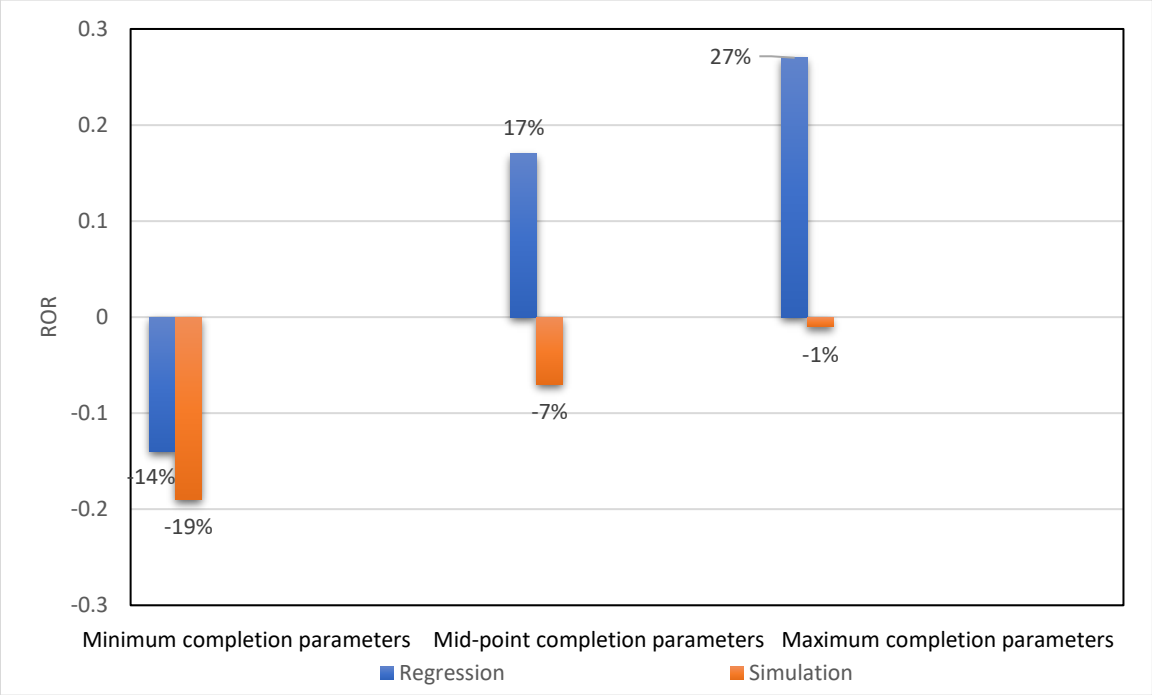

Fig. 5.34—ROR of regression and simulation methodologies for the minimum, mid-point, and maximum completions

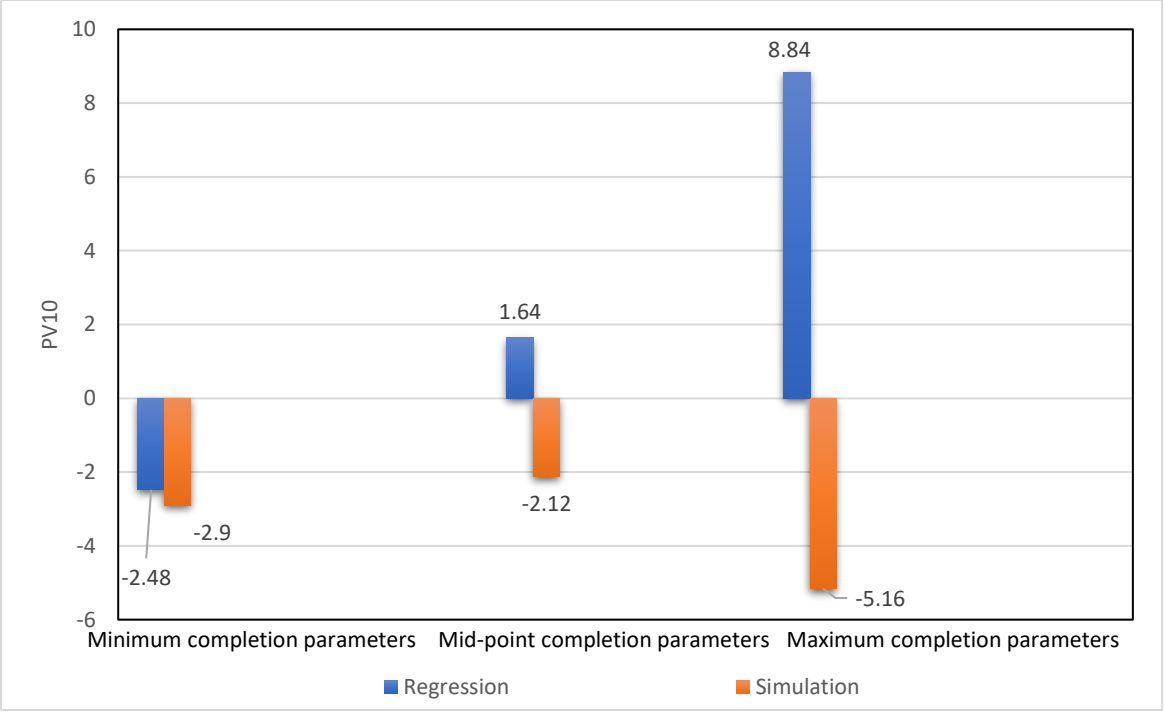

Fig. 5.35—PV10 ($MM) of regression and simulation methodologies for the minimum, mid-point, and maximum completions

Table 5.31 to Table 5.42 present summaries of optimum completion designs that maximize rate of return or PV10 using multivariable regression and reservoir simulation process for existing completion practices in the industry as well as those beyond the past observed practices using CAD$2/MMbtu, CAD$3/MMbtu and CAD$4/MMbtu.

As mentioned earlier in this chapter, the regression method tends to predict greater short and long-term production volumes compared to the simulation model. Therefore, given the same well cost, calculated economic gain using the regression method is greater than the simulation method. Inside the range of values of the observed dataset, the higher forecast of production in regression method is not as severe as the higher forecast outside range of observed values.

As shown in Table 5.31 to Table 5.42, within the current range of completion practices both multivariable regression and reservoir simulation methods generate the same optimum

completion design regardless of commodity price. A net effect of using the regression method is an inflated estimate of ROR and PV10 for any designs being evaluated.

Outside the range of current industry practices the regression and simulation methods generate different optimum completion designs across the evaluated commodity prices. For ROR optimization, the net impact of using the regression methodology rather than the simulation methodology is only to significantly increase the sand intensity and, in the CAD$2/MMbtu gas price case, increasing the number of entry points. For PV10 optimization outside the range of current practices, the net impact of using the regression methodology rather than the simulation methodology is to significantly increase the sand intensity and the number of entry points, and again in the CAD$2/MMbtu gas price case to increase the lateral length.

Gas Price, (CAD)/MMbtu	Methodology	Lateral length, ft	Sand intensity, lb/ft	Entry point	ROR
$2	Simulation	6,560	942	50	4%
	Regression	6,560	942	50	13%

Table 5.31—Optimum ROR completion for current completion designs for a well spacing of 1,312 ft and CAD$2/MMbtu gas price

Gas Price, (CAD)/MMbtu	Methodology	Lateral length, ft	Sand intensity, lb/ft	Entry point	ROR
$2	Simulation	9,840	942	100	12%
	Regression	9,840	2,688	150	31%

Table 5.32—Optimum ROR completion for future completion designs for a well spacing of 1,312 ft and CAD$2/MMbtu gas price

Gas Price, (CAD)/MMbtu	Methodology	Lateral length, ft	Sand intensity, lb/ft	Entry point	ROR
$3	Simulation	6,560	942	50	31%
	Regression	6,560	942	50	43%

Table 5.33—Optimum ROR completion for current completion designs for a well spacing of 1,312 ft and CAD$3/MMbtu gas price

Gas Price, (CAD)/MMbtu	Methodology	Lateral length, ft	Sand intensity, lb/ft	Entry point	ROR
$3	Simulation	9,840	471	150	57%
	Regression	9,840	2,688	150	86%

Table 5.34—Optimum ROR completion for future completion designs for a well spacing of 1,312 ft and CAD$3/MMbtu gas price

Gas Price, (CAD)/MMbtu	Methodology	Lateral length, ft	Sand intensity, lb/ft	Entry point	ROR
$4	Simulation	6,560	942	50	60%
	Regression	6,560	942	50	74%

Table 5.35—Optimum ROR completion for current completion designs for a well spacing of 1,312 ft and CAD$4/MMbtu gas price

Gas Price, (CAD)/MMbtu	Methodology	Lateral length, ft	Sand intensity, lb/ft	Entry point	ROR
$4	Simulation	9,840	471	150	118%
	Regression	9,840	2,688	150	148%

Table 5.36—Optimum ROR completion for future completion designs for a well spacing of 1,312 ft and CAD$4/MMbtu gas price

Gas Price, (CAD)/MMbtu	Methodology	Lateral length, ft	Sand intensity, lb/ft	Entry point	PV10 (MM$)
$2	Simulation	6,560	942	50	-0.89
	Regression	6,560	942	50	0.54

Table 5.37—Optimum PV10 completion for current completion designs for a well spacing of 1,312 ft and CAD$2/MMbtu gas price

Gas Price, (CAD)/MMbtu	Methodology	Lateral length, ft	Sand intensity, lb/ft	Entry point	PV10 (MM$)
$2	Simulation	9,840	942	100	0.29
	Regression	13,120	2,688	400	8.84

Table 5.38—Optimum PV10 completion for future completion designs for a well spacing of 1,312 ft and CAD$2/MMbtu gas price

Gas Price, (CAD)/MMbtu	Methodology	Lateral length, ft	Sand intensity, lb/ft	Entry point	PV10 (MM$)
$3	Simulation	6,560	942	50	2.96
	Regression	6,560	942	50	5.73

Table 5.39—Optimum PV10 completion for current completion designs for a well spacing of 1,312 ft and CAD$3/MMbtu gas price

Gas Price, (CAD)/MMbtu	Methodology	Lateral length, ft	Sand intensity, lb/ft	Entry point	PV10 (MM$)
$3	Simulation	13,120	1,413	100	7.27
	Regression	13,120	2,688	400	29.03

Table 5.40—Optimum PV10 completion for future completion designs for a well spacing of 1,312 ft and CAD$3/MMbtu gas price

Gas Price, (CAD)/MMbtu	Methodology	Lateral length, ft	Sand intensity, lb/ft	Entry point	PV10 (MM$)
$4	Simulation	6,560	942	50	6.84
	Regression	6,560	942	50	10.92

Table 5.41—Optimum PV10 completion for current completion designs for a well spacing of 1,312 ft and CAD$4/MMbtu gas price

Gas Price, (CAD)/MMbtu	Methodology	Lateral length, ft	Sand intensity, lb/ft	Entry point	PV10 (MM$)
$4	Simulation	13,120	1,413	100	15.45
	Regression	13,120	2,688	400	49.27

Table 5.42—Optimum PV10 completion for future completion designs for a well spacing of 1,312 ft and CAD$4/MMbtu gas price

As the results show in the Table 5.31 to Table 5.42, within the range of current completion practices, the regression and simulation models generate the same optimal completion design of 6,560 ft of lateral length, 942 lb/ft of sand intensity and 50 entry points and are at the upper limit of current practices for all completion parameters. However, outside the range of current completion practices, the regression and simulation model generate different optimal completion designs:

- In both regression and simulation methodologies, lateral length of the optimum completion designs (ROR and PV10) are considerably longer than the upper limit of current lateral length in the Town field.
- In both regression and simulation methodologies, number of entry points of optimum completion designs (ROR and PV10) are greater than the upper limit of current number of entry points in the Town field.

- The optimized sand intensities (ROR and PV10) using the regression method are considerably higher than upper limit of sand intensities currently used in the Town field. In the simulation method, optimized sand intensities for ROR are within current practices and optimized sand intensities for PV10 are within and beyond current practices used in the field, depending on commodity prices.

CHAPTER 6 LIMITATIONS AND FUTURE WORK

One limitation of this study in particular is that the optimization was not normalized for the size of the development area. That is, as the lateral length increases, not as many wells can be drilled per section, the well inventory decreases and infrastructure costs (e.g., roads, pads) change. This study was performed for individual-well optimization, not multi-well optimization of an area. Future work should encompass multi-well optimization by area.

Another limitation was the lack of geologic/reservoir data in the dataset. For the regression methodology these data were completely omitted and for the simulation methodology an average set of values was used. These data were excluded primarily due to the difficult and time-consuming nature of accurately acquiring these data. Future work should consider including these data, spatially distributed across the study area for both methodologies.

In this work, optimization using multivariable regression and reservoir simulation were conducted separately. Future work should investigate how to combine two these methodologies into a single optimization. Moreover, future work should quantify the uncertainty that exists in both models.

CHAPTER 7 CONCLUSIONS

The objectives of this research were, first, to develop methodologies to identify the economic optimum completion in heterogeneous, low-permeability horizontal wells that require hydraulic fracturing to flow at commercial rates, within and beyond the current industry completion practices and, second, apply the methodologies to 44 hydraulic-fractured horizontal wells in the Town field, located in the Montney formation in Canada, British Columbia. The conclusions of the study are as following:

- Two different methodologies were used to identify the economic optimum completion design in the Town field:
  - First, an empirical multivariable methodology incorporating individual-well completion and production data was used to predict B3 which was then projected into a 40-year production forecast using an average type curve.
  - Second, a physics-based reservoir simulation methodology using reservoir properties, was calibrated to match the average flowing pressure and production performance of an average production type curve. This calibrated simulator was then used to predict B3 and a 40-year production forecast.
  - Each methodology was used to generate production forecasts for a wide variety of completion designs. Single-well economics were generated on each of those designs and the optimum designs were identified that maximize either ROR or PV10.
- For the empirical multivariable regression section, I developed five multivariable regression models using completion parameters of 44 wells in the Town field to predict

short-term well performance. The conclusions from the multivariable regression modeling are as follows:

- The best model among the five models in the Town Upper Montney is the per-entry-point model, not the per-fluid model that was chosen for the analysis in this study.
- The predicted values from the per-fluid multivariable regression model of the Town field do not exhibit as large a range of values as the observed values. This is probably due to missing data in the model such as rock properties.
- The model does a poor job of predicting individual wells.
- I applied multivariable regression on the full BC Montney dataset of 1040 wells along with three different reduced datasets for the Town, Altares and Parkland fields:
  - For the Town field, the reduced dataset generated a better predictive model. For Altares and Parkland fields, there was no meaningful difference between the full and reduced models.
- Multivariable regression model was used to predict short-term well performance for 300 sets of completion parameters within and beyond the range of current completion practices in the Town field. The B3 of each set of completion parameters was converted to a 40-year monthly production forecast by scaling with the Town Field production type curve.

- For the physics-based reservoir simulation modeling, I calibrated a reservoir simulation model to match the average flowing pressures and production of a 44-well type curve in the Town field and used that calibrated model to predict well performance. The conclusions from the reservoir simulation modeling are as follows:
  - The model does a poor job of predicting individual wells.

- The predicted B3 values from the simulation model do not exhibit as large a range of values as the observed values. This is probably due to a single set of rock properties being used in the simulation model while the 44-well Town area probably includes a significant range of rock properties.
- The simulation model does a better job of predicting the B3 extremes than the regression model, but results in a lower R^2 of predicted vs. observed B3 than the regression model.

- Economic optimization was performed using the both regression and simulation models with an assumed well spacing of a 1,312 ft. The conclusions from the economic modeling are as follows:
  - The regression model predicts higher ROR & PV10 compared to the simulation model for the same completion parameters.
    - The higher forecast ROR is because of a higher forecast B3. This is due to a lack of parameters relating to the physics of wellbore friction losses in the regression model.
    - The higher forecast PV10 is because of a higher forecast EUR. This is due to a lack of parameters relating to the physics of the drainage area size in the regression model.
  - Within the range of current completion practices, the regression and simulation models generate the same optimal completion design of 6,560 ft of lateral length, 942 lb/ft of sand intensity and 50 entry points. The optimal completion design is at the upper limit of current industry practices in the Town field for all completion

parameters, indicating the optimal completion is likely beyond the current completion practices.

- Outside the range of current completion practices, the regression and simulation model generate different optimal completion designs. In both methods, lateral length and number of entry points of the optimum completion designs (ROR and PV10) are considerably greater than the upper limit of current values in the Town field. The optimized sand intensities (ROR and PV10) using the regression method are considerably higher than upper limit of sand intensities currently used in the Town field. In the simulation method, optimized sand intensities for ROR are within and optimized sand intensities for PV10 are within and beyond current practices used in the field, depending on commodity prices.
- These results suggest that the optimal completion is beyond current practices.
- Although the regression method is faster, the simulation method is recommended for optimization beyond the range of current completion practices. This is because the reservoir simulation method specifically models several physics-based realities that regression does not, such as material balance as dictated by the size of the reservoir (OGIP) and fluid-flow friction losses through the casing and tubing.
- B3 is mostly influenced by and positively correlated to the number of entry points. Larger B3's generate larger ROR's and thus impact the economic optimum completion.
- EUR is mostly influenced by and positively correlated to the lateral length. Larger EUR's generate larger PV10's and thus impacts the economic optimum completion.

REFERENCES

A&D Drill Bits. 2015. Best in Class Where is 2015 Capital Being Spent, BMO Capital Market, Montreal, Canada. https://www.bmoaddeals.com/uploads/pdf/Drill-Bits-Best-in-Class-August-2015.pdf

Crew Energy. 2016. Crew Energy Inc. Corporation report. https://www.desmogblog.com/sites/beta.desmogblog.com/files/2016-Shale-Factbook_0.pdf

Curtis, T. and Montalbano, B. 2017. Oxfordenergy.org. Completion Design Changes and the Impact on US Shale Well Productivity, https://www.oxfordenergy.org/wpcms/wp-content/uploads/2017/11/Completion-Design-Changes-and-the-Impact-on-US-Shale-Well-Productivity-Insight-21.pdf

EIA. 2015. Energy Information Administration 2015. DOE/EIA-0383(2015), Annual Energy Outlook 2015 With Projections to 2040, U.S. Energy Information Administration, Washington, DC. https://www.eia.gov/outlooks/aeo/pdf/0383(2015).pdf

EIA. 2016. U.S. Energy Information Administration, Trends in U.S. Oil and Natural Gas Upstream Costs, U.S. Energy Information Administration, Washington, DC. https://www.eia.gov/outlooks/aeo/pdf/0383(2016).pdf

Grieser, B., Hobbs, J., Hunter, J. and Ables, J. 2003. The Rocket Science Behind Water Frac Design. Presented at the SPE Production and Operations Symposium, Oklahoma City, Oklahoma, USA, 22-25 March 2003. SPE-80933-MS. http://dx.doi.org/10.2118/80933-MS.

Gong, X., McVay, D., Bickel, J. et al. 2011. Integrated Reservoir and Decision Modeling to Optimize Northern Barnett Shale Development Strategies. Presented at the Canadian Unconventional Resources Conference, Calgary, Canada. SPE-149459. http://dx.doi.org/10.2118/149459-MS.

Hislop, J. 2018. Energy News. Innovation is key performance driver for modern gas wells: Montney Formation one of North America's biggest gas resources, https://energi.news/alberta/innovation-driver-performance-imodern-gas-wells-montney formation/

Hryb, D., Archimio, A., and Badessich, M. 2014. Unlocking the True Potential of the Vaca Muerta Shale via an Integrated Completion Optimization Approach. Presented at the SPE Annual Technical Conference and Exhibition, Amsterdam, Netherlands. SPE-170580. https://doi.org/10.2118/170580-MS

James, G. and Witten, D. 2017. An Introduction to Statistical Learning, second edition. New York: Springer.

Krause, F.F., Deutsch, K.B. et al. 1994. Atlas of the Western Canada Sedimentary Basin. Available at: http://www.cspg.org/CSPG/IMIS20/Publications/Geological_Atlas/CSPGIMIS20/Publications/Geological Atlas.aspx?hkey=dd3bbc73-ab4f-4ca3-aeae-0a65cf7a3b05

LaFollette, R. and Holcomb, W. 2011. Practical Data Mining: Lessons-Learned from the Barnett Shale of North Texas. Presented at the SPE Hydraulic Fracturing Technology Conference, The Woodlands, Texas. SPE-140524. http://dx.doi.org/10.2118/140524-MS.

Lafollette, R., Holcomb, W., and Aragon, J. 2012. Practical Data Mining: Analysis of Barnett Shale Production Results with Emphasis on Well Completion and Fracture Stimulation.

Presented at the SPE Hydraulic Fracturing Technology Conference, The Woodlands, Texas. SPE-152531. http://dx.doi.org/10.2118/152531-MS.

Mangha, O., Nair, N., Miller, M. et al. 2012. Play wide Well Performance Analysis in Montney Siltstone. Presented at the Canadian Unconventional Resources Conference, Calgary, Alberta, Canada. SPE-162843. http://dx.doi.org/10.2118/162843-MS.

NEB. 2013. National Energy Board, The Ultimate Potential for Unconventional Petroleum from the Montney Formation of British Columbia and Alberta. BC OGC, BC, Canada. https://www.nebone.gc.ca/nrg/sttstc/ntrlgs/rprt/ltmtptntlmntnyfrmtn2013/ltmtptntlmntnyfrmtn2013-eng.pdf

Petersen, K.B. and Pedersen, M.S. 2005. The Matrix CookBook, math.uwaterloo.ca/~hwolkowi/, 5 January 2005, http://www2.imm.dtu.dk/pubdb/views/edoc_download.php/3274/pdf/imm3274.pdf (accessed 17 May 2019).

Reimer, J., 2015. Hydrocarbon Recovery Optimization in the Montney Formation: Framing Key Challenges Relating to Shale Gas Development for Industry and External Stakeholders. Presented at the CSUR Technical Luncheon, Calgary, Canada.

Reynolds, M., Batchman, R., Buendia, J. et al. 2015. A Critical Review of Well Performance by Production Analysis of Over 2,000 Montney Multi-Stage Fractured Horizontal Gas Wells. Presented at the SPE/CSUR Unconventional Resources Conference, Calgary, Canada. SPE-175948. http://dx.doi.org/10.2118/175948-MS.

Rokosh, C. D. 2012. Summary of Alberta's Shale and Siltstone Hosted Hydrocarbons. ERCB/AGS Open File Report, Alberta, Canada. https://ags.aer.ca/document/OFR/OFR_2012_06.PDF

Sereda, R. 2017. The Lower Montney Turbidite Complex of Northwest Alberta and Northeast British Columbia: Evolution of an Oil and Gas Play from Conventional to Unconventional. Presented at the AAPG, Houston, Texas. http://www.searchanddiscovery.com/documents/2017/10987sereda/ndx_sereda.pdf

Sheather, S. J. 2009. A Modern Approach to Regression with R. Springer Texts in Statistics, first edition. New York: Springer.

Stack exchange. 2016. What is Wrong with Extrapolation? (20 June 2016), https://stats.stackexchange.com/questions/219579/what-is-wrong-with-extrapolation (accessed 29 January 2019).

Veatch, W. 1983. Overview of Current Hydraulic Fracturing Design and Treatment Technology--Part 1. Journal of Canadian Petroleum Technology 35 (1): 677—687. https://doi.org/10.2118/10039-PA

Voneiff, G., Sadeghi, S., and Bastian, P. 2014. Probabilistic Forecasting of Horizontal Well Performance in Unconventional Reservoirs Using Publicly-Available Completion Data. Presented at the Unconventional Resources Conference, The Woodlands, Texas. SPE-168978. https://doi.org/10.2118/168978-MS.

Voneiff, G., Sadeghi, S., and Bastian, P. 2013. A Well Performance Model Based on Multivariate Analysis of Completion and Production Data from Horizontal Wells in the Montney Formation in British Columbia. Presented at the Unconventional Resources Conference Canada, Alberta, Canada. SPE-167154. https://doi.org/10.2118/167154-MS

Wilson, B., Lui, D., Kim, J. et al. 2011. Comparative Study of Multistage Cemented Liner and Openhole System Completion Technologies in the Montney Resource Play. Presented at

the Unconventional Resources Conference Canada, Alberta, Canada. SPE-149437. https://doi.org/10.2118/149437-MS

Zinselmeyer, R. 2015. Tower Montney Unconventional Oil Project – New Completion Technology Unlocks a Significant New Resource in BC. Presented at the 9th Annual British Columbia Unconventional Gas Technical Forum, Victoria, Canada.